February 1990 Thesis/Dissertation

Examples of Isallobaric Forcing in Surface Frontal Motion and Surface Frontogenesis over the Central United States

Steven R. Christy

AFIT Student at: Creighton University

AFIT/CI/CIA - 90-098

AFIT/CI
Wright-Patterson AFB OH 45433

Examples of Isallobaric Forcing in Surface Frontal Motion and Surface Frontogenesis over the Central United States

A Description of Graduate Research

By

Steven R. Christy

Department of Atmospheric Sciences

Creighton University

23 February 1990

1. Introduction

It has long been known that surface fronts sometimes move at higher velocities than the crossfrontal component of the actual surface wind would support. In these cases, the crossfrontal component of the geostrophic wind has been demonstrated to provide a somewhat more satisfactory explanation of surface frontal motion. However, frontal motion faster than the geostrophic crossfrontal component would support has also been observed. Past research has suggested that the isallobaric component of the ageostrophic wind may be responsible for this phenomenon. However, to date, the isallobaric wind has not been shown to directly influence processes which contribute to surface frontal motion; specifically, isallobarically induced enhancement of crossfrontal wind components and apparent propagation through isallobaric frontogenetical forcing. This paper will examine the role of isallobaric forcing on surface frontal motion and frontogenesis through its influence upon these two processes in three cases studies over the Central United States.

Studies of the factors involved in surface frontal motion have yielded a wide variety of results. For instance, Brundidge (1965) in his study of cold fronts, noted that the frontal speed was approximately double the normal wind component measured after frontal passage at 30 feet (ft) and found better agreement in most cases with the normal wind component measured at 600 ft. Brundidge's results suggest that geostrophic flow normal to the frontal surface might provide better agreement with the observed surface frontal motion

than the actual surface winds. Geostrophic balance across a front was used by Hoskins and Bretherton (1972) in their model of frontogenesis, but they noted that tangential accelerations are also important. Recent studies (Hobbs and Pearson, 1982; Bond and Fleagle, 1985) have noted that in some cases surface cold frontal motion is accurately determined by the gravity current equation; however, Smith and Reeder (1988) have questioned this apparent agreement of observed surface frontal speeds with the calculated speeds of internal gravity waves and noted that except where cold fronts become orographically trapped, there is little evidence to suggest that frontal speed is controlled by gravity waves rather than by processes which operate on the frontal scale itself, where the ageostrophic crossfront circulation plays a central role. One component of the ageostrophic wind was considered by Brunt and Douglas in 1928. In particular, they presented some evidence of isallobaric forcing's impact on surface frontal motion, but due to a sparse observation network which did not allow the computation of accurate frontal positions, geostrophic winds, or isallobaric winds their hypothesis remained unproved.

Another mechanism by which fronts may propagate is by the frontogenetical forcing associated with the actual wind. Two-dimensional models of horizontal shear frontogenesis have demonstrated that when a significant along-front temperature gradient exists, it is possible for a cold front to propagate faster than the wind behind the cold front (Reeder and Smith 1986, 1987; Reeder 1986). Furthermore, Saucier (1955) noted that the isallobaric wind is frontogenetical near the regions of pressure falls and that the

magnitude of the frontogenesis in the lower troposphere is large in the same areas. In conditions similar to those noted above (strong along-front temperature gradient), isallobaric forcing on frontogenesis may also influence surface frontal motion through an "apparent" propagation.

In this study the isallobaric contribution to surface frontal motion and surface frontogenesis is estimated by use of the frictionless isallobaric wind. A representation of typical pressure tendencies associated with a mid-latitude cyclone is depicted in Fig. 1. The frictionless isallobaric wind should reach its maximum magnitude between the region of pressure rises behind the cold front and the pressure fall region ahead of the cold front. Also, the frictionless isallobaric wind should have a local maximum of magnitude around the pressure fall center north of the warm front. Based upon these distributions, it is expected that the frictionless isallobaric wind will be found to contribute to increased speed of surface frontal propagation. Defining frontogenesis as the Lagrangian rate of change of the magnitude of the temperature gradient, the frictionless isallobaric wind in Fig. 1 would act as a frontogenetic wind field through redistribution of the maximum temperature gradient.

2. Data and Methods

2.1 Data

Locations of the 336 surface observation stations used to compile

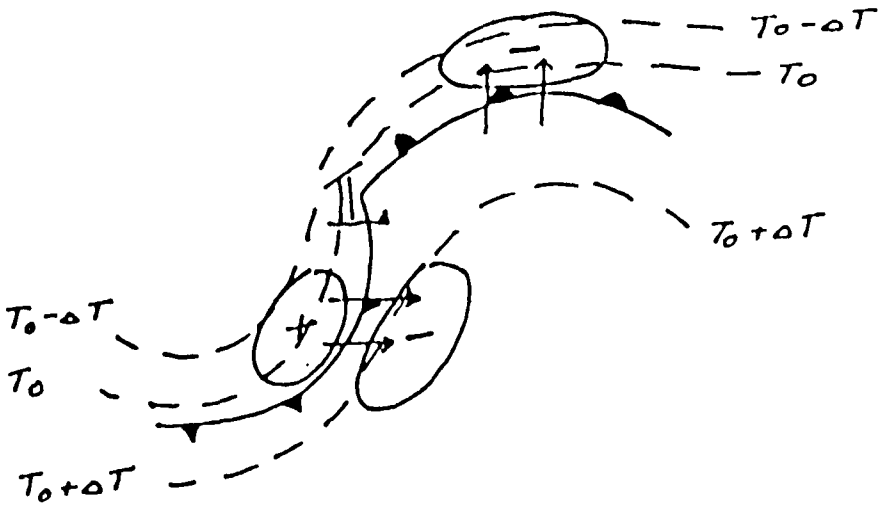

Fig. 1. A typical isallobaric distribution for an extratropical cyclone. A (+) represents a pressure rise center and a (-) represents a pressure fall center. Arrows represent maxima of the frictionless isallobaric wind and broken lines are isotherms.

the data base for this study are indicated in Fig. 2. Data input from each observation location included the following: temperature, dewpoint, wind direction, wind speed, and altimeter setting. The above mentioned elements from hourly and corrected surface airway reports were manually entered into computer input files. In addition to possible error from incorrect dissemination of the observed elements, this methodology introduced the additional possibility of error due to incorrect transfer of the data to the data sheets and incorrect typing into the input files. The methods used to screen the data set for errors are discussed in Appendix A.

Brundt and Douglas (1928) and Saucier (1955) both noted that correct representation of the isallobaric wind requires the evaluation of the pressure tendency field over the shortest time interval possible. In the absence of barometric traces for each observation location and given the meteorological data available, the shortest time period for which pressure tendencies can be computed is 1-hour. Saucier (1955) alluded to the use of 3-hour pressure tendencies for determining the pressure change due to synoptic influences, but he noted that in the middle latitudes the effect of the semi-diurnal pressure wave is large enough to make 3-hour local pressure changes misleading. Smaller scale influences such as pressure changes due to thunderstorms can also influence the tendencies. In the absence of a spectral analysis to identify the different components of the pressure tendency, the easiest way to smooth the influences discussed earlier is to use the average change over a 2-hour period.

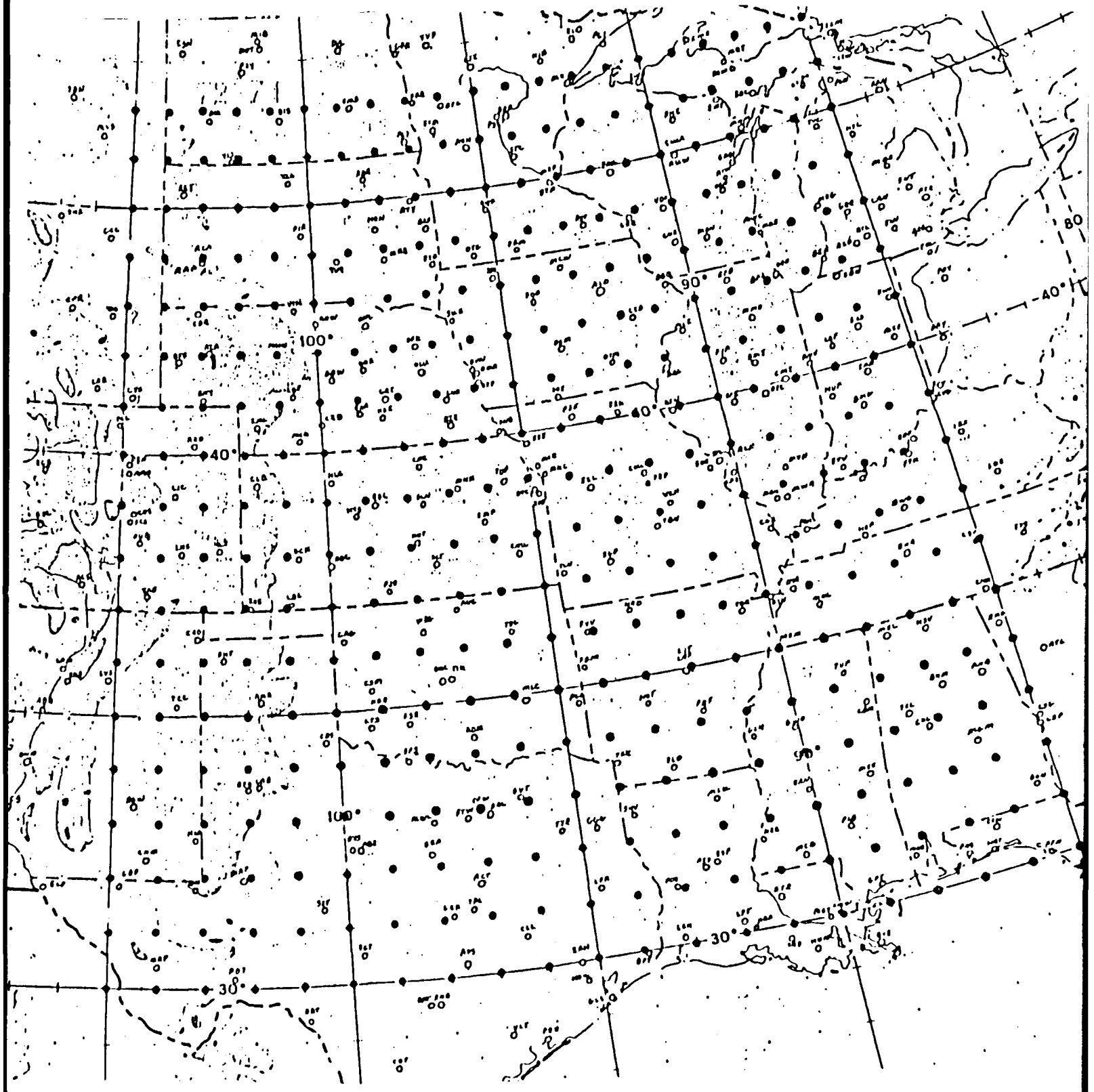

Fig. 2. Locations of grid points and surface stations used in this study.

2.2 Methods

The actual wind at any point is defined as the sum of the geostrophic and ageostrophic winds. Therefore, it is possible to compute the ageostrophic wind at that point by subtracting the geostrophic wind from the actual wind. Actual winds at each observation location were broken into u and v components and fitted to a one degree latitude-longitude grid using the Cressman (1959) objective analysis scheme which is described in Appendix B. The grid is located over the Central United States and extends from 47°N to 30°N and from 85°W to 105°W (Fig. 2). The total number of grid points is 378. Gridspacing is 111.19 kilometers (km) between grid points in the north-south direction and the distance between grid points in the east-west direction varies from 75.83 km to 96.29 km at the northern and southern grid boundaries, respectively. Surface geostrophic wind computations require an accurate representation of the surface horizontal pressure gradient force which is easily obtained over level terrain; however, the area under consideration is sloping terrain which introduces the problem of eliminating the vertical variation of pressure with height in order to obtain the true horizontal pressure gradient force.

2.2.1 Horizontal Pressure Gradient Force Computations

Sangster (1960, 1967) among others, has noted the problems with using station pressures reduced to sea level for the representation of the surface horizontal pressure gradient force and subsequent

computations of the surface geostrophic wind. Sangster (1987) notes that the plateau correction, which is implicitly included in the reduction of station pressures to sea level for station elevations above 305 meters (m), has the effect of producing a northerly geostrophic wind component in the summer over the Great Plains, and a southerly geostrophic wind component there in winter with values of around 10 m s^{-1} for the components under extreme conditions. Sangster (1960, 1987) has also shown that it is possible to compute the slope of a constant pressure surface in non-isobaric coordinates by use of the altimeter correction method developed by Bellamy (1945). Hereafter, all references to Bellamy will be from his 1945 paper. The altimeter correction (D) is defined as follows:

$$D = Z - Z_p, \tag{1}$$

where Z is the elevation of the station above sea level and Zp is the pressure altitude of the station pressure. Following Bellamy, the value of D can be used to approximate the height of any constant pressure level. For a given station pressure, the pressure altitude is the height of the observed station pressure in a defined standard atmosphere using the hypsometric equation

$$Z_{p2} = -R_d g^{-1} \bar{T}_p \ln(P_2/P_1) + Z_{p1}, \tag{2}$$

where Rd is the dry gas constant, g is the acceleration due to gravity, $\bar{T}_p$ is the mean standard atmospheric temperature of the layer, P_1 is the pressure at level 1, Zp_1 is the pressure altitude at

level 1, P_2 is the pressure at level 2, and Zp_2 is the pressure altitude at level 2.

In this study the National Advisory Committee for Aeronautics (NACA) standard atmosphere was used. The NACA standard atmosphere has the following characteristics (Haltiner and Martin, 1957):

a. Assume dry air.

b. Base level pressure, P_0 = 1013.25 mb.

c. Base temperature T = 15°C.

d. Lapse rate = 0.65°C 100 m^{-1} for $z \leq 10769$ m.

e. gravity = 980.665 cm sec^{-2}.

The correction for temperature and moisture may be derived by starting with the hypsometric equation for the actual atmosphere.

$$Z_2 - Z_1 = -R_d g^{-1} \bar{T}_v \ln(P_2/P_1), \tag{3}$$

where $\bar{T}v$ is the mean virtual temperature for the layer. Multiplying Eq. (3) by $\bar{T}p\ \bar{T}p^{-1}$, defining the pressure at level 1 as 1013.25 mb, and substituting Eq. (2) for the pressure altitude of the observed station pressure (Zp_2) results in

$$Z_2 - Z_{1013.25} = \bar{T}_v \bar{T}_p^{-1} Z_{p2}, \tag{4}$$

where Zp_2 was calculated using Eq. (5) (Haltiner and Martin, 1957),

$$Z_{p2}\ (m) = 44,3081 [1 - (P_2/1013.25)^{0.19023}]. \tag{5}$$

Now by taking $Tv\ Tp^{-1}$ as approximately equivalent to $\bar{T}v\ \bar{T}p^{-1}$ we are assuming that the virtual temperature and the standard atmospheric temperature at the station elevation are representative of the mean temperatures of the column, respectively. Following Haltiner and Martin (1957), the quantity

$$Z_{1013.25} = Z_2 - T_v T_p^{-1} Z_{p2}, \tag{6}$$

represents the height of the 1013.25 mb surface. Bellamy defined a quantity called the specific temperature anomaly S^* which is the deviation of the actual virtual temperature, corrected for gravity variations between the actual and standard atmospheres, from the standard atmospheric temperature

$$S^* = (T^* - T_p)T_p^{-1}. \tag{7}$$

Bellamy's definition of virtual temperature (T^*) is given as

$$T^* = g_p g^{-1} T_v, \tag{8}$$

where g_p is the acceleration of gravity in the standard atmosphere. The method used to calculate Tv and variations in gravity is discussed in Appendix C. Substitution of $1 + S^*$ for $Tv\ Tp^{-1}$ and D for $Z_2 - Zp_2$ in Eq. (6) yields

$$Z_{1013.25} = D_2 - S^* Z_{p2}. \tag{9}$$

Equation (9) shows that the height of the 1013.25 mb surface is the sum of the deviation of the observed column thickness from the standard column thickness and the correction due to differences of the observed virtual temperature from the standard atmospheric temperature. Sangster (1967) illustrated that the temperature averaging process used in the reduction of station pressures to sea level effectively "masked" the diurnal variation of the surface geostrophic wind over the Great Plains. More importantly for the purposes of the present study is the effect that 12 hour temperature averaging would have on an accurate determination of the surface geostrophic wind where a change of air mass has occurred due to frontal passage since the temperature change associated with some fronts can be greater than the normal diurnal temperature change.

The slope of the constant pressure surface may be obtained by substitution of D in the coordinate transfer equation

$$\vec{\nabla}_{H}D = \vec{\nabla}_{P}D + (\partial D \partial Z_{p}^{-1})\vec{\nabla}_{H}Z_{p}, \qquad (10)$$

where the H subscript means horizontal in cartesian coordinates and the p subscript implies isobaric coordinates. Since $\partial D \partial Z_{p}^{-1} = S^{*}$, the hydrostatic equation in the D system, substitution of S^{*} into Eq. (10) with some rearrangement yields

$$\vec{\nabla}_{P}D = \vec{\nabla}_{H}D - S^{*}\vec{\nabla}_{H}Z_{p}. \qquad (11)$$

Further examination of Eq. (11) will demonstrate the problems of this method that Sangster (1960, 1987) discusses. Reintroduction of the

subscripts for the pressure levels defined earlier and remembering that the pressure altitude of the base level (Zp_1) is equal to zero, Eq. (11) can be written in the following form:

$$\vec{\nabla}_P Z_{1013.25} = (1 + S^*)\vec{\nabla}_H D_2 - S^*\vec{\nabla}_H Z_2. \qquad (12)$$

The second term on the right hand side shows that the slope of the 1013.25 mb surface depends partially on the sloped terrain. Values of D computed at the observation locations depend upon the station elevations and if the elevations at the grid points differ greatly from the station elevations, introduction of a fictitious effect occurs. A satisfactory solution to this problem was achieved by fitting station elevations to the grid using the same Cressman (1959) weighting scheme as was used for computing the D values and specific temperature anomalies at the grid points. Sharp changes in grid point elevations can also introduce a fictitious slope that are not the result of the horizontal pressure differences. To minimize sharp elevation changes, grid point elevations where then smoothed by a two-pass five-point formula given in Appendix C. The smoothed elevations used are shown in Fig 3. The other problem results from the assumption of the mean standard atmospheric temperature of the column as equivalent to the standard atmospheric temperature at the station elevation. By using the standard atmospheric temperature at station elevation, a temperature that will always be colder than the mean standard atmospheric temperature is used. Referring to Eq. (7) the specific temperature anomaly would be greater than if the mean standard atmospheric temperature was used. Reduction of the error

caused by this assumption was achieved by the use of an approximate mean standard atmospheric temperature taken as the average of the surface and station elevation standard atmospheric temperature.

2.2.2 Geostrophic Wind in the D System

The expression for the geostrophic wind in isobaric coordinates is

$$\vec{V}_g = -gf^{-1}\vec{\nabla}_p Z \times \hat{k}, \tag{13}$$

where f is the coriolis parameter and $\hat{k}$ is the vertical unit vector. Substitution of Eq. (12) for the slope of a constant pressure surface in Eq. (13) gives

$$\vec{V}_g = -gf^{-1}[(1 + S^*)\vec{\nabla}D - S^*\vec{\nabla}Z] \times \hat{k}. \tag{14}$$

The u and v components of the geostrophic wind (u_g, v_g) obtained from Eq. (14) are as follows:

$$u_g = -gf^{-1}[(\partial D\partial y^{-1} + S^*\partial D\partial y^{-1}) - S^*\partial Z\partial y^{-1}], \tag{15a}$$

$$v_g = -gf^{-1}[(-\partial D\partial x^{-1} - S^*\partial D\partial x^{-1}) + S^*\partial Z\partial x^{-1}]. \tag{15b}$$

Equations (15a) and (15b) are equivalent to the method used by Bonner and Paegle (1970) to confirm the diurnal variation of the surface geostrophic wind discovered by Sangster (1967). D values and specific temperature anomalies were computed at each station and the

Cressman (1959) weighting scheme was used to fit the values to the grid points. Equations (15a) and (15b) allowed the computation of the u and v components, respectively, of the surface geostrophic winds at each grid point (excluding boundary grid points) using centered finite differencing to approximate the derivatives.

2.2.3 The Ageostrophic Wind

The vector form of the equation for the ageostrophic wind may be written as (Saucier, 1955)

$$\vec{V}_{ag} = \hat{k} \times (f^{-1}\underset{1}{\frac{\partial \vec{V}_g}{\partial t}} + f^{-1}\underset{2}{\vec{V}_H \bullet \vec{\nabla} \vec{V}_g} + wf^{-1}\underset{3}{\frac{\partial \vec{V}_g}{\partial z}} + f^{-1}\underset{4}{\frac{d\vec{V}_{ag}}{dt}}), \qquad (16)$$

where t is time and $\vec{V}_H$ is the actual horizontal wind vector. Term 1 in Eq. (16) represents the ageostrophic wind due to a changing height distribution with time in isobaric coordinates (isallohypsic wind), or in cartesian coordinates is the acceleration due to changes in pressure gradient and specific volume over time. Term 2 represents the ageostrophic wind due to the horizontal advection of the geostrophic wind. Term 3 represents the convective ageostrophic wind due to the vertical advection of the geostrophic wind. Term 4 is the component due to the acceleration of the ageostrophic wind. Note that the frictional term was not included in Eq. (16). As shown by Saucier (1955), there is a component of the ageostrophic wind (antitriptic wind) due to frictional accelerations.

The expression for the isallobaric wind was derived by Brunt and

Douglas (1928) and can be expressed as (Haltiner and Martin, 1957)

$$\vec{V}_{is} = -\alpha f^{-2}\vec{\nabla}_H(\partial P/\partial t^{-1}), \tag{17}$$

where $\vec{V}_{is}$ is the isallobaric wind and α is the specific volume.

2.2.4 Isallobaric Wind in the D System

Since the surface geostrophic wind was computed in isobaric coordinates, consistency required an expression for the frictionless isallobaric wind in the same coordinate system. With the assumption of hydrostatic equilibrium, the equivalency of the isallobaric wind in cartesian coordinates to the expression on the left hand side of Eq. (18) can be shown.

$$-gf^{-2}(1 + S^*)\vec{\nabla}_H(\partial D/\partial t^{-1}) = -\alpha f^{-2}\vec{\nabla}_H(\partial P/\partial t^{-1}). \tag{18}$$

The u and v components of the isallobaric wind (u_{is} , v_{is}) obtained from the left hand side of Eq. (18) are as follows:

$$u_{is} = -gf^{-2}[(1 + S^*)(\partial(\partial D/\partial t^{-1})/\partial x)], \tag{19a}$$

$$v_{is} = -gf^{-2}[(1 + S^*)(\partial(\partial D/\partial t^{-1})/\partial y)]. \tag{19b}$$

In order to evaluate Eqs. (19a) and (19b), the change of D was computed from

$$(\partial D \partial t^{-1})_t = (D_{t-1} - D_{t+1})/2, \quad (20)$$

where the subscript t is the time in hours. D change values from Eq. (20) and the specific temperature anomalies at each station were computed and the Cressman (1959) weighting scheme was used to fit the values to the grid points. Centered finite differencing was used to evaluate the derivatives in Eqs. (19a) and (19b). Young (1973) demonstrated the deviation of the isallobaric wind in the boundary layer to the left due to the effects of friction (Fig. 4). Thus the frictionless isallobaric wind as an estimator of the surface isallobaric wind will not posses the deviation to the left as well as having a somewhat larger magnitude.

2.2.5 Locating Surface Fronts and Computing Surface Frontal Velocities

Objectively defining a front at the surface is still at best a difficult procedure. For example, defining a front based upon the magnitude of the gradient of temperature may work well for anafronts (the prefixes 'ana' and 'kata' are as defined by Bergeron (1937)) which are usually defined by sharp changes in temperatures however, the katafront is usually accompanied only by a drop in relative humidity (Browning and Monk, 1982). An example of the magnitude of the temperature gradient for one hour from the 31 Jan 89 case study illustrates the difficulty of defining the front based soley on magnitude of the temperature gradient (Fig. 5). It is generally accepted that the maximum temperature gradient should be located

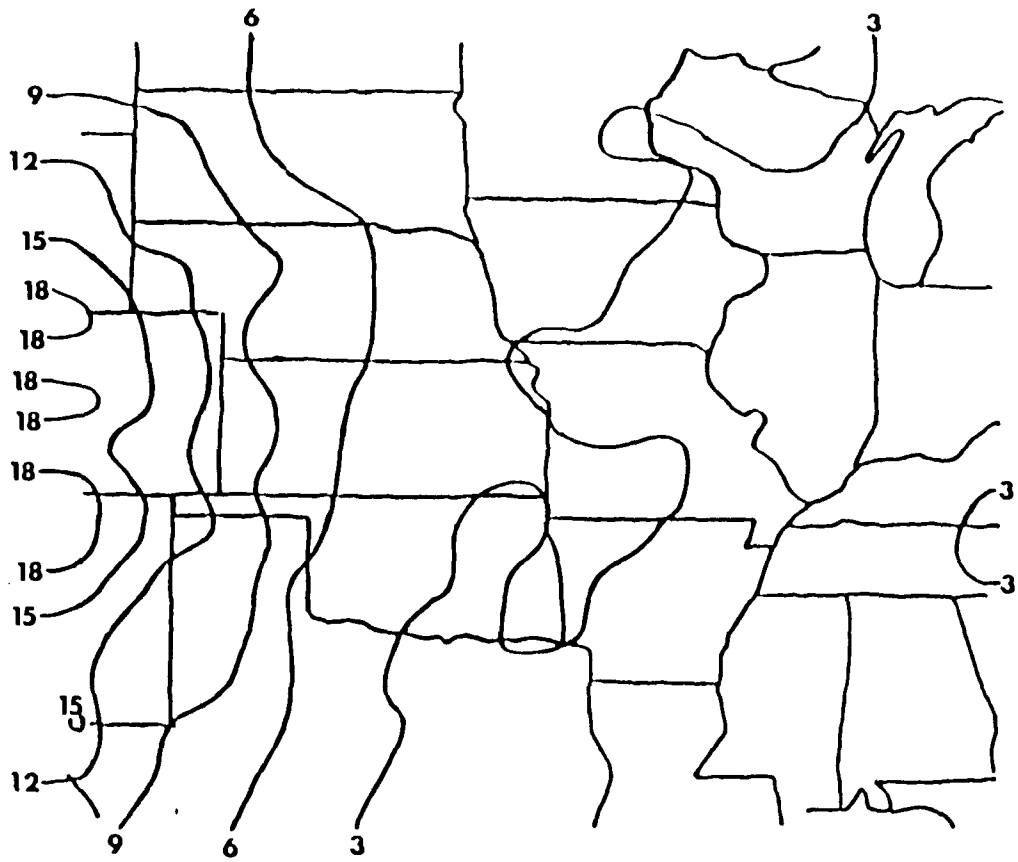

Fig. 3. Smoothed terrain used in the computations. Elevations above sea level are in hectometers (hm) with a contour of 3 hm.

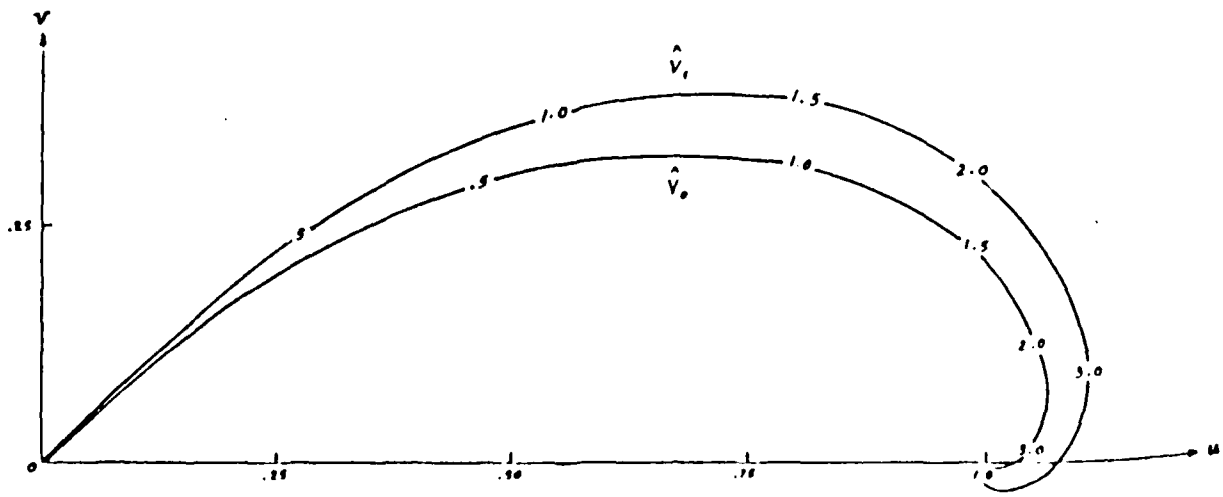

Fig. 4. Wind vector hodographs for Ekman ($\hat{V}o$) flow and frictional isallobaric flow ($\hat{V}_r$). After Young, 1973

behind a cold front. If this criterion is used as the only parameter by which to locate the front, the western one-third of the cold front is well defined; however, the eastern two-thirds of the cold front does not conform to this pattern. Based upon the uncertainty of frontal postioning in areas of weak temperature gradient, it was decided to use the more subjective approach of defining the surface frontal positions using all available surface parameters. In order to reduce the bias that may result from this procedure, surface analyses produced at the National Meteorological Center were used as guides for location of the surface fronts at 1500, 1800, 2100, and 0000 G.M.T.. Surface frontal positions at intermediate hours were determined from plotted station data.

Frontal velocities were determined from hourly surface positions for various hours within each case study. Some error in the determination of surface frontal velocities is to be expected with the subjective method of frontal location; however, the resultant frontal velocities are considered accurate enough for the purposes of this study. The component of the geostrophic, actual, and frictionless isallobaric winds normal to the surface front were determined for the same periods as the frontal velocities. The normal component of the respective wind for each segment of the frontal zone (segment defined as the length of front one-half the distance from each grid point) is determined from the nearest grid point. The nearest grid point definition is based upon one-third of the distance from the middle of the front to the grid point. If the front was located more than this distance away from the two nearest grid points, the crossfrontal component was taken as a linear average

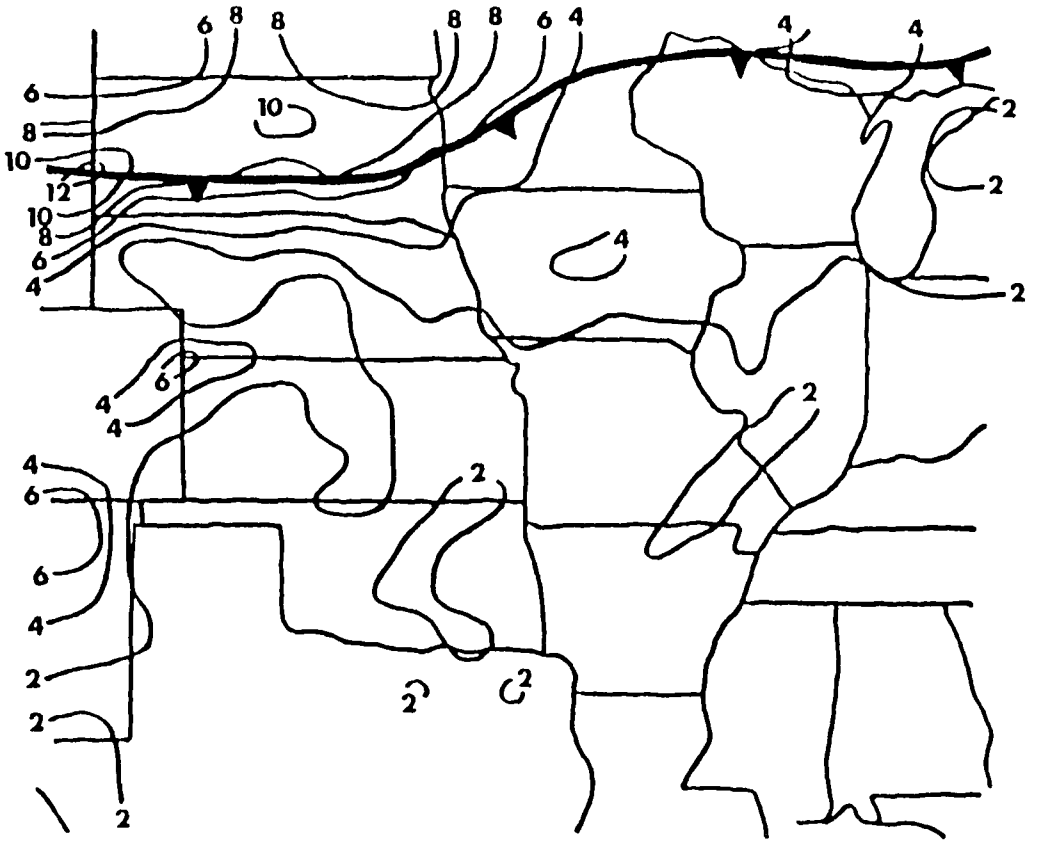

Fig. 5. Magnitude of the temperature gradient $|\nabla T|$ from 31 January 1989 for 1900 G.M.T. Units are $^{\circ}K\ Km^{-1}\ X\ 10^{2}$ with a contour of $2^{\circ}K$. Surface frontal position is superimposed.

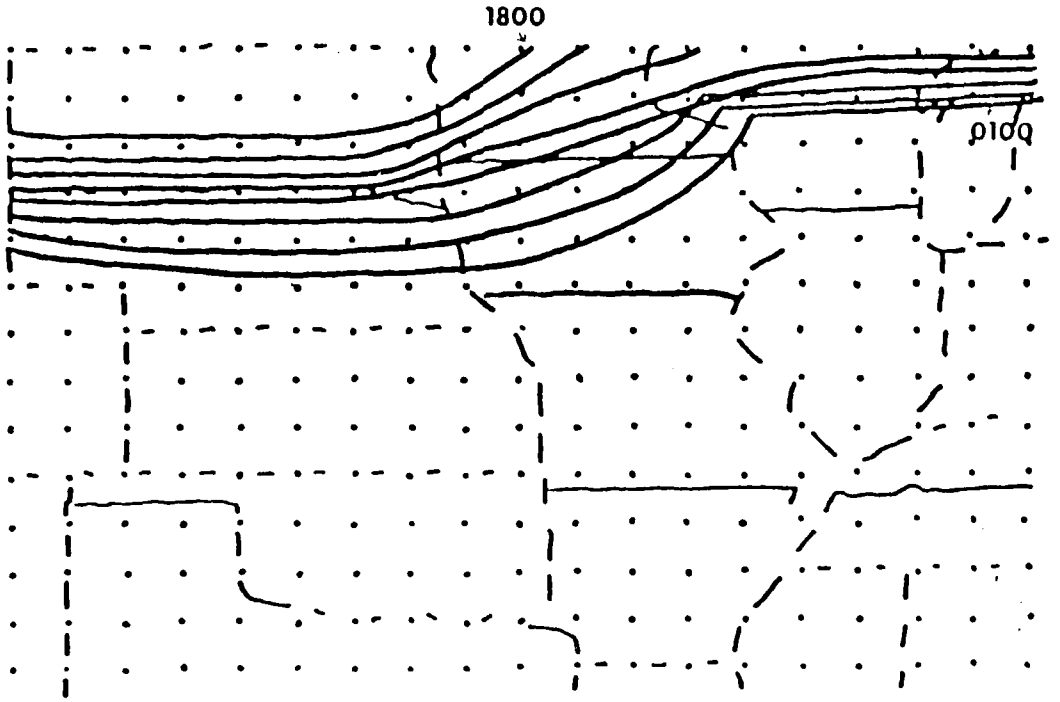

Fig. 6. Hourly frontal positions over the central United States for 1800-0100 G.M.T. 31 January-1 February 1989.

of the crossfrontal components from the two nearest grid points. Frontal velocities along with the crossfrontal component by the actual, geostrophic, and frictionless isallobaric winds are displayed together in figures hereafter called frontal velocity maps.

2.6 Computation of Surface Frontogenetical Forcing

Petterson (1956) demonstrated that by assuming adiabatic motion and neglecting the vertical component of motion, the kinematic factors involved in surface frontogenesis of a potential temperature field may be expressed in terms of the deformation, divergence, and the angle of the isotherms from the axis of dilitation. Petterson further demonstrated that for synoptic scale motions the divergence term may be neglected and obtained the now classical result that if the angle from the isotherms to the axis of dilitation is less than 45 degrees frontogenesis occurs and if the angle exceeds 45 degrees frontolysis occurs. In the scale of motion associated with a developing cyclone or a front, it is possible for the divergence term of the surface frontogenetical function to be of the same order of magnitude or larger than the deformation term. For example, in their case study of a developing cyclone, Moore and Blakey (1988) had contributions to the surface frontogenesis from the divergence term of the same order of magnitude as the deformation term. By definition the contribution to surface frontogenesis by convergent or divergent motions of the actual wind field has to come from the ageostrophic component. Surface frontogenesis evaluated as the Lagrangian rate of change of the horizontal temperature gradient

magnitude and with the vertical component of motion removed may be written as (Jascourt et al., 1988):

$$\mathfrak{F} = d(\|\vec{\nabla}T\|)/dt = -\{\partial T\partial x^{-1}[\partial T\partial y^{-1}\partial u\partial x^{-1} + \partial T\partial y^{-1}\partial v\partial x^{-1}] + \partial T\partial y^{-1}[\partial T\partial x^{-1}\partial u\partial y^{-1} + \partial T\partial y^{-1}\partial v\partial y^{-1}] - [\partial T\partial x^{-1}\partial(dTdt^{-1})\partial x^{-1} + \partial T\partial y^{-1}\partial(dTdt^{-1})\partial y^{-1}]\}/\|\vec{\nabla}T\|, \quad (21)$$

where $\|\vec{\nabla}T\|$ is the magnitude of the temperature gradient. By using the quantities defined below

$$\text{Shearing Deformation} = S_r = \partial u\partial y^{-1} + \partial v\partial x^{-1},$$
$$\text{Stretching Deformation} = S_t = \partial u\partial x^{-1} - \partial v\partial y^{-1},$$
$$\text{Divergence} = \vec{\nabla} \bullet \vec{V} = \text{Div} = \partial u\partial x^{-1} + \partial v\partial y^{-1},$$

it can be shown that Eq. (21) may be written as

$$\mathfrak{F} = -\{(\partial T\partial x^{-1}\partial T\partial y^{-1})S_r + [((\partial T\partial x^{-1})^2+(\partial T\partial y^{-1})^2)\text{Div}]/2 + [((\partial T\partial x^{-1})^2-(\partial T\partial y^{-1})^2)S_t]/2 - [\partial T\partial x^{-1}\partial(dTdt^{-1})\partial x^{-1} + \partial T\partial y^{-1}\partial(dTdt^{-1})\partial y^{-1}]\}/\|\vec{\nabla}T\|. \quad (22)$$

The last term on the right hand side of Eq. (22) represents the temperature tendencies portion of the frontogenesis function

$$[\partial T\partial x^{-1}\partial(dTdt^{-1})\partial x^{-1} + \partial T\partial y^{-1}\partial(dTdt^{-1})\partial y^{-1}]/\|\vec{\nabla}T\|. \quad (23)$$

Other studies (i.e., Jascourt et. al., 1988) have often ignored this term. A short discussion on the validity of neglecting the temperature tendencies term is presented in the first case study.

Breaking Eq. (23) into its advective and local change components and reuniting the result with Eq. (22) gives a form of the frontogenetical function that can be evaluated for the u and v components of the actual and isallobaric winds,

$$\begin{aligned} \mathcal{F} = -\{[(\partial T/\partial x^{-1}\partial T/\partial y^{-1})S_r] + [((\partial T/\partial x^{-1})^2 + (\partial T/\partial y^{-1})^2)Div]/2 \\ + [((\partial T/\partial x^{-1})^2 - (\partial T/\partial y^{-1})^2)S_t]/2 - [\partial T/\partial x^{-1}\partial(\partial T/\partial t^{-1})/\partial x^{-1} \\ + \partial T/\partial x^{-1}\partial(\vec{V}\bullet\vec{\nabla}T)/\partial x^{-1} + \partial T/\partial y^{-1}\partial(\partial T/\partial t^{-1})/\partial y^{-1} \\ + \partial T/\partial y^{-1}\partial(\vec{V}\bullet\vec{\nabla}T)/\partial y^{-1})/\|\vec{\nabla}T\|, \end{aligned} \tag{24}$$

where $\vec{V}\bullet\vec{\nabla}T$ was evaluated as

$$\vec{V}\bullet\vec{\nabla}T = u(\partial T/\partial x) + v(\partial T/\partial y).$$

Equation (24) was evaluated for the actual and frictionless isallobaric winds. The frictionless isallobaric wind was available on all except the exterior grid points (latitudes 47°N and 30°N, longitudes 105°W and 85°W). The derivatives in Eq. (24) were approximated using centered finite differencing except for the exterior grid points where uncentered finite differencing was used. Because the times when the actual wind is measured at observation locations can vary considerably, a sensitivity study was performed to determine how frontogenetical forcing can be influenced by small changes in the actual wind. This is discussed in Appendix D.

3. Results

Contributions by the isallobaric wind to surface frontal motion and surface frontognetical forcing are examined in three case studies. Differing synoptic conditions in each case study allow observation of varied isallobaric patterns in the vicinity of

surface fronts. The 31 January 1989 case study investigates the isallobaric effects on a cold front that serves as a boundary for an arctic air mass moving south from Canada. The other two case studies (15 November 1988 and 7 January 1989) examine isallobaric influences associated with developing mid-latitude cyclones.

3.1 31 January 1989 Case Study

On 31 January 1989 a cold front located over South Dakota and Minnesota at 1800 G.M.T. moved south and was located from south-central Nebraska through Iowa and into central Wisconsin by 0100 G.M.T. 1 February 1989 (Fig. 6). Referring to Fig. 6, it is apparent that the frontal zone did not demonstrate a constant movement; decreased frontal speed is observed during the period 2000-2100 G.M.T. followed by increased frontal speed from 2200-0000 G.M.T. These frontal velocity changes correspond to pronounced changes in the D value (pressure) tendency field during the same period. The National Meteorological Center (NMC) 1200 G.M.T. 850 mb, 700 mb, and 500 mb maps (Figs. 7, 8, and 9) reveal that the southerly push of cold air through the period of interest was in response to northerly flow in the lower levels created by an intense closed low over Hudsons Bay and the high pressure ridge over Northwestern North America. Closer scrutiny of the upper air maps reveals several other features. For example, the warm air over Nebraska and Kansas is the result of flow over the Rocky Mountains as indicated by the lee side trough in the lower troposphere. Surface temperatures in response to this adiabatic warming reached maximums in the mid to upper 70's over

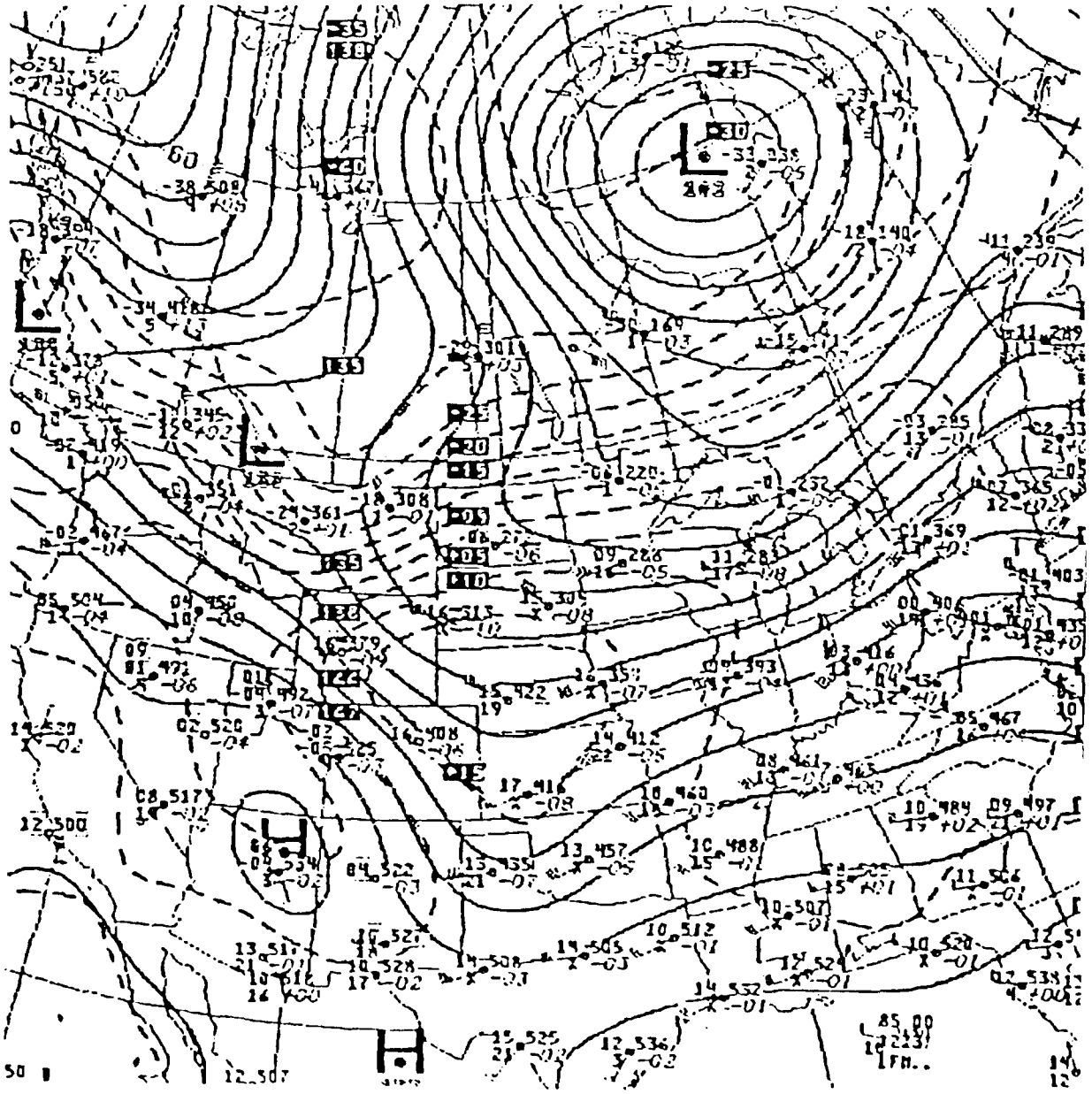

Fig. 7. National Meteorological Center 850 mb chart for 1200 G.M.T. 31 January 1989. Solid lines are height contours (decameters) and dashed lines are isotherms (°C).

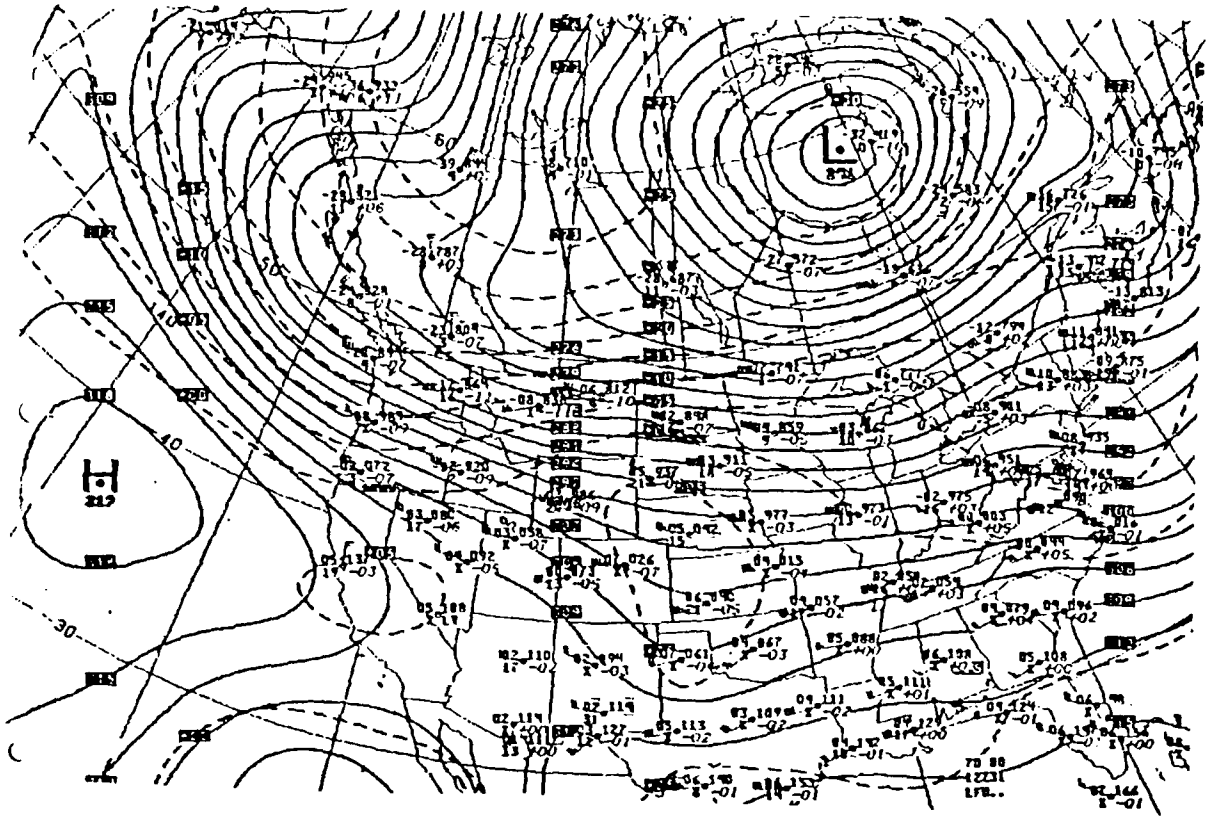

Fig. 8. Same as Fig. 7, except at 700 mb.

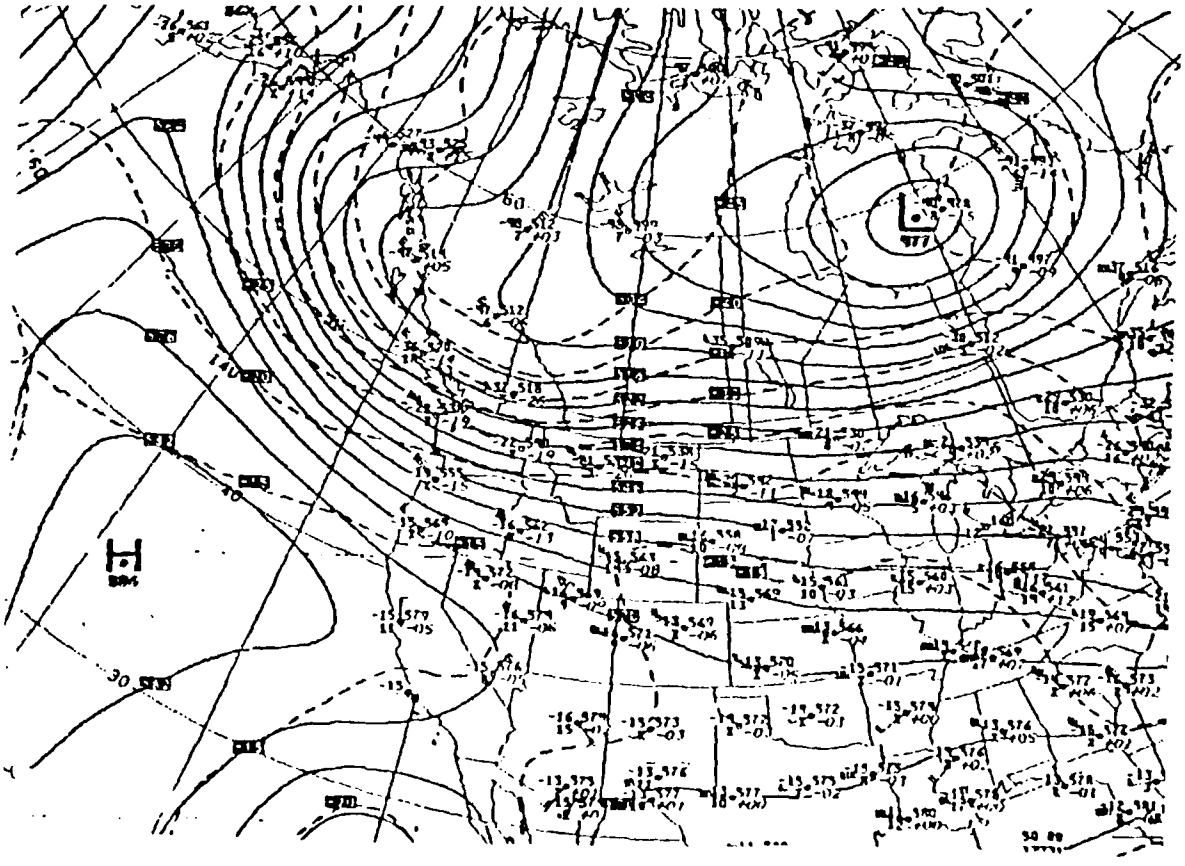

Fig. 9. Same as Fig. 7, except at 500 mb.

Kansas and southern Nebraska. Notice the short northwesterly tilt of the trough up to 700 mb above which it became almost vertically stacked to 500 mb just north of the United States-Canadian Border. In addition, a decreasing temperature gradient with height is observed.

The gridded surface temperature field at the beginning of the case study is shown in Fig. 10. This remarkable gradient created some very interesting temperature and pressure changes as the air mass moved southward. For example, at 2200 G.M.T. Valentine, Nebraska reported a temperature of 69°F while at Pierre, South Dakota (located approximately 150 km to the north) the temperature was 26° F. At 2300 G.M.T., one hour after frontal passage occurred, Valentine reported a temperature of 32°F. During the same one hour period when the temperature drop occurred, Valentine reported an incredible pressure rise of 6.4 mb! Precipitation associated with the front was in the form of light snow well behind the surface front. Intense pressure rises behind the front along with pressure falls ahead of the front, coupled with a frontal zone well defined by temperature, made for an ideal case study to test the hypothesis.

The 1900 G.M.T. actual, geostrophic, and isallobaric winds in the vicinity of the frontal zone are indicated in Figs. 11-13, respectively. Frontal segment labels and the ageostrophic winds at the same grid points used to compute the crossfrontal components by the actual, geostrophic, and isallobaric winds are displayed in Fig. 14. The most apparent difference, illustrated by the 1900 G.M.T. winds, is the larger degree of perpendicularity to the frontal zone by the actual and isallobaric winds as compared to the geostrophic

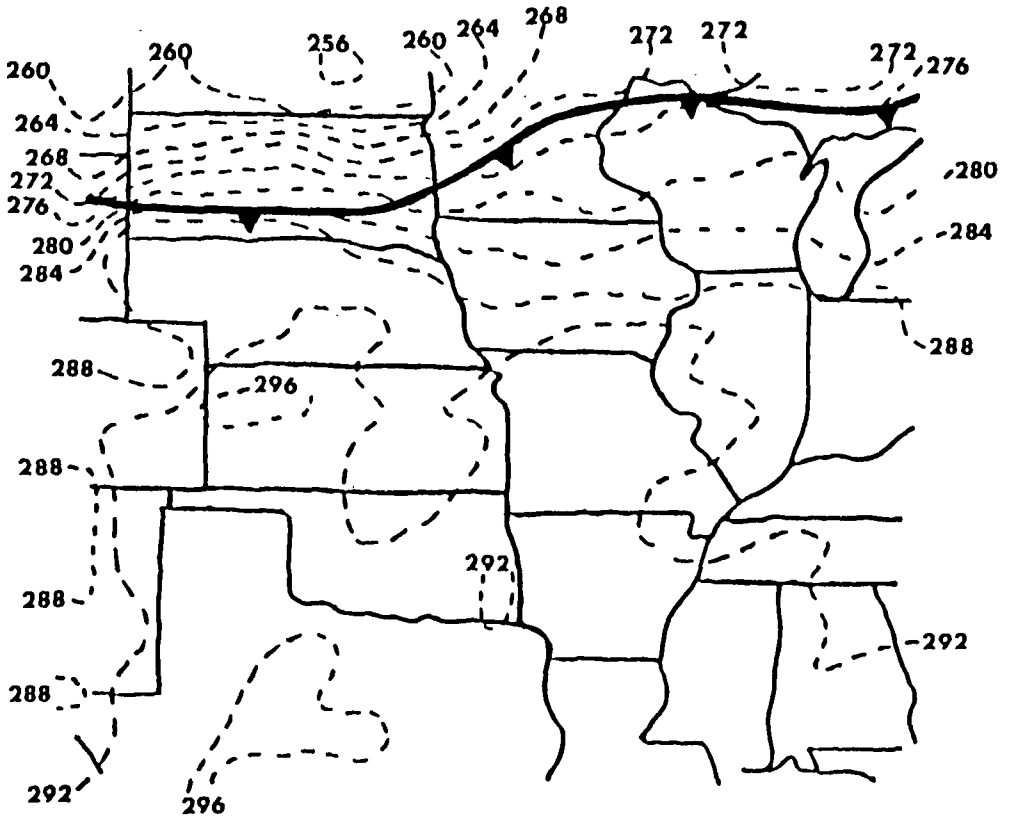

Fig. 10. Temparatures (^{o}K) fitted to the grid points for 1900 G.M.T 31 January 1989. Dashed lines are isotherms analysed at 4^{o}K intervals. Surface frontal postion is superimposed.

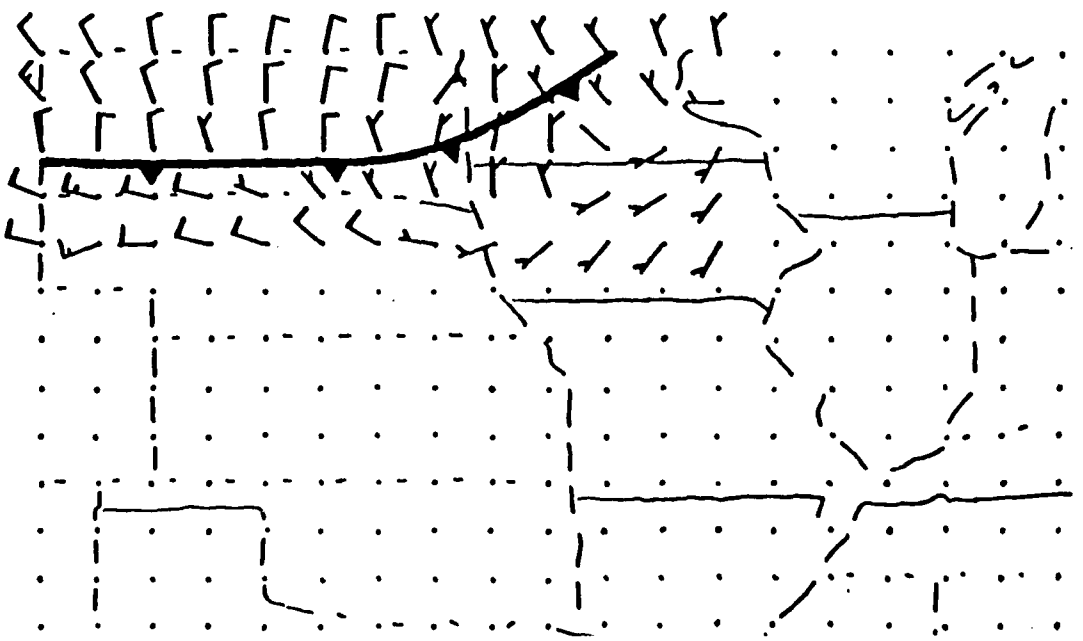

Fig. 11. Gridded actual surface winds at 1900 G.M.T. 31 January 1989 (m s^{-1}) plotted according to the usual convention. Surface frontal position is superimposed.

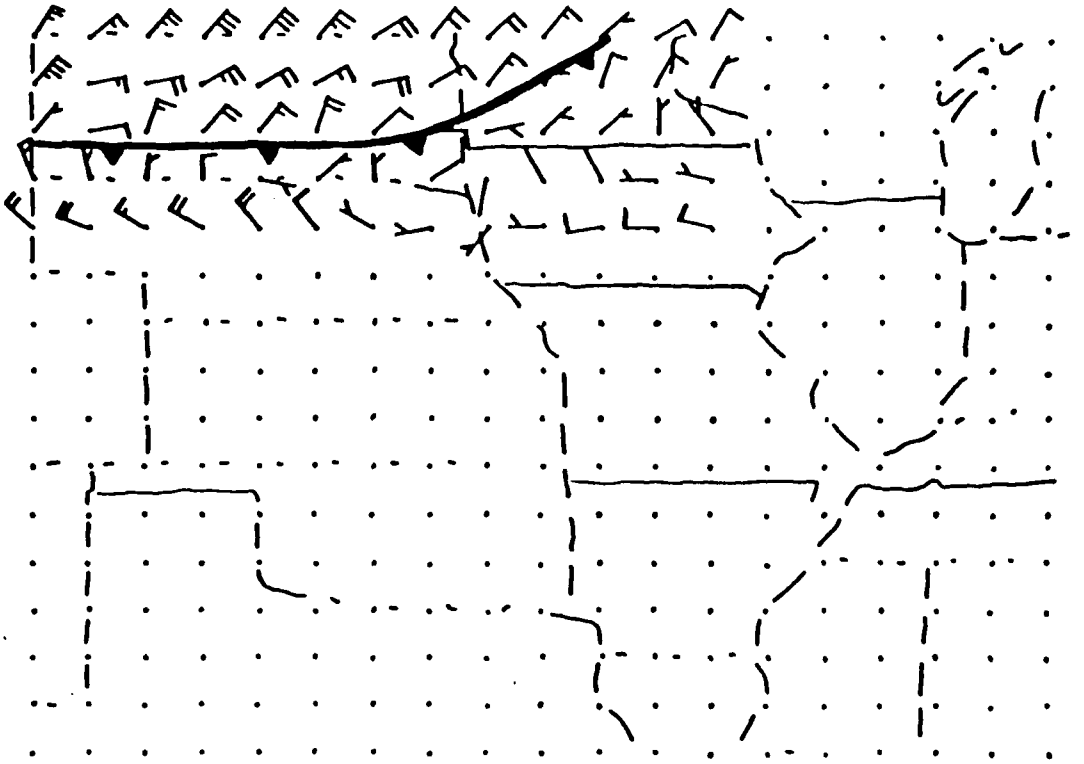

Fig. 12. Same as Fig. 11, but for geostrophic winds.

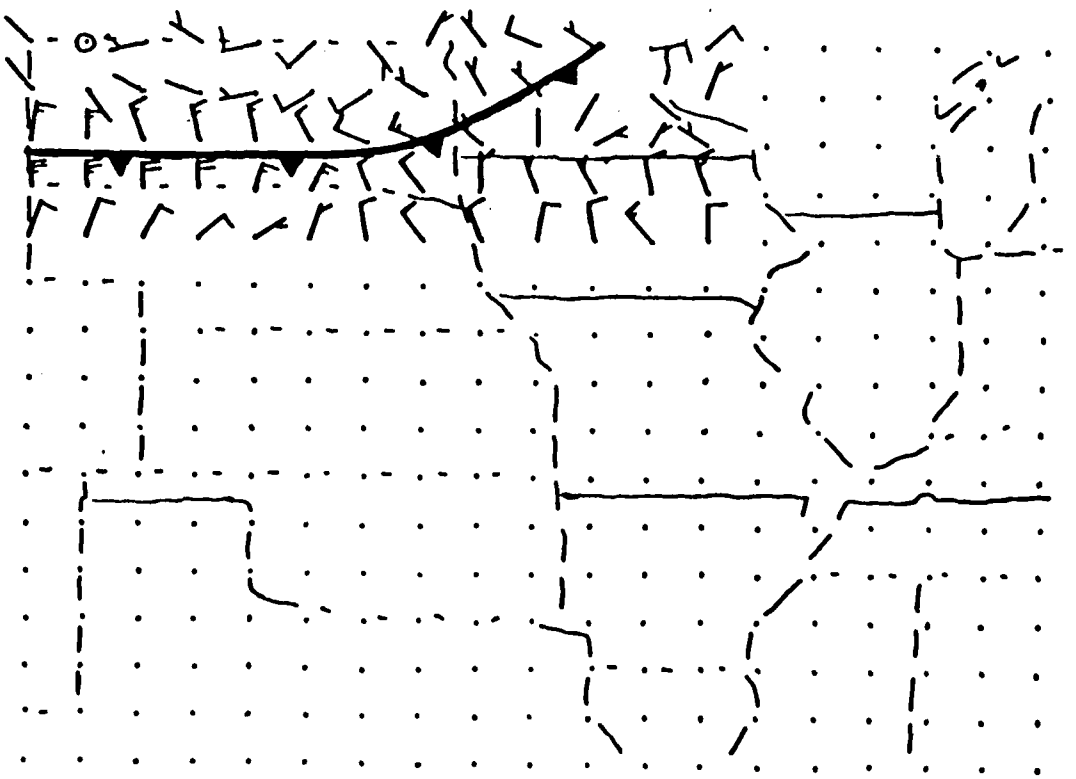

Fig 13. Same as Fig. 11, but for isallobaric winds.

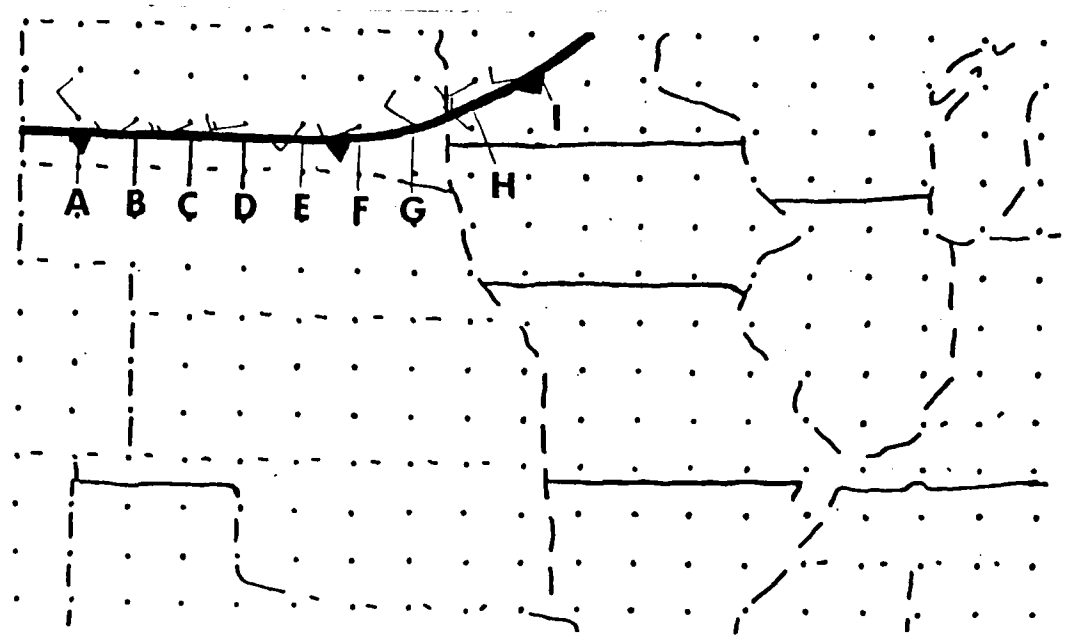

Fig. 14. 1900 G.M.T. ageostrophic winds plotted at the grid points used to determine the crossfrontal components by the actual, geostrophic, and isallobaric winds. Letters designate frontal segments on the superimposed front.

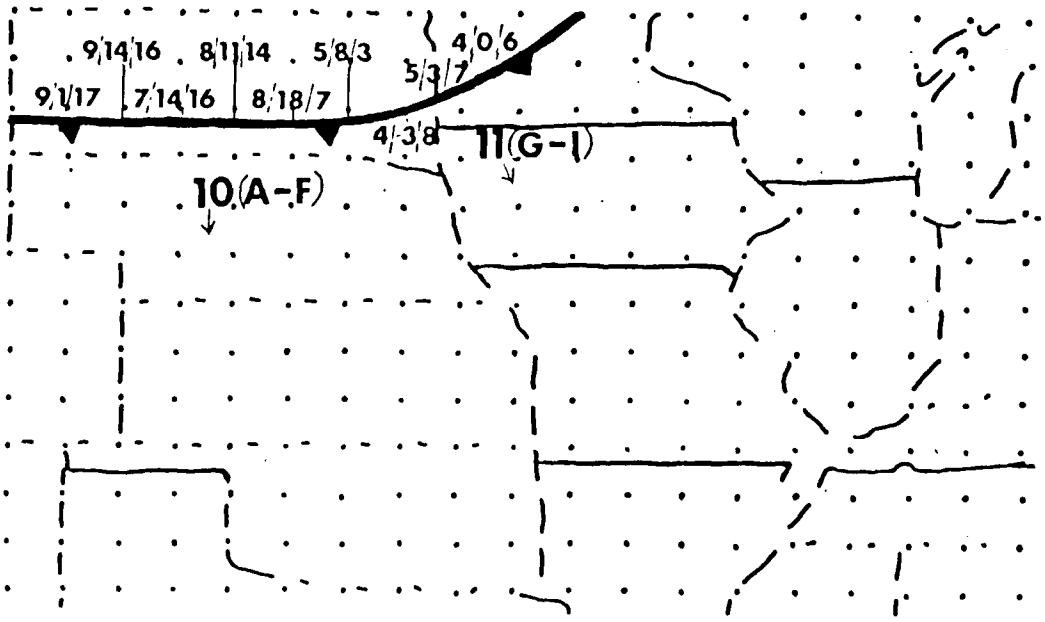

Fig. 15. Frontal velocity map for the period 1900-2000 G.M.T. 31 January 1989. Frontal velocities (m s^{-1}) are indicated by the larger numbers and correspond to the frontal segments indicated in parenthesis by the frontal velocity. Arrows indicate the approximate direction of motion. Small numbers indicate the crossfrontal component (m s^{-1}) by the actual/geostrophic/isallobaric winds. Positive (negative) cross frontal components indicate flow in the same (opposite) direction of frontal motion.

winds, especially over frontal segments G-I. However, the larger magnitude of the geostrophic winds over frontal segments B-D and F made for positive (in the direction of motion) crossfrontal components (Fig. 15) that were generally similar to the observed frontal motion. The 1900 G.M.T. frontal velocities map (Fig. 15) shows that the geostrophic crossfrontal components do not support the observed frontal motion at segments A and G-I. The actual wind crossfrontal components are much closer to the observed velocity at these segments. The reason may be due to the ageostrophic crossfrontal component. The question then becomes how much of the ageostrophic crossfrontal component is due to the isallobaric acceleration.

Assuming that the frictional and isallobaric forces are the dominant components of the observed ageostrophic wind, it is possible to estimate the isallobaric contribution by comparison of the observed ageostrophic wind to the ageostrophic wind resulting from friction. Frictional effects will be parameterized by using a 40 degree cross-contour flow and 30% reduction (a conservative value) of the geostrophic wind speed at three grid points used to compute crossfrontal components. Starting with segment A (Fig. 16(1)), the ageostrophic wind due to the frictional acceleration ($\vec{V}agf$) has a much smaller magnitude and would not posses the normal component that the observed ageostrophic wind ($\vec{V}ag$) posses. The ageostrophic wind due to the frictional parameterization at segment D (Fig. 16(2)) is similar to the observed ageostrophic wind. However, since the 30% reduction in geostrophic wind speed is probably too small, the ageostrophic wind due to friction would have a larger magnitude and

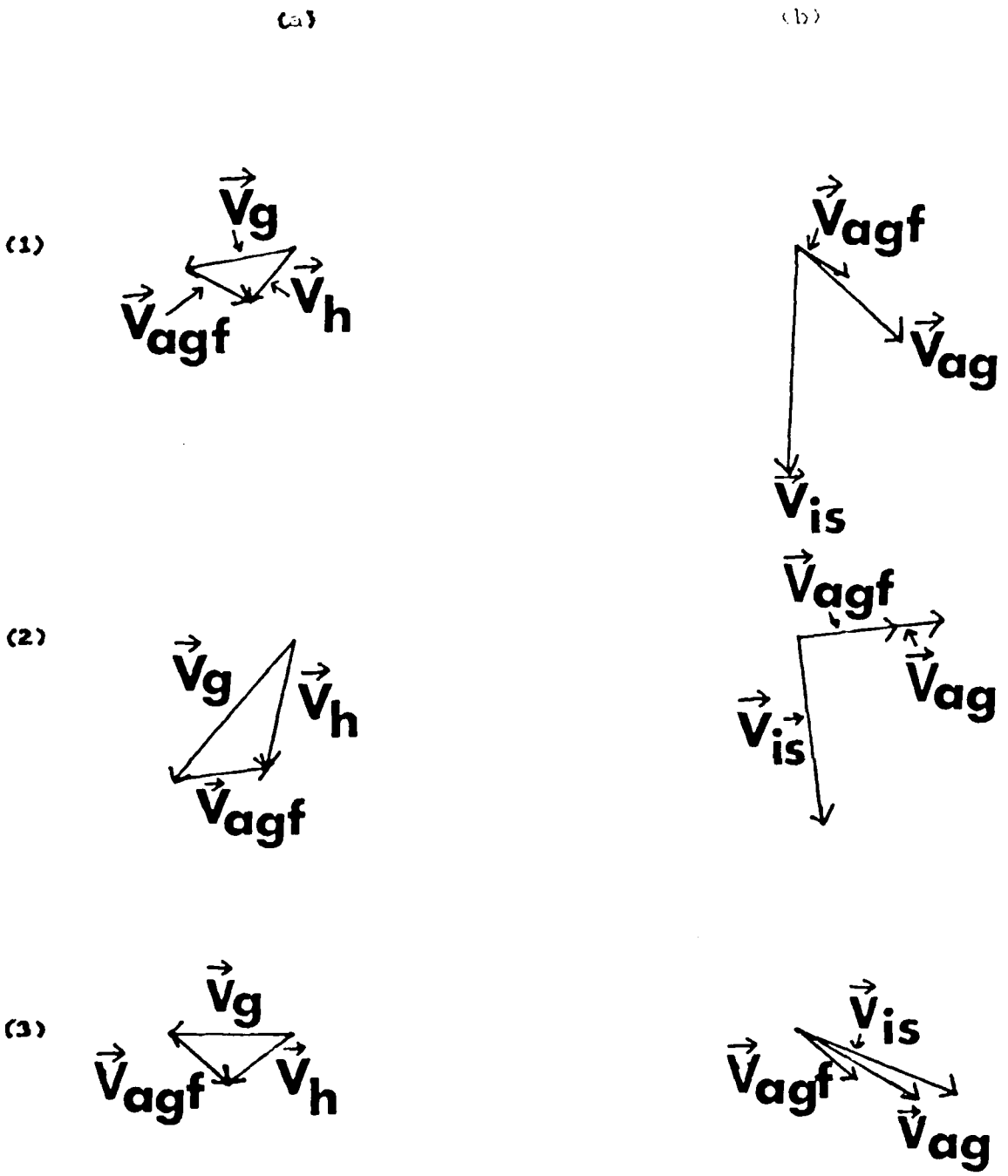

Fig. 16. (a). Ageostrophic wind ($\vec{V}agf$) at 1900 G.M.T. from estimate of the actual wind ($\vec{V}_h$) due to frictional parameterization on the geostrophic wind ($\vec{V}g$). (b). Comparison of the ageostrophic wind due to fricition ($\vec{V}agf$) with the observed ageostrophic wind ($\vec{V}ag$) and the fricitionless isallobaric wind ($\vec{V}is$). Geostrophic and ageostrophic winds are from the grid points used to compute the crossfrontal components at frontal segments A (1), D (2), and G (3). Vector magnitude is based upon a ratio of two millimeters to one m s^{-1}.

point more towards the northeast. This suggests that the isallobaric acceleration is counteracting the frictional acceleration resulting in a larger actual wind crossfrontal component. This simple analysis demonstrates that it is not necessary for the ageostrophic wind to posses a positive crossfrontal component to indicate an isallobaric contribution. Segment G (Fig. 16(3)) represents a case where the geostrophic crossfrontal component is negative, but the positive actual wind crossfrontal component is primarily the result of friction. The above examination suggests that the magnitude of isallobaric influence on the actual wind crossfrontal components can vary from dominant to insignificant.

Frontogenetical forcing by the actual wind and contributions by the various terms (shearing and stretching deformation, divergence, and temperature tendencies) in Eq. (24) are shown in Figs. 17-21. Given the number of points that comprise the area of interest, a simple analysis to estimate the frontogenetical forcing due to the ageostrophic wind resulting from friction is beyond the scope of this study. Magnitudes of the component terms were not smoothed prior to analysis. Notice that in areas where pronounced cyclonic shearing is indicated (western South Dakota and northwestern Iowa), the frontogenetical forcing due to shearing deformation of the actual wind (Fig. 17) is contributing to frontolysis. As in Moore and Blakey's (1988) results, the magnitude of the divergence term (Fig. 19) is equivalent to the magnitude by the deformation terms (Figs. 17 and 18). The frontogenesis maximum due to the divergence term (Fig. 19) along frontal section A-D occurs in an area where the actual winds (Fig. 11) are convergent within with a north-south temperature

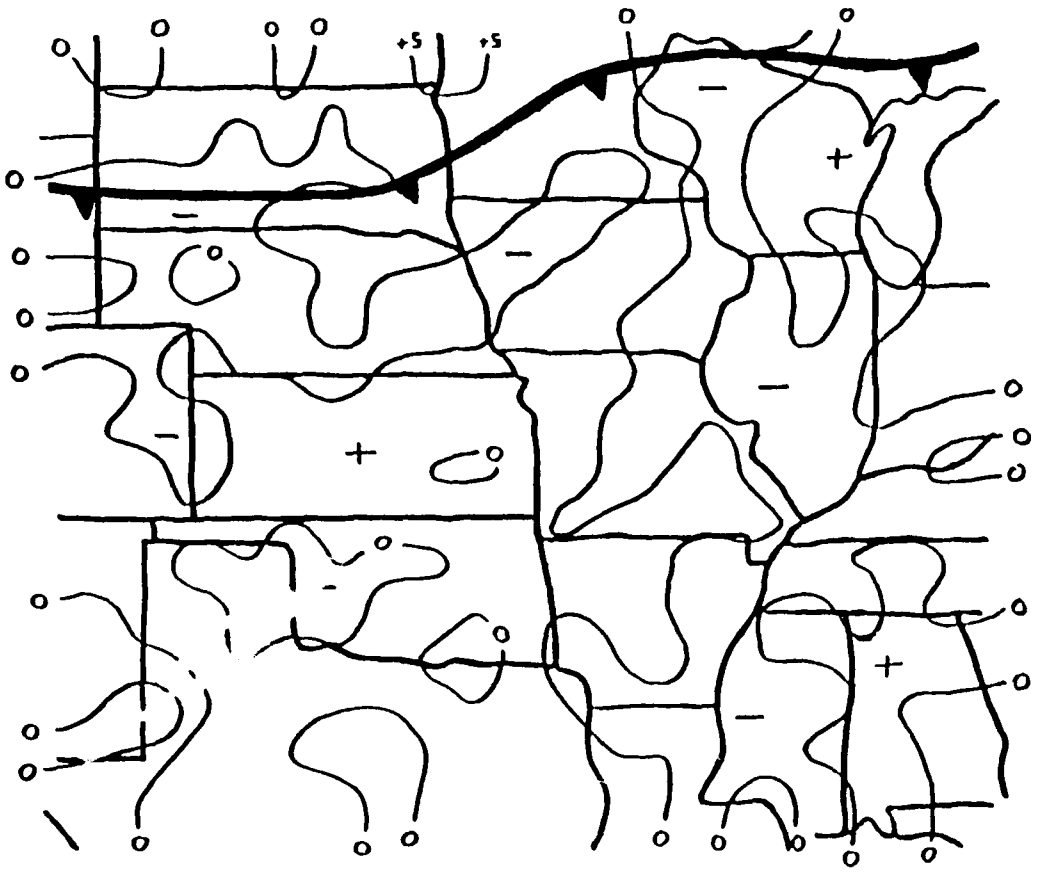

Fig. 17. Frontogenetical forcing due to shearing deformation of the actual surface wind at 1900 G.M.T. 31 January 1989 ($X\ 10^{3}\ ^{o}K\ km^{-1}\ hr^{-1}$). Positive (negative) values represent frontogenesis (frontolysis). Surface frontal position is superimposed.

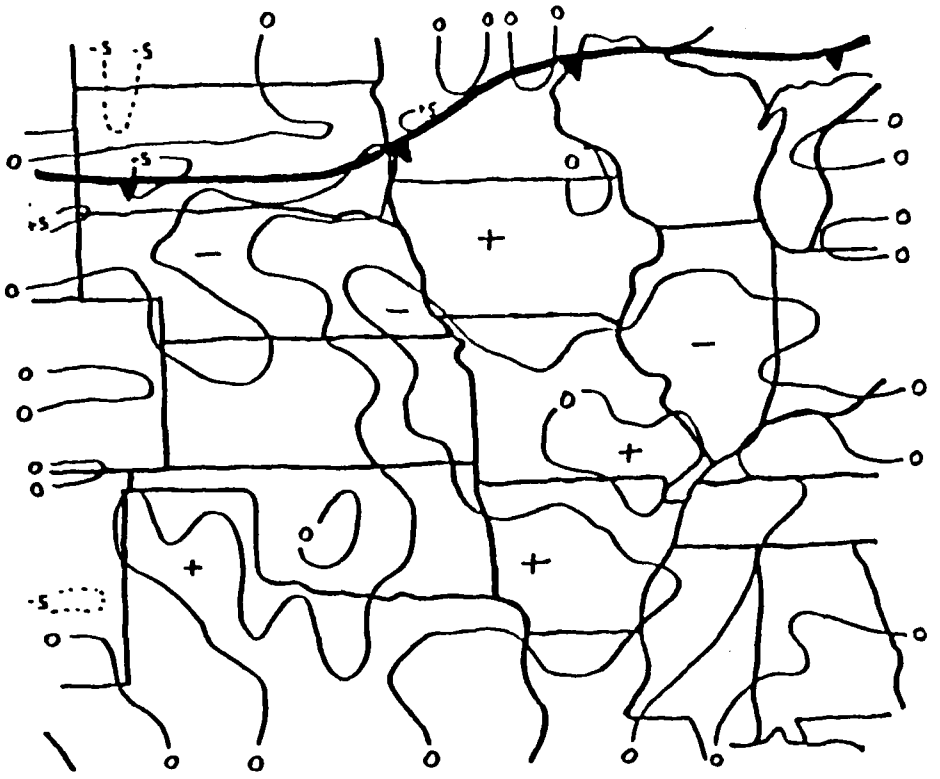

Fig. 18. Same as Fig. 17, but due to stretching deformation.

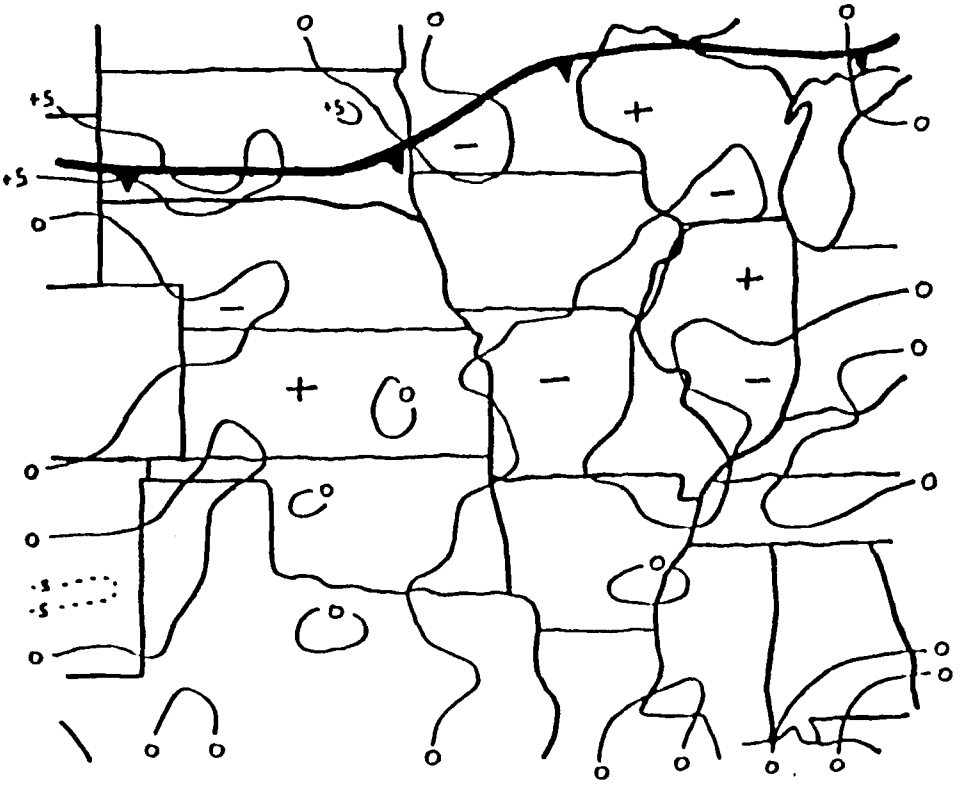

Fig. 19. Same as Fig. 17, but due to divergence.

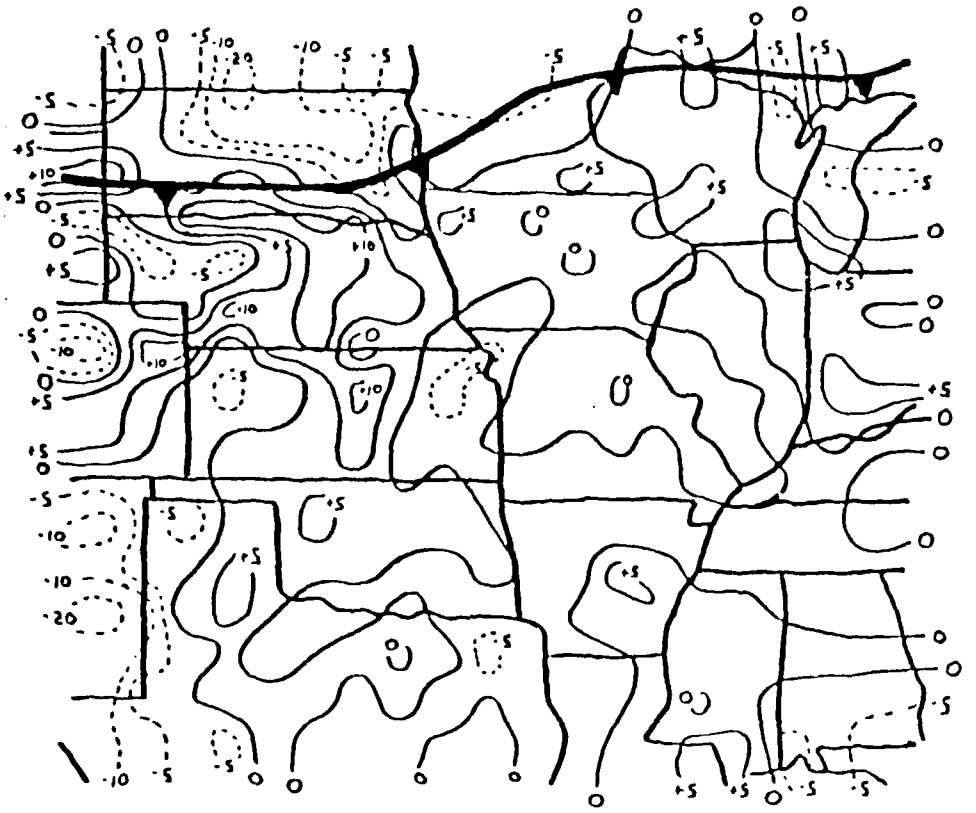

Fig. 20. Same as Fig. 17, but due to temperature tendencies term.

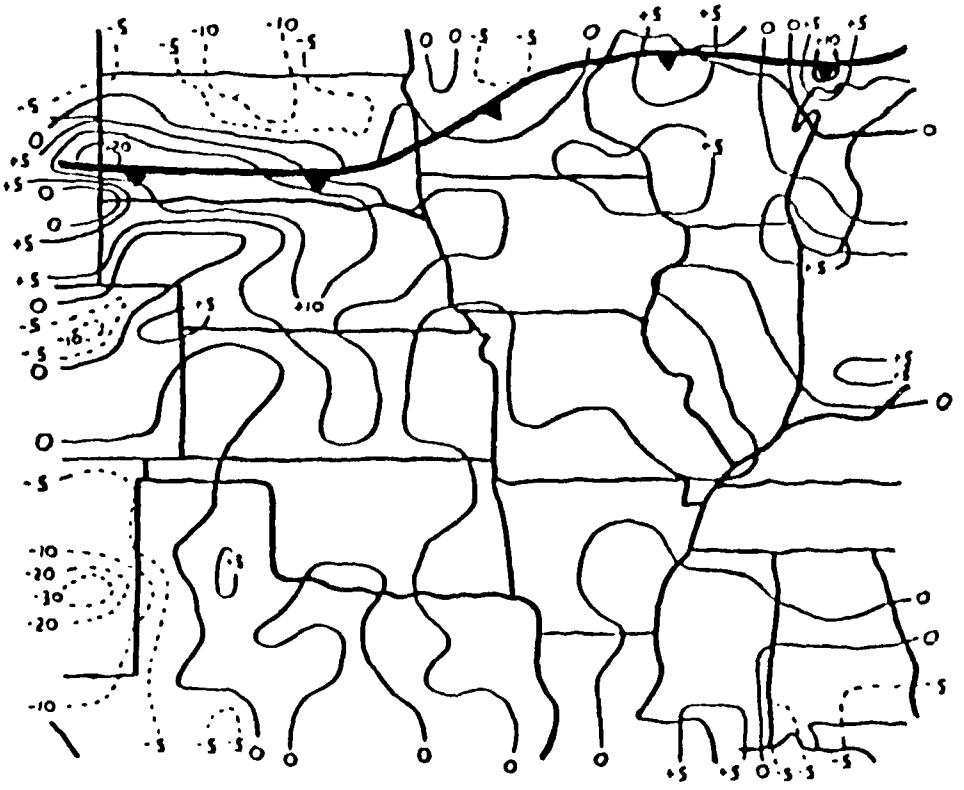

Fig. 21. Same as Fig. 17, but for the total frontogenetical forcing.

gradient (Fig. 10). One of the more interesting results of this study was the significance of the temperature tendencies term (Fig. 20) contribution to the total frontogenetical forcing by the actual wind (Fig. 21). Notice that frontal segments G and I (Fig. 21) are in a frontogenetical forcing pattern indicative of movement in response to a redistribution of the temperature gradient ("apparent" propagation).

Contributions by the isallobaric frontogenetical forcing terms (Figs. 22-25) have somewhat larger magnitudes than for the actual wind; this is not surprising given the larger magnitudes of the frictionless isallobaric wind. The convergent/divergent nature of the frictionless isallobaric wind is illustrated by the divergence term (Fig. 24). As expected, the magnitudes of the divergence term are larger than for either shearing (Fig. 22) or stretching deformation (Fig. 23). The divergence term contribution is easily visualized by observing the D value tendencies (Fig. 27) together with the temperature gradient (Fig. 10). In addition, frontal section A-D and to a lesser extent frontal segments H and I are located in a frontogenetical forcing pattern due to the divergence term conducive of "apparent" propagation. An approximate estimate of the pressure change in millibars may be obtained from Fig. 27 by using the ratio of one millibar pressure change to 10 meters of D value change as required for hydrostatic equilibrium near the surface. The temperature tendencies term (Fig. 25) was the primary contributor to the total frontogenetical forcing by to the isallobaric wind (Fig. 26). Closer examination of the total frontogenetical forcing (Fig. 26) reveals a pattern, through which

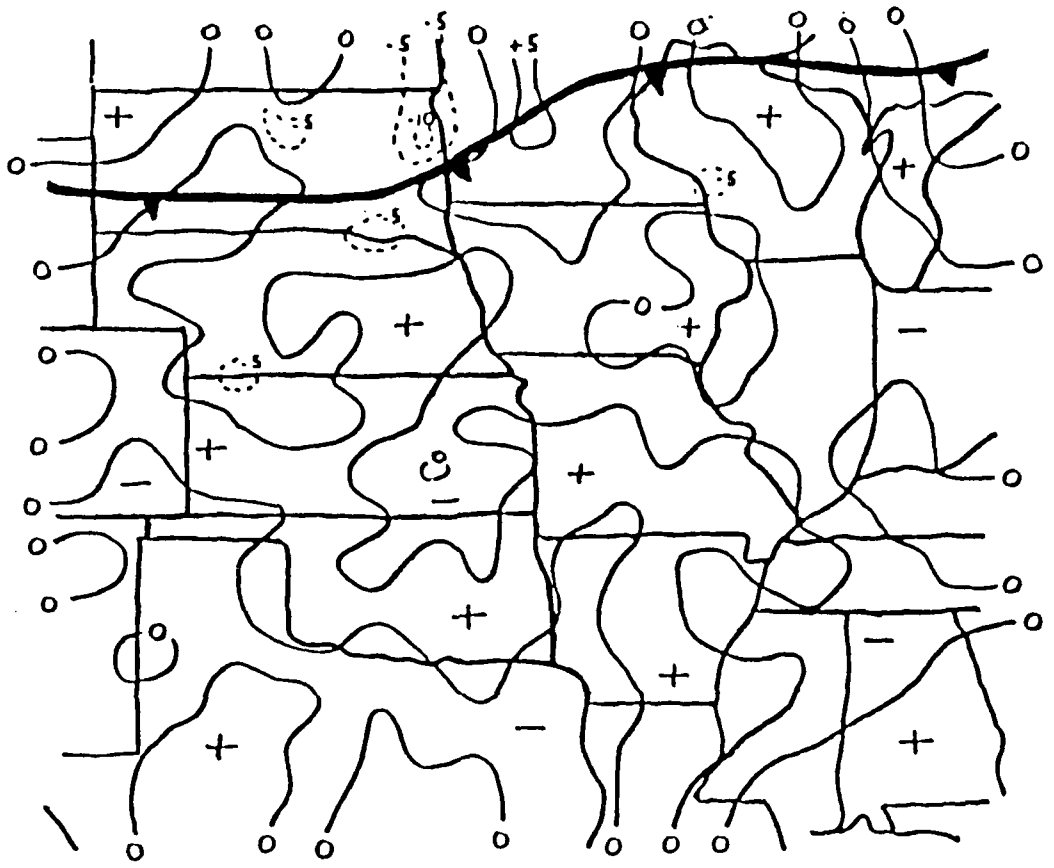

Fig. 22. Frontogenetical forcing due to shearing deformation of the isallobaric wind at 1900 G.M.T. 31 January 1989 ($\times 10^{-3}$ °K km^{-1} hr^{-1}). Positive (negative) values represent frontogenesis (frontolysis). Surface frontal position is superimposed.

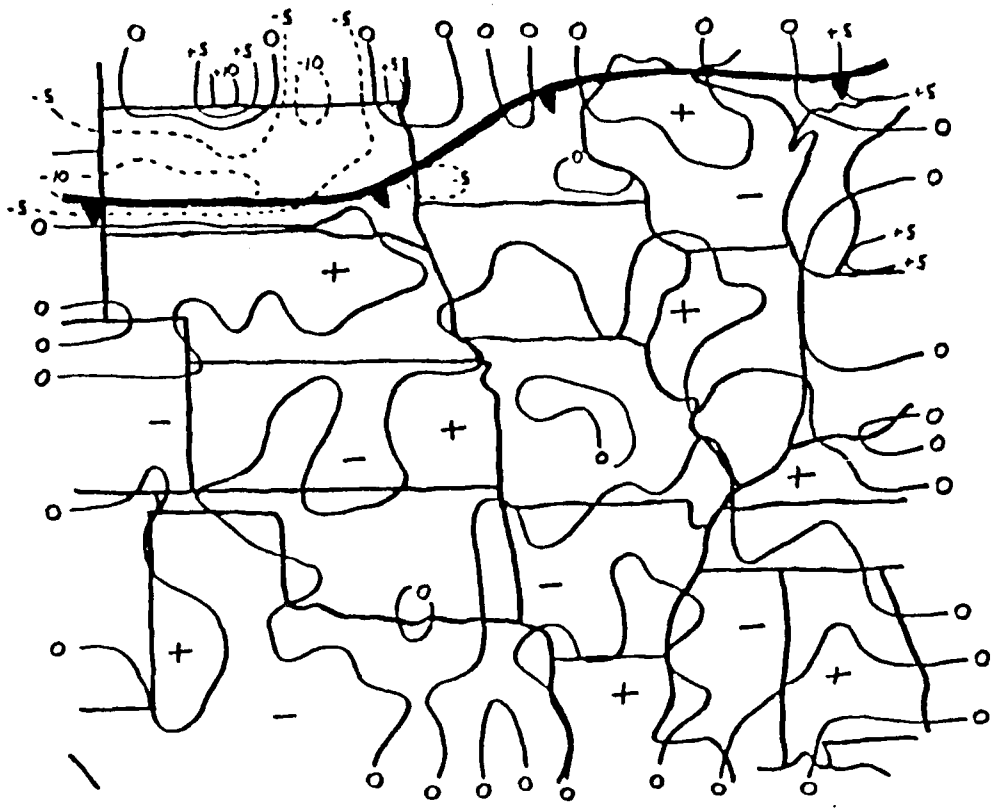

Fig. 23. Same as Fig. 22, but due to isallobaric stretching deformation.

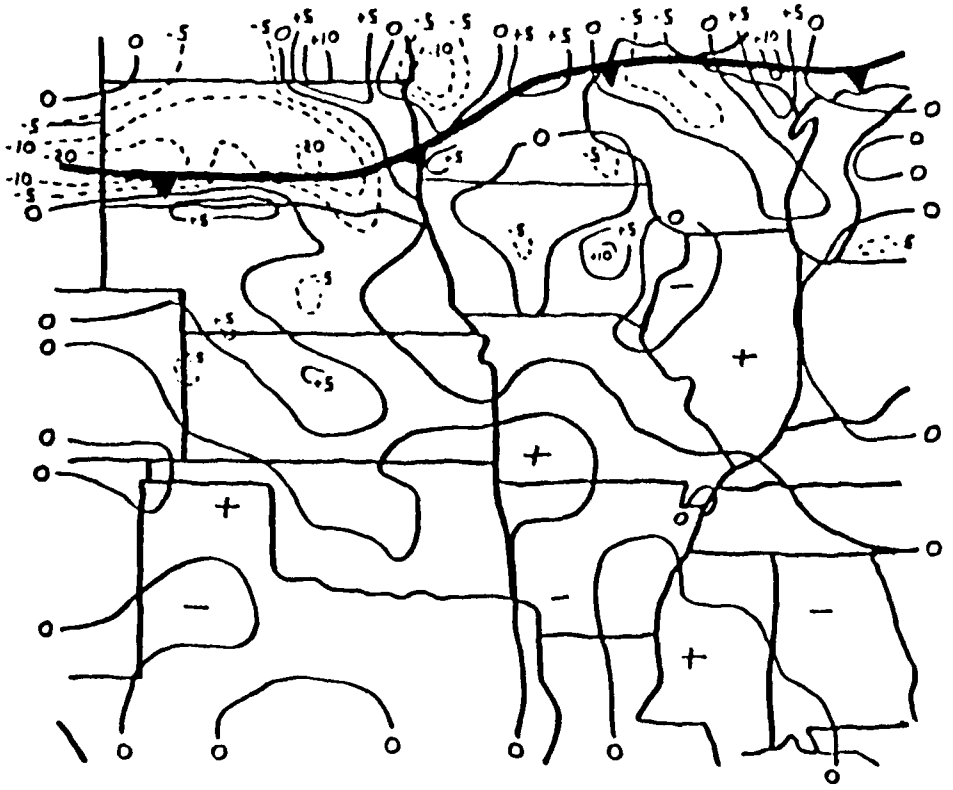

Fig. 24. Same as Fig. 22, but due to isallobaric divergence.

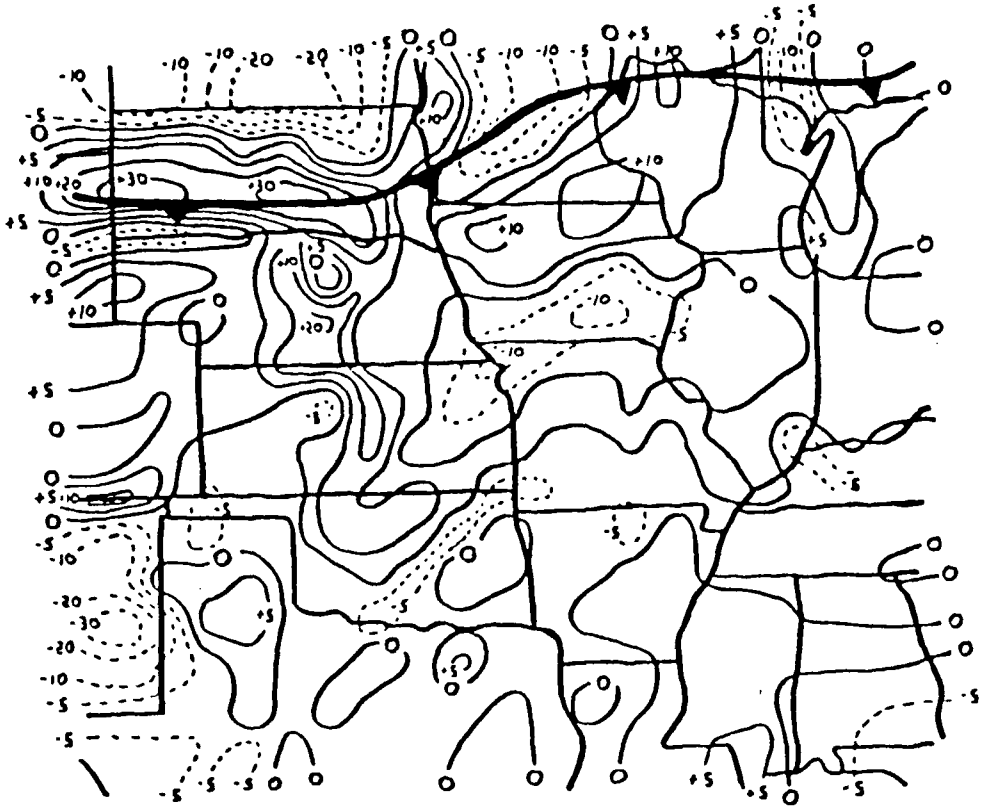

Fig. 25. Same as Fig. 22, but due to isallobaric temperature tendencies term.

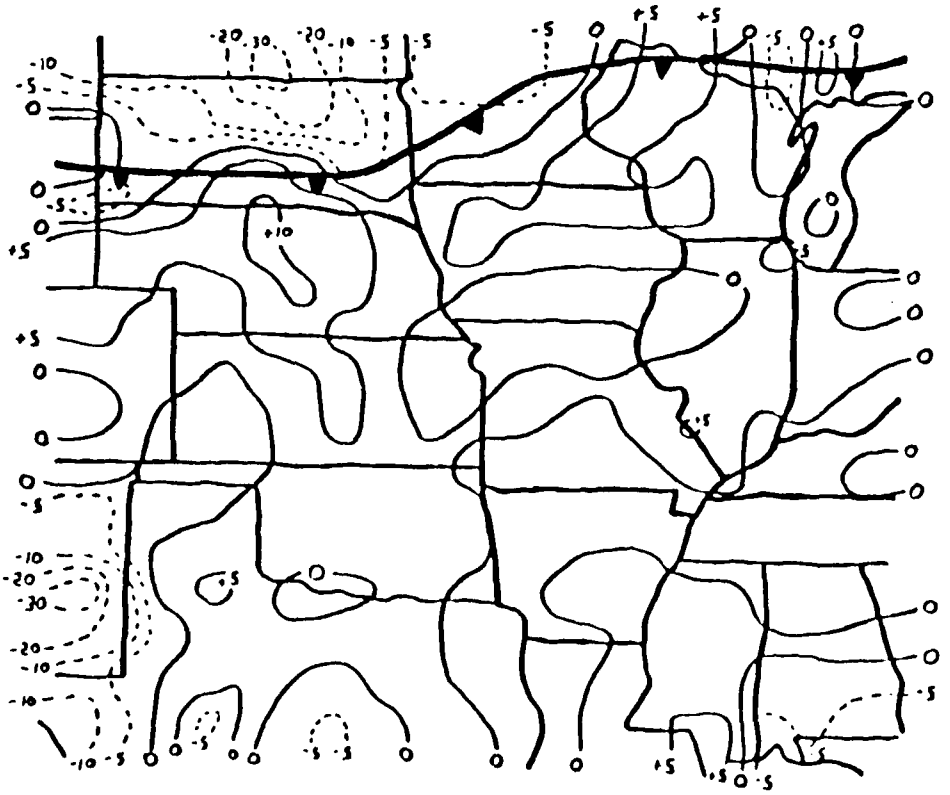

Fig. 26. Same as Fig. 22, but for total isallobaric frontogenetical forcing.

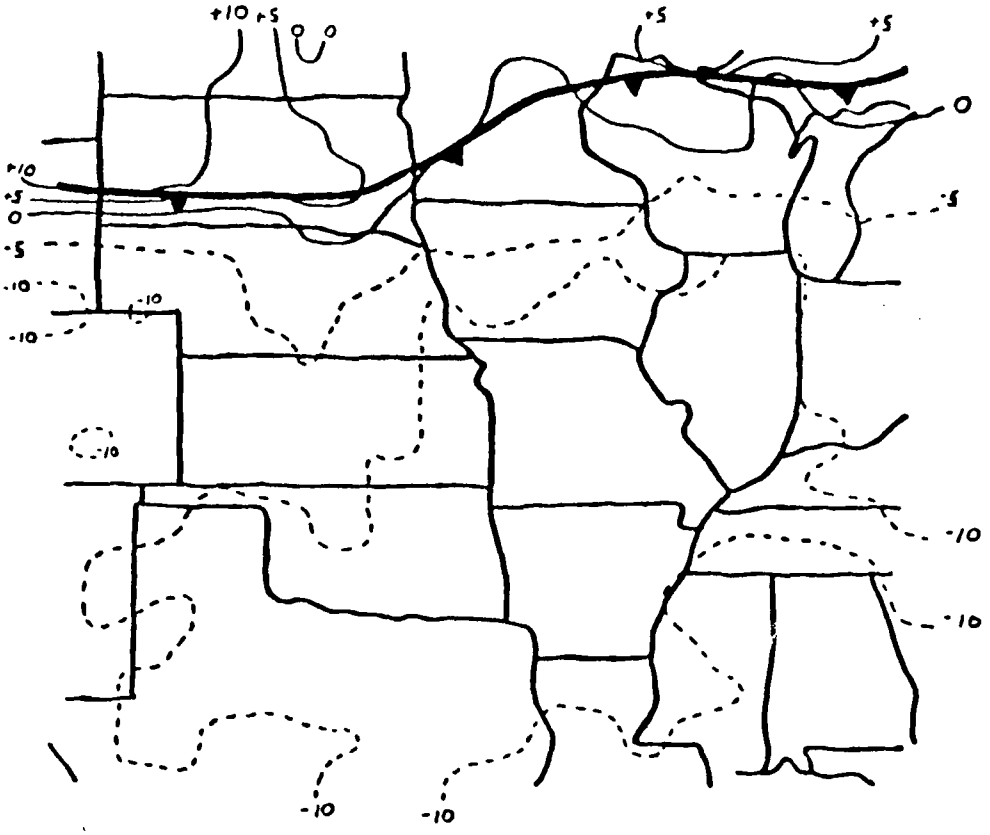

Fig. 27. Tendency of D values at 1900 G.M.T. 31 January 1989 (mhr^{-1}). Height falls are indicated by dashed lines and height rises by solid lines. Surface frontal position is superimposed.

frontal section F-I lies, favorable for "apparent" propagation. The coincidental agreement of the isallobaric and actual total frontogenetical forcing over frontal segments G and I would suggest that some of the observed frontal motion was indeed occurring through frontogenetical forcing produced by the isallobaric wind.

The magnitude of the temperature tendencies term has implications for future frontogenetical forcing studies. Argument for inclusion of the term can best be made by examination of the assumption under which it has frequently been eliminated. For example, Jascourt et. al. (1988) neglects the term based upon an observed pattern of little temperature change over time. Recall from Eq. (24) that the temperature tendencies term is a combination of the gradient of temperature change and the gradient of advection. Figure 28 identifies the location of two grid points ahead and behind the front were the contribution by the gradient of temperature change and the gradient of advection for each wind have been calculated and presented in Table 1. It is apparent from Table 1 that the contribution to the temperatures tendencies term by the gradient of advection can be of equal or greater magnitude than the contribution by the gradient of local temperature change. These calculations demonstrate that even with strong temperature change, the spatial gradient of advection can be the dominant portion of the temperature tendencies term.

Isallobaric forcing has been subjectively demonstrated as a contributor to the actual wind crossfrontal components at frontal segments (A, D, H, and I). At other frontal segments (B, C, E, F, and G) isallobaric influence on the actual wind crossfrontal

components was small or unclear. Differences between the observed frontal motion and the actual wind crossfrontal components over frontal segments G and I are not explained by the frontogenetical forcing by the actual wind. Magnitudes of the actual frontogenetical forcing give a temperature gradient realignment over 100 km of only .5°C for segment I increasing to 1.5°C for segment G. Given the magnitude of the temperature gradient associated with the front (Fig. 5), the amount of "apparent" propagation induced by isallobaric forcing is does not appear large enough to account for the difference.

GRID POINT NUMBER	LOCATION	WIND	TOTAL	GRADIENT TEMP CHANGE	GRADIENT ADVECTION
1	44 N 100 W	ACTUAL	3.8	18.4	-14.6
		ISALL	35.1	18.4	16.7
2	44 N 98 W	ACTUAL	-8.0	-2.9	-5.1
		ISALL	10.2	-2.9	13.1
3	42 N 100 W	ACTUAL	2.3	8.2	-5.9
		ISALL	16.7	8.2	8.5
4	42 N 98 W	ACTUAL	14.0	17.1	-3.1
		ISALL	9.9	17.1	-7.2

Table 1. Frontogenetical forcing by the temperature tendencies term (Total), contribution by the gradient of temperature change, and contribution by the gradient of advection. (X 10^{3}°K $km^{-1}hr^{-1}$).

The period 2200 to 2300 G.M.T. marked the beginning of increased frontal speed over frontal section A-K (Figs. 29 and 30). Note the strength of the isallobaric crossfrontal components in response to a north-south D change gradient over frontal section E-G (Fig. 31).

This intense gradient was the result of the D rise center having a closer proximity to the front than in previous hours. The isallobaric influence on the actual wind crossfrontal components over frontal segments E and F is unclear due to friction; however, a significant isallobaric contribution is suggested on frontal segment G by virtue of a positive ageostrophic crossfrontal component (Fig. 29) not indicative of friction. Smaller isallobaric contributions are possible over frontal segments A, G, H, I, and Q.

Frontogenetical forcing due to the actual and isallobaric winds (Figs. 32 and 33, respectively) during this period also demonstrated an interesting change. This change was the frontolysis by both winds behind frontal section D-F. With the reposition of the D value rise center over the maximum temperature gradient, the divergence term became a substantial contributor to the isallobaric frontolysis. Disappointingly, the magnitude of the temperature gradient realignment due to the actual wind frontogenetical forcing (Fig. 32) is only 2^{0}C over 100 km and is not large enough to explain the difference between the actual crossfrontal components and the observed frontal motion. The coincidental occurrence of increased frontal velocity with an increased D value rise center in close proximity to the front suggest an isallobaric contribution. The diagnosed isallobaric contribution has been subjectively illustrated on both the actual wind crossfrontal components and on frontogenetical forcing. The limited geographical extent of influence relegates the isallobaric role to one of many potential contributors.

By 2300 G.M.T. a west-southwest shift of a further increased D

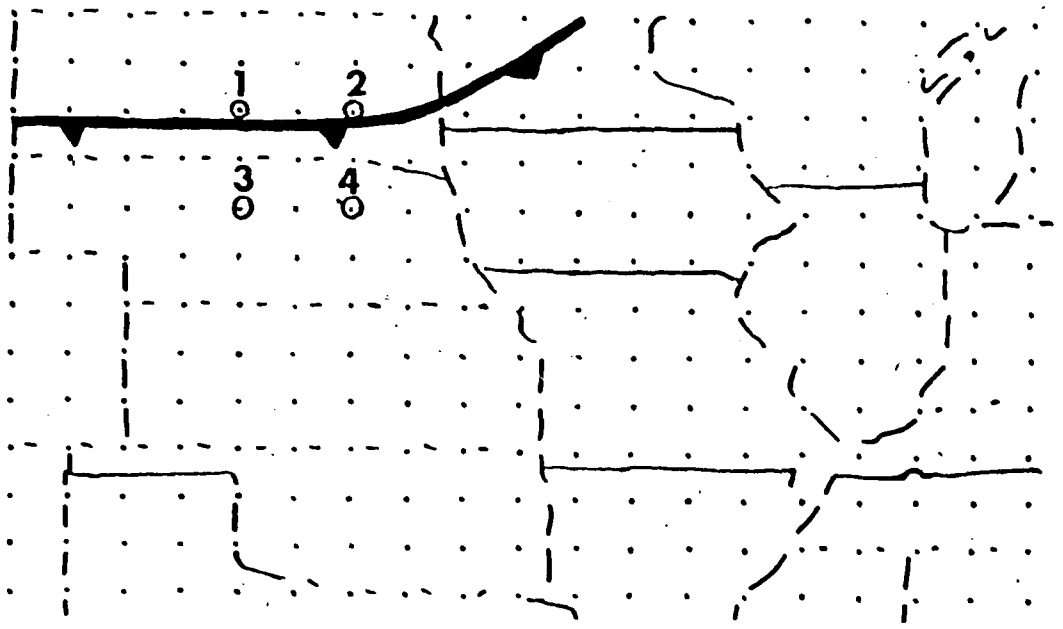

Fig. 28. Location of the points listed in Table 1. Surface frontal position is superimposed.

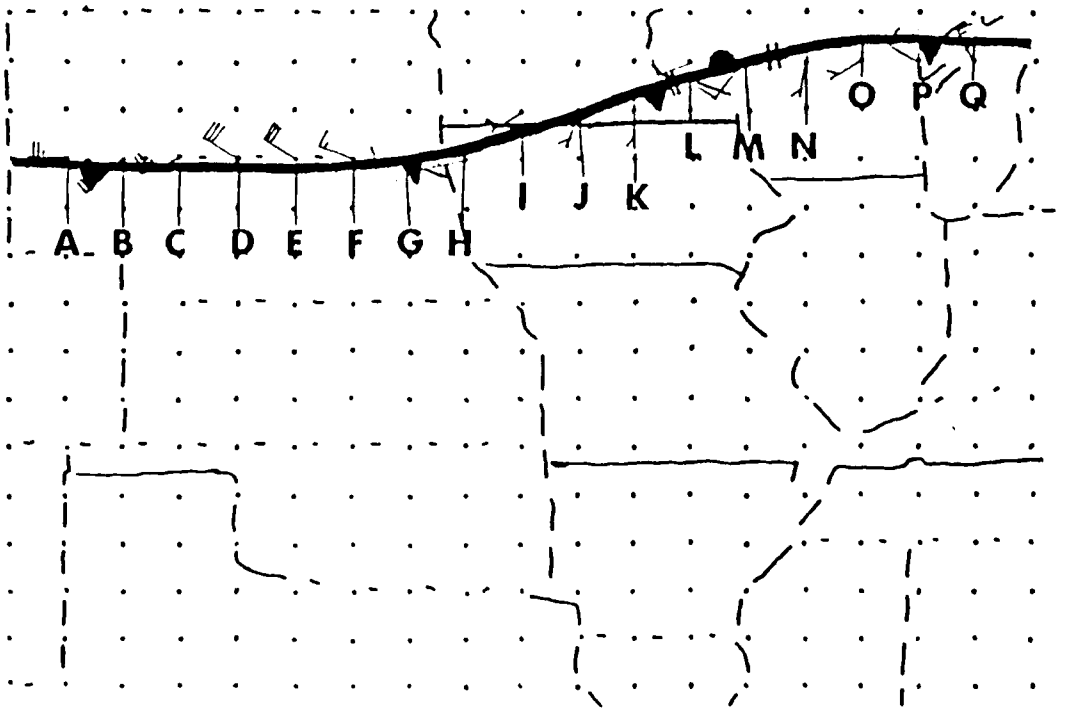

Fig. 29. Same as Fig. 14, except for 2200 G.M.T..

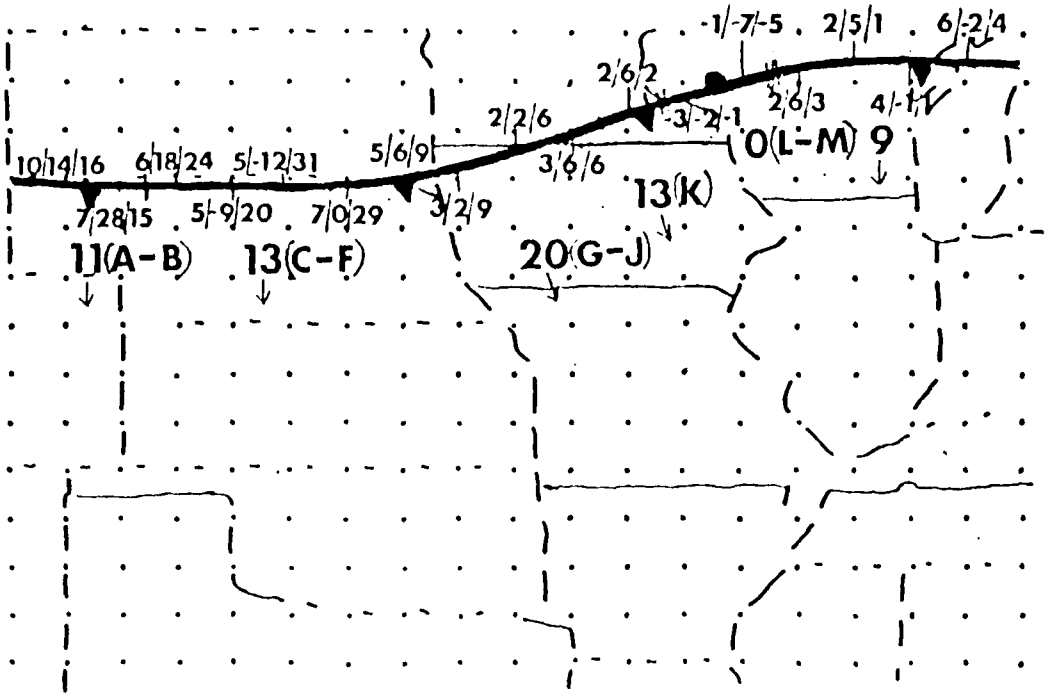

Fig. 30 Same as Fig. 15, except for 2200 G.M.T..

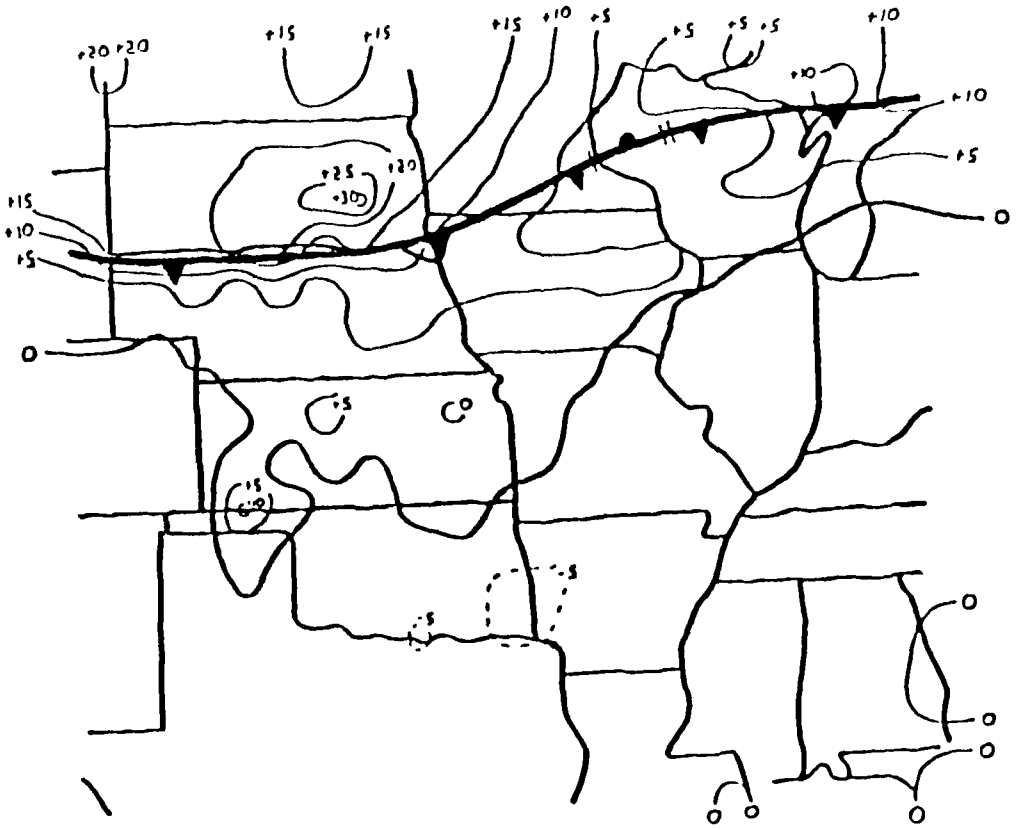

Fig. 31. Same as Fig. 27, except for 2200 G.M.T..

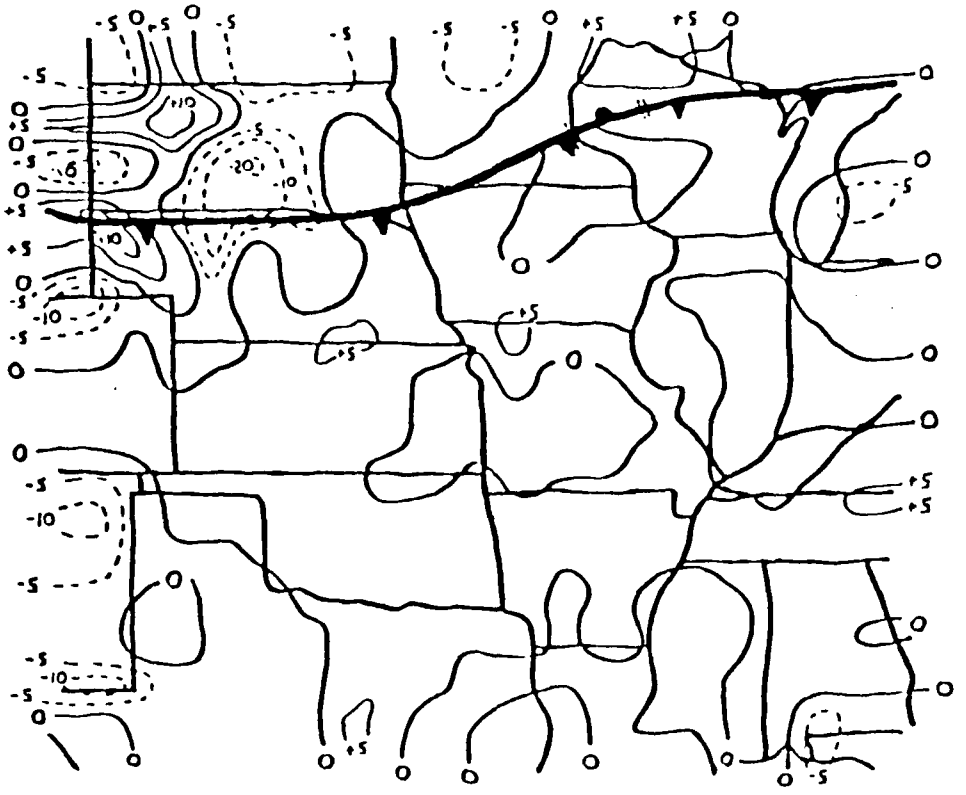

Fig. 32. Same as Fig. 21, except for 2200 G.M.T..

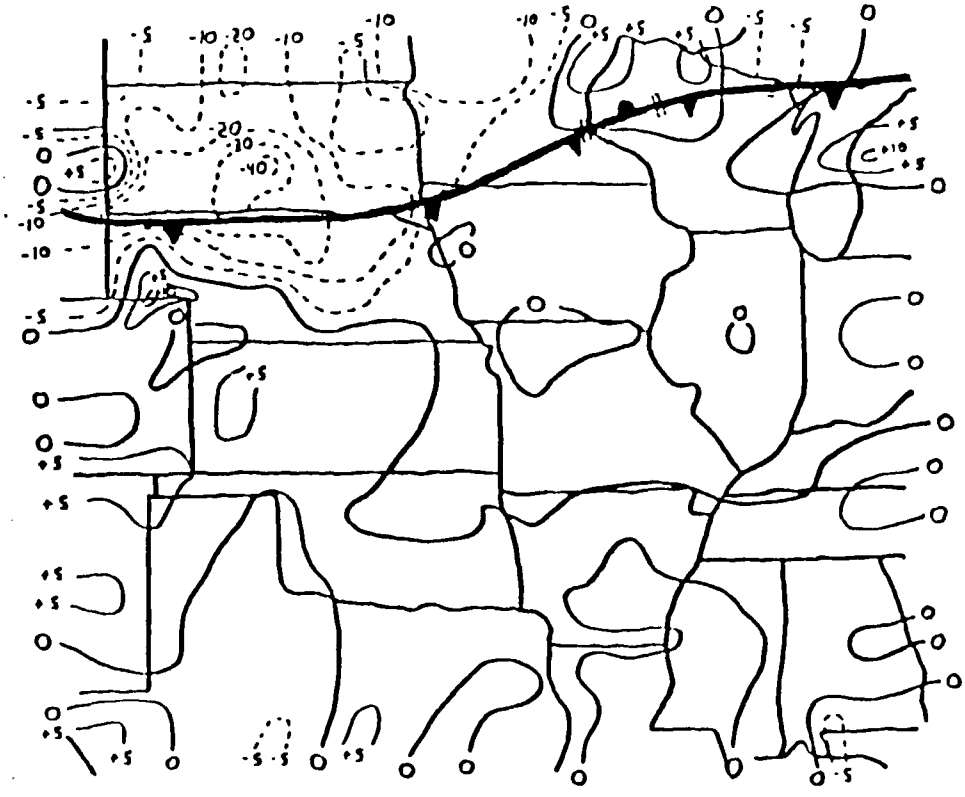

Fig. 33. Same as Fig. 26, except at 2200 G.M.T..

value rise center to extreme southern South Dakota (Fig. 34) correspondingly moved the largest isallobaric crossfrontal components through frontal section A-J (Figs. 35 and 36). Notice that frontal acceleration (from the previous hour) is indicated over frontal sections A-F and K-L (Fig. 36). Counteraction of friction over frontal segments A, C, D, and F is indicated by ageostrophic winds parallel to the front (Fig. 35) and actual crossfrontal components similar to geostrophic crossfrontal components (Fig. 36). Unlike previous hours, a somewhat consistent isallobaric influence was indicated where the maximum isallobaric crossfrontal components occurred. Unfortunately, no improvement of frontal motion diagnostics by the actual crossfrontal components is indicated at any frontal segment where an isallobaric influence is suggested. Isallobaric influence (Fig. 37) on the actual wind frontogenetical forcing (Fig. 38) would again appear to be manifested as frontolysis behind frontal section B-L. While the addition of velocity induced by the actual wind frontogenetical forcing to the actual wind crossfrontal components would appear to provide better agreement with observed frontal motion than the geostrophic crossfrontal components at some segments (C, D, and F), it is unclear that this would be the case at other segments (A, B, and E). The limited area of isallobaric influence is shown by little or contribution on the other frontal section (K-L) displaying increased velocity.

In summary, significant isallobaric kinematic and frontogenetical forcing contributions were indicated at some frontal segments in this case study. The appearance of "apparent" propagation in this case study suggests that some frontal motion occurs through frontal

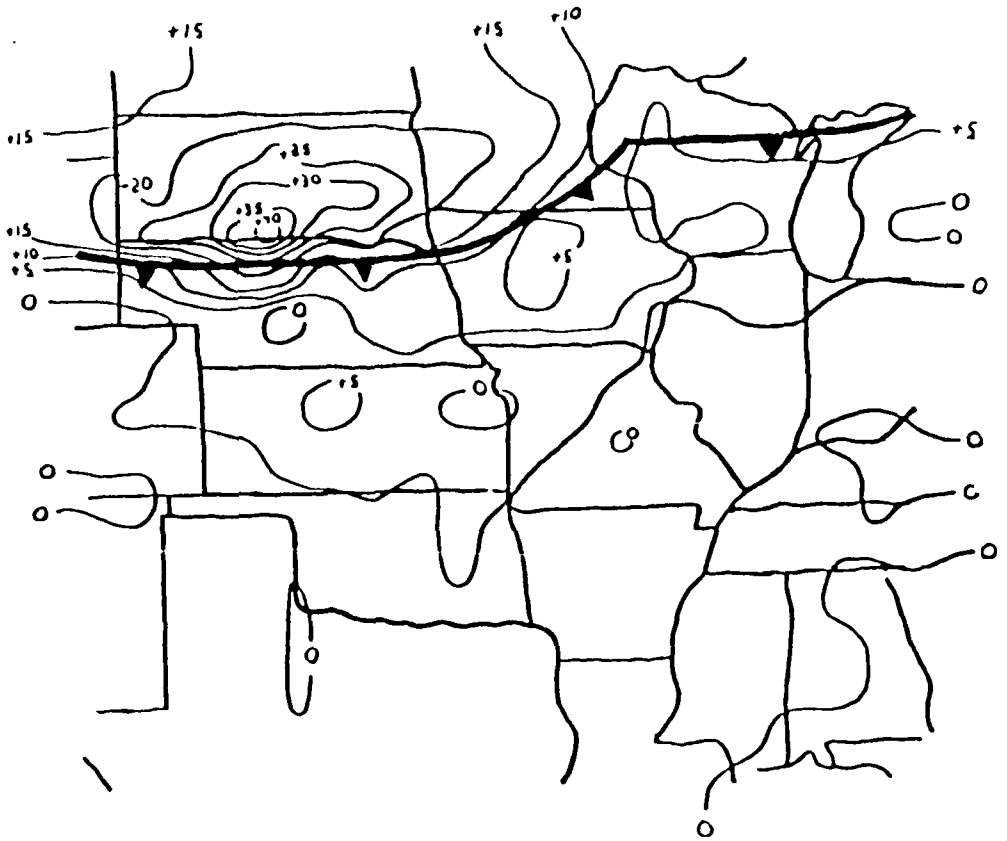

Fig. 34. Same as Fig. 31, except for 2300 G.M.T..

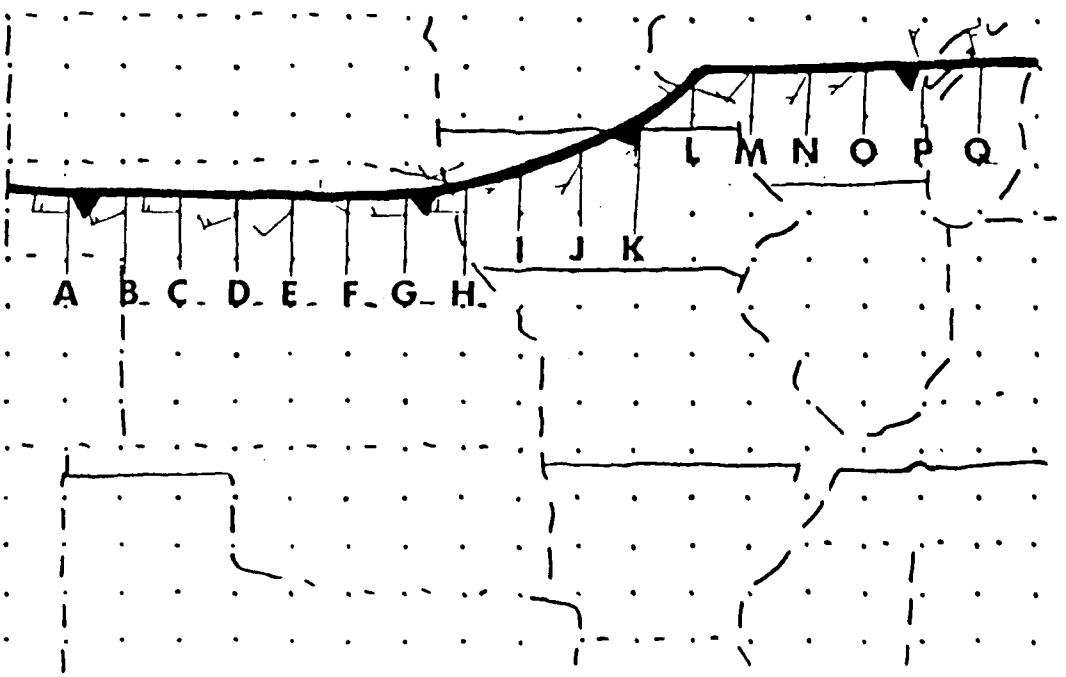

Fig. 35. Same as Fig. 29, except for 2300 G.M.T..

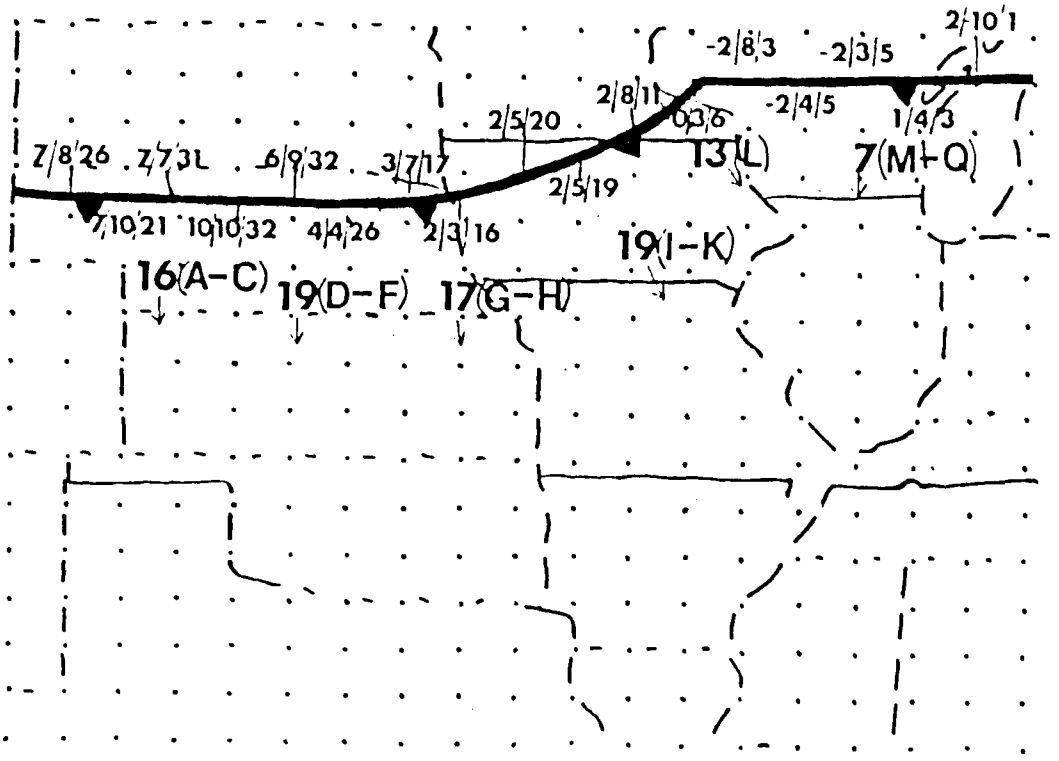

Fig. 36. Same as Fig. 30, except for 2300 G.M.T..

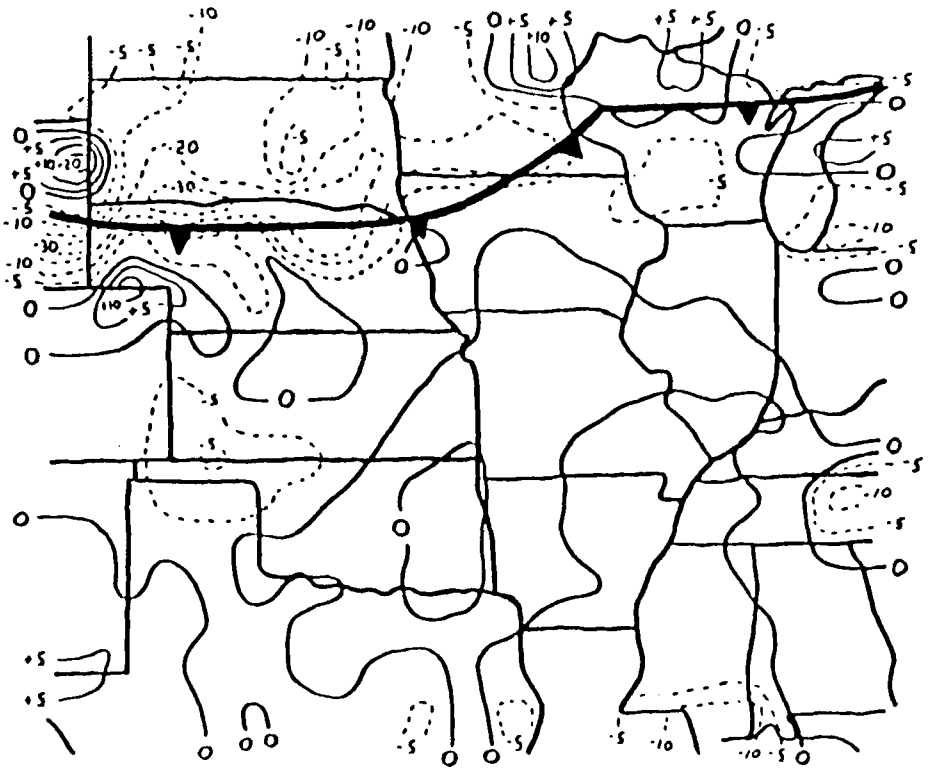

Fig. 37. Same as Fig. 33, except at 2300 G.M.T..

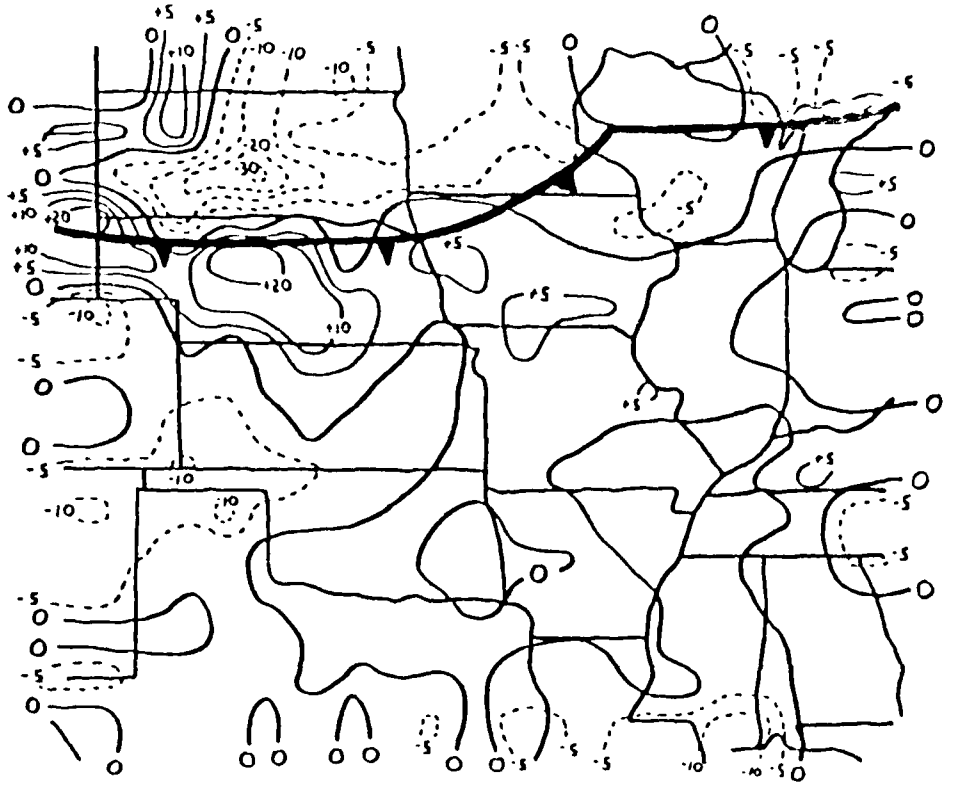

Fig. 38. Same as Fig. 32, except at 2300 G.M.T..

redevelopment. The isallobaric acceleration has been shown as a contributor to this frontogenetically induced motion. Diagnosing an isallobaric contribution to surface frontal motion through the actual wind crossfrontal components makes the significance of isallobaric crossfrontal components difficult to determine. However, strong isallobaric crossfrontal components were indicated across many frontal segments. The fact that the actual wind crossfrontal components on these segments did not consistently (until the isallobaric acceleration became unusually large) display an isallobaric influence suggests that the contribution may have been somewhat random. When some consistency of isallobaric influence on the actual wind crossfrontal components was indicated (2300 G.M.T.), evidence of a limited isallobaric contribution was given by the geostrophic crossfrontal components in better agreement with the observed frontal velocity than the actual wind crossfrontal components.

3.2 15 November 1988 Case Study

At 1200 G.M.T. an intense shortwave moved out of the southwestern United States (note the strength of the 500 mb height falls over northern New Mexico, Fig. 39) into a baroclinic environment favorable for rapid surface cyclogenesis (Fig. 40). This well defined baroclinic zone over Kansas and Nebraska was predominately due to vigorous warm air advection in the lower levels (Fig. 40). This warm air advection over the past 12 hours moved the warm front from Kansas to the 1600 G.M.T. position over Minnesota and Wisconsin (Fig. 41).

As indicated by the NMC 1200 G.M.T. 850 mb chart (Fig. 40), cold air advection extended from South Dakota to western Nebraska. By the beginning of the case study (1600 G.M.T., Fig. 41), cold air advection promoted the development of the cold front from the Oklahoma Panhandle to northern New Mexico and was partially responsible for the cold front from Kansas to eastern Nebraska. The upper level shortwave concurrent with the baroclinic zone facilitated the development of an intense surface cyclone over southwestern Kansas that moved into northeast Kansas by 2300 G.M.T. (Fig. 41). The cold front extending from Oklahoma into Texas at 1600 G.M.T. (Fig. 41) stemmed from advection of dry air (Fig. 40) and subsequent frontal development due to an abrupt change in moisture.

In addition to surface cyclone development, this case study differs from the 31 January case study in two important respects: First, widespread convective precipitation was indicated throughout the entire period of consideration (Figs. 42, 43, and 44). Many tornadoes were reported in the impressive line of thunderstorms that materialized from Iowa to Texas. Thundersnows were reported in the isolated convection over central and northwestern Kansas. Second, rapidly changing D value tendencies at the surface created a myriad of isallobaric forcing patterns, while the 31 January case study exhibited a more consistent isallobaric pattern. In this case study, cold air advection initially resulted in D value rises (1600 to 1800 G.M.T.) behind the cold front extending from Kansas to Nebraska. As the surface cyclone moved northeast out of southwestern Kansas, the isallobaric acceleration on the actual winds in the vicinity of this front was in response to D value falls. For example, a pressure fall

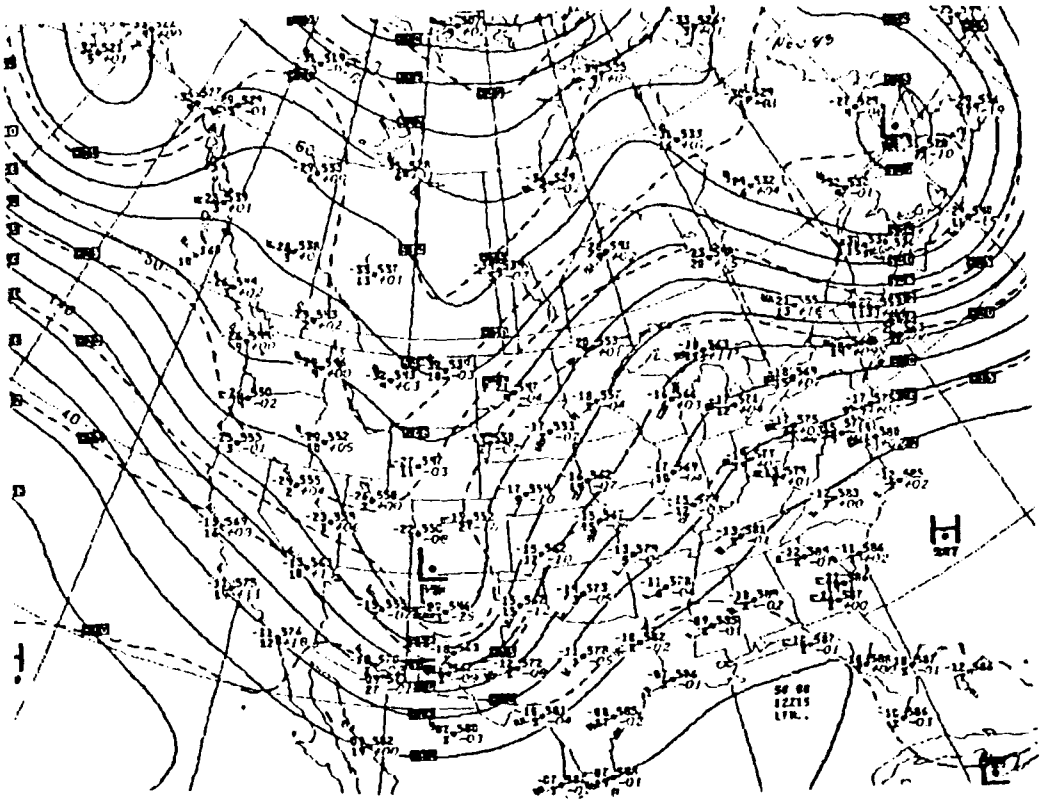

Fig. 39. National Meteorological Center 500 mb chart for 1200 G.M.T. 15 November 1988. Solid lines are height contours (decameters) and dashed lines are isotherms (^{0}C).

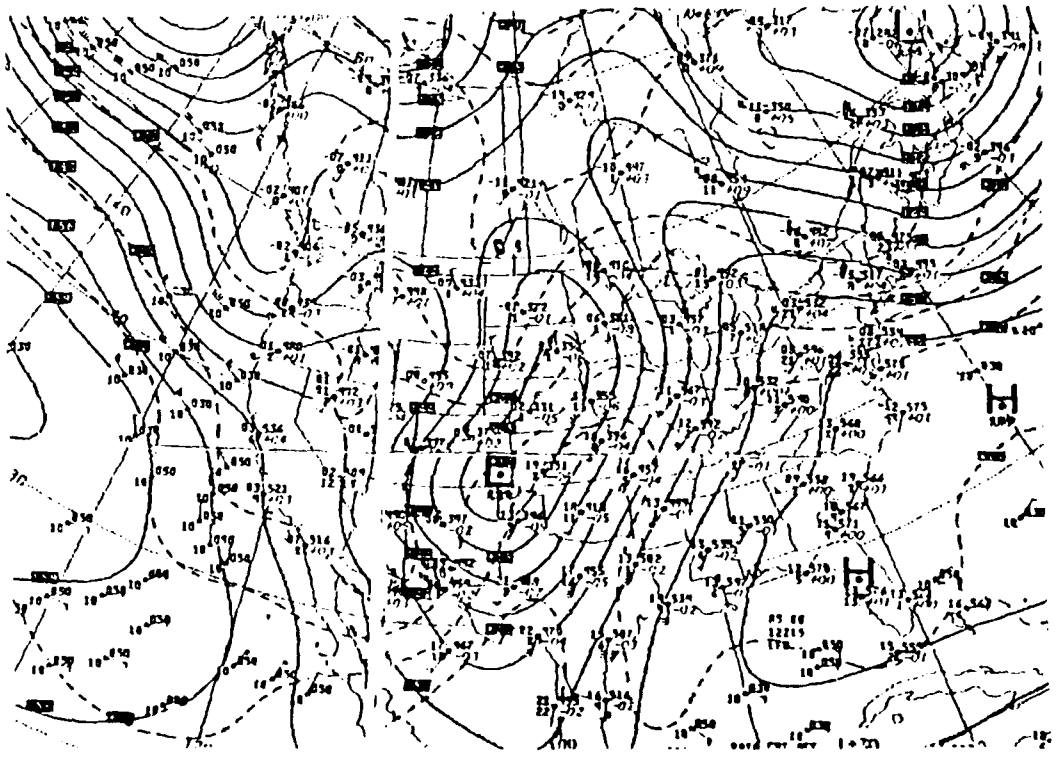

Fig. 40. Same as Fig. 39, except at 850 mb.

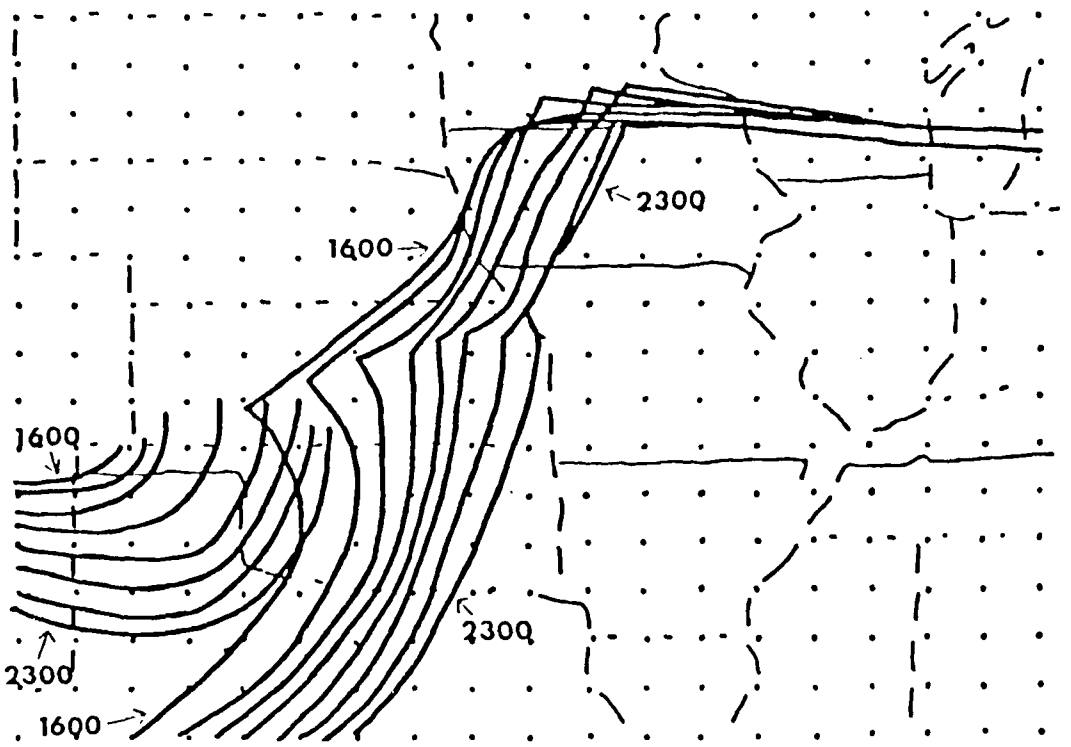

Fig. 41. Hourly frontal positions over the central United States for 1600-2300 G.M.T. 15 November 1988.

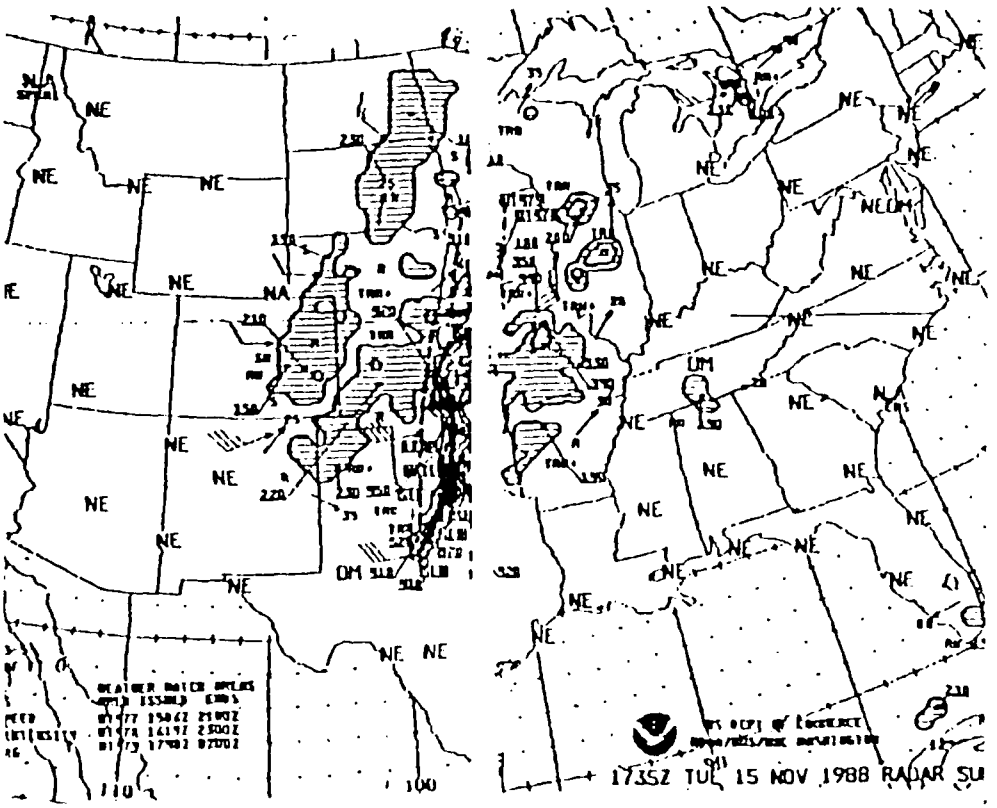

Fig. 42. National Meteorological Center Radar Summary at 1735 G.M.T. Hatched areas are precipitation. Contours are at intensity levels one, three, and five. Area movements (kts) are given by arrows with pennants. Cell movements (kts) are given by arrows with numbers. Precipitation bases and tops (X 10^2 feet) are overlined and underlined, respectively.

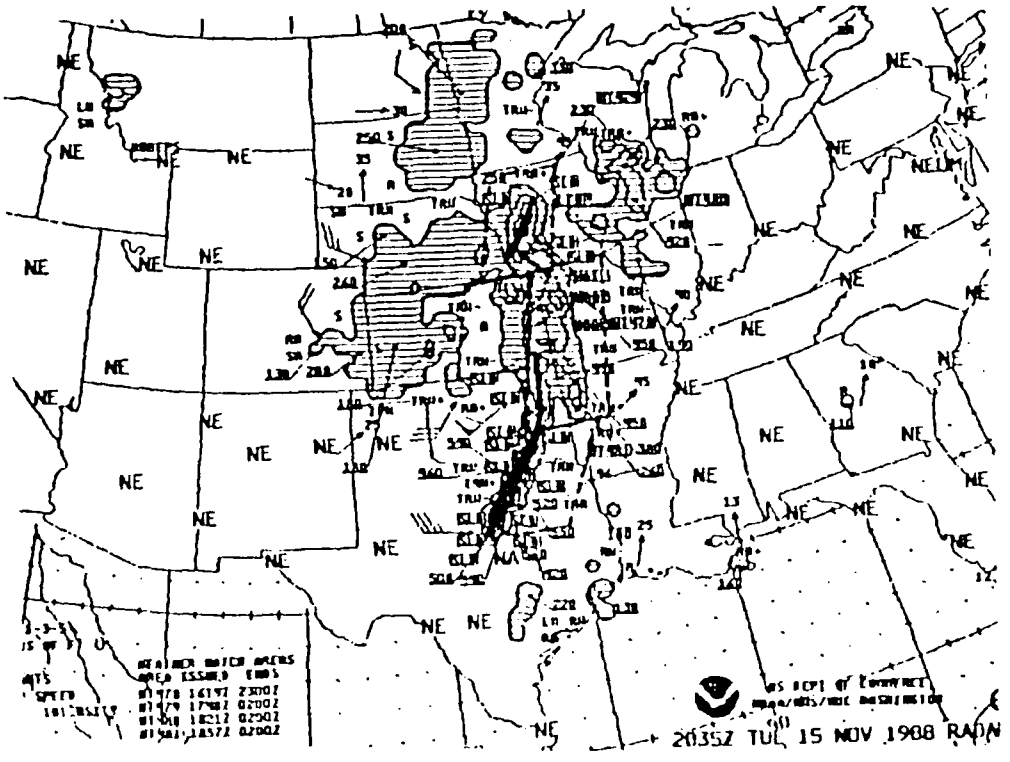

Fig. 43. Same as Fig. 42, except at 2035 G.M.T..

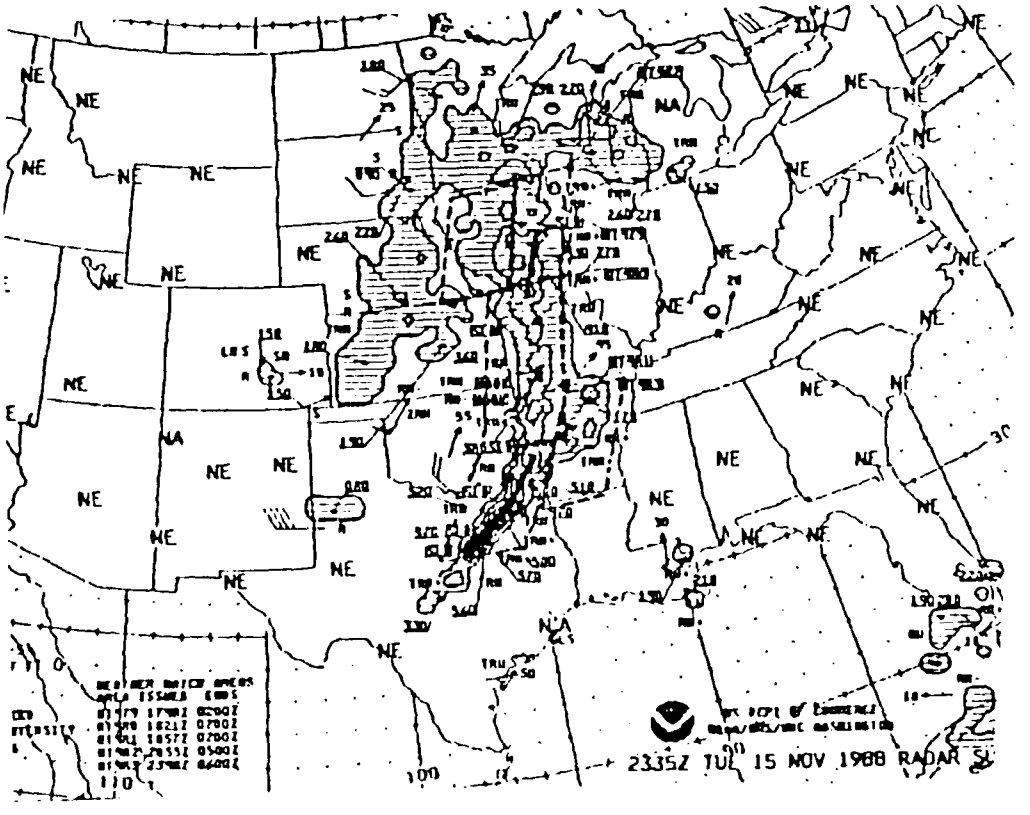

Fig. 44. Same as Fig. 42, except at 2335 G.M.T..

of 3.6 mb was reported at Topeka, Kansas from 1700 to 1800 G.M.T. Given the movement and continued development of the surface cyclone over Kansas, the cold front extending from Kansas to Nebraska displayed an anomalous movement. Isallobaric forcing appears to provide a partial explanation for the movement of this front.

In response to the D value tendencies over Nebraska and Kansas (Fig. 45), the 1600 G.M.T. ageostrophic winds (Fig. 46) and frontal velocities (Fig. 47) hint of an isallobaric contribution over frontal section G-I. Despite the presence of strong isallobaric crossfrontal components, an isallobaric influence on the actual wind crossfrontal components appears limited to frontal segment H. Frontogenetical forcing due to the isallobaric wind (Fig. 48) indicated a maxima of frontogenesis concurrent with the D value rise center (Fig. 45) behind frontal section G-K. A similar frontogenesis pattern displayed by the frontogenetical forcing due to the actual wind (Fig. 49) alludes to isallobaric forcing as a contributor.

The actual wind frontogenetical forcing would contribute to slower movement of frontal section G-K, but the magnitude of temperature gradient realignment is small ($1^{\circ}K\ hr^{-1}\ 100\ km^{-1}$). While the actual wind crossfrontal components provide a more consistent (in the direction of motion) indication of movement for frontal section G-I, an isallobaric contribution is difficult to diagnose at frontal segments G and I. The limited area of isallobaric influence on the actual crossfrontal components is demonstrated by geostrophic crossfrontal components in better agreement with the observed frontal motion for frontal section A-F. In contrast, the actual wind crossfrontal components conform better to the observed frontal

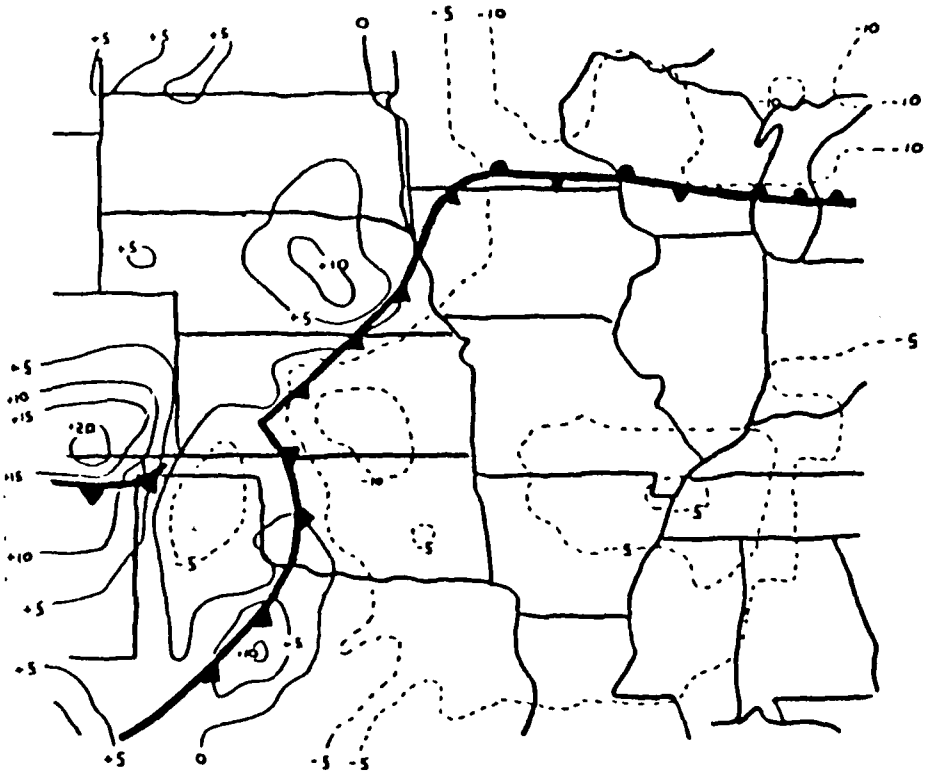

Fig. 45. Tendency of D values at 1600 G.M.T. 15 November 1988 (mhr^{-1}). Height falls are indicated by dashed lines and height rises by solid lines. Surface frontal positions are superimposed.

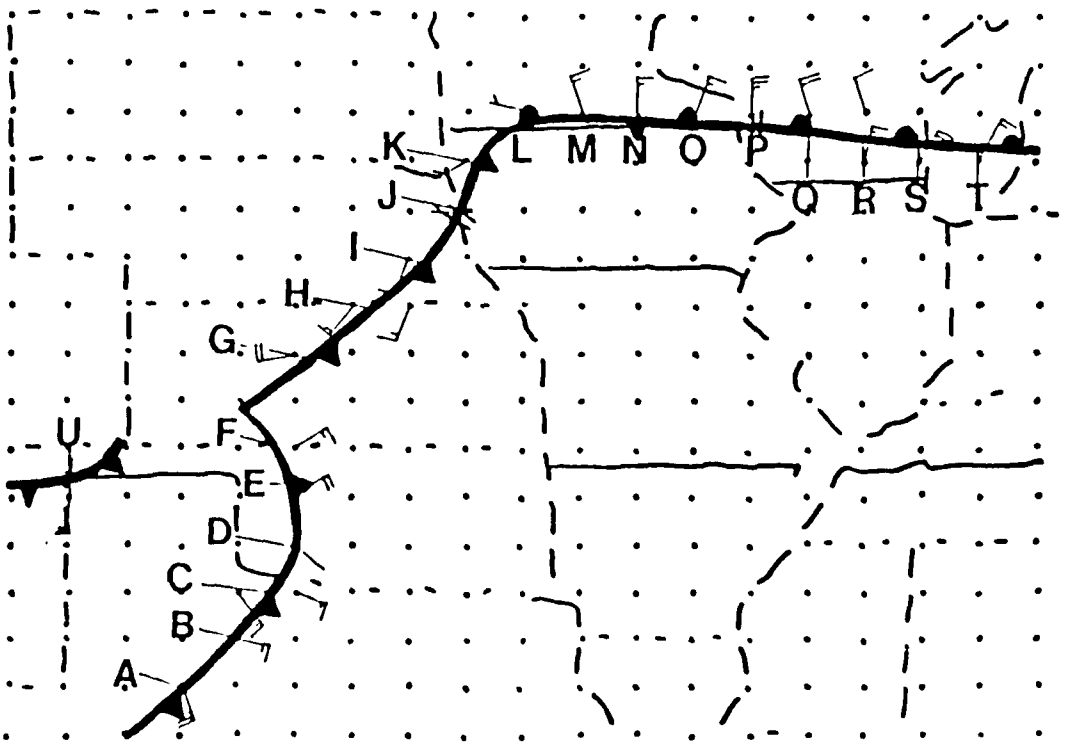

Fig. 46. 1600 G.M.T. ageostrophic winds plotted at the grid points used to determine the crossfrontal components by the actual, geostrophic, and isallobaric winds. Letters designate frontal segments on superimposed fronts.

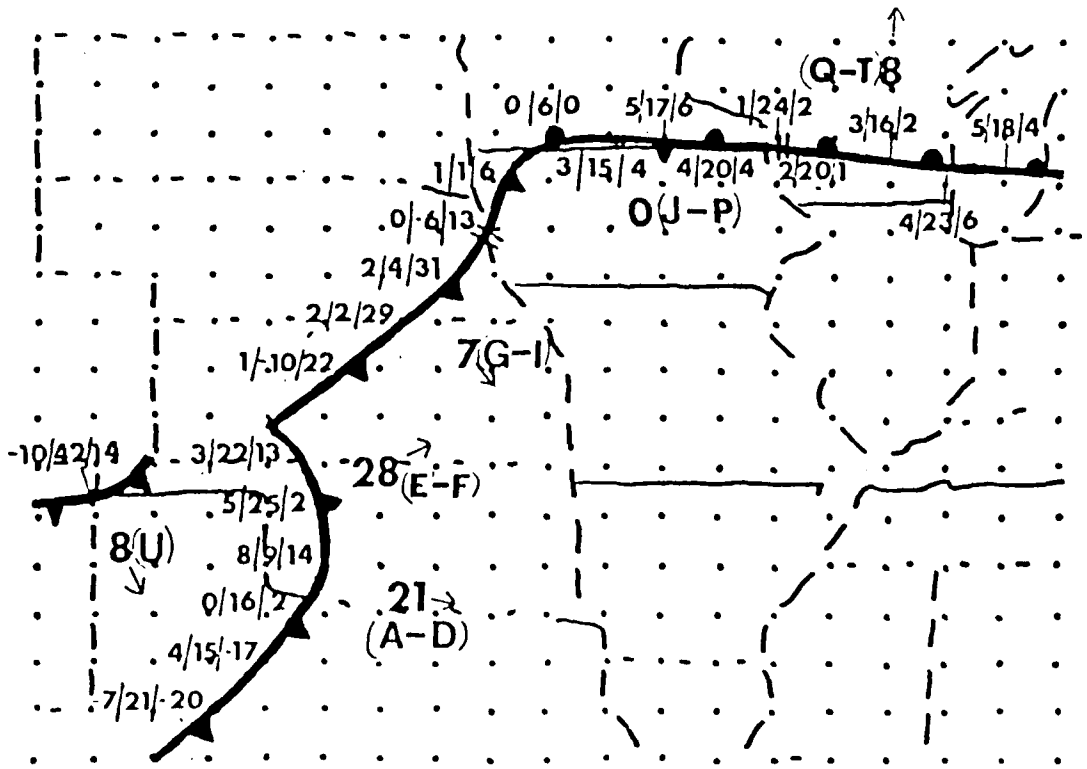

Fig. 47. Frontal velocity map for the period 1600-1700 G.M.T. 15 November 1988. Frontal velocities (m s^{-1}) are indicated by the larger numbers and correspond to the frontal segments indicated in parenthesis by the frontal velocity. Arrows indicate the approximate direction of motion. Small numbers indicate the crossfrontal component (m s^{-1}) by the actual/geostrophic/isallobaric winds. Positive (negative) cross frontal components indicate flow in the same (opposite) direction of frontal motion.

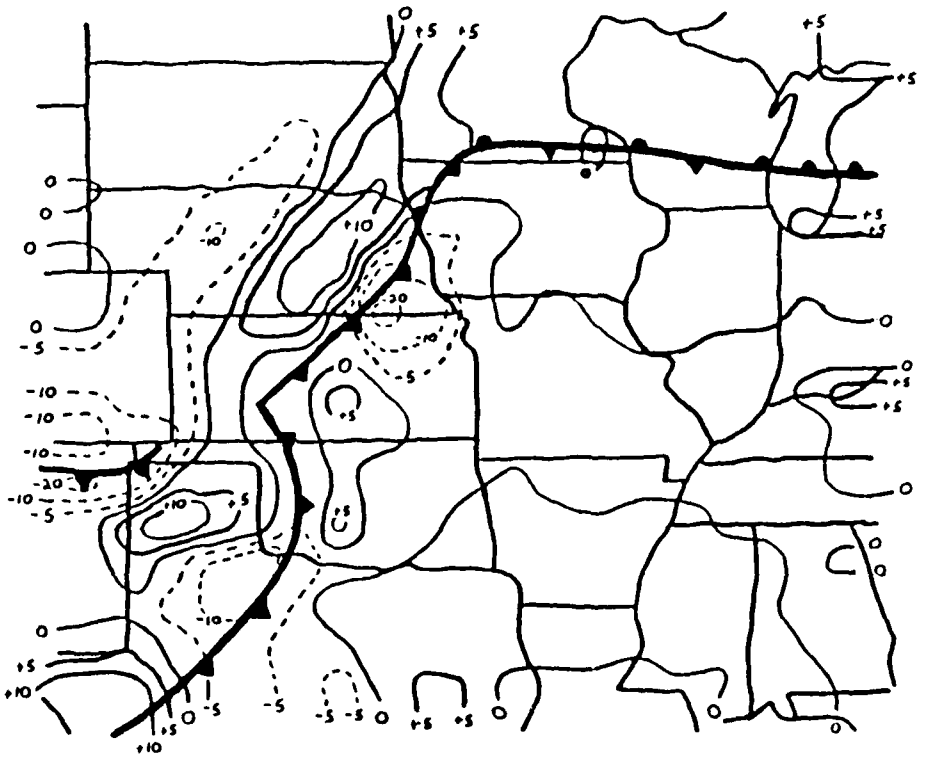

Fig. 48. Frontogenetical forcing due to the isallobaric wind at 1600 G.M.T. 15 November 1988 (X 10^{30}K $km^{-1}hr^{-1}$). Positive (negative) values represent frontogenesis (frontolysis). Surface frontal positions are superimposed.

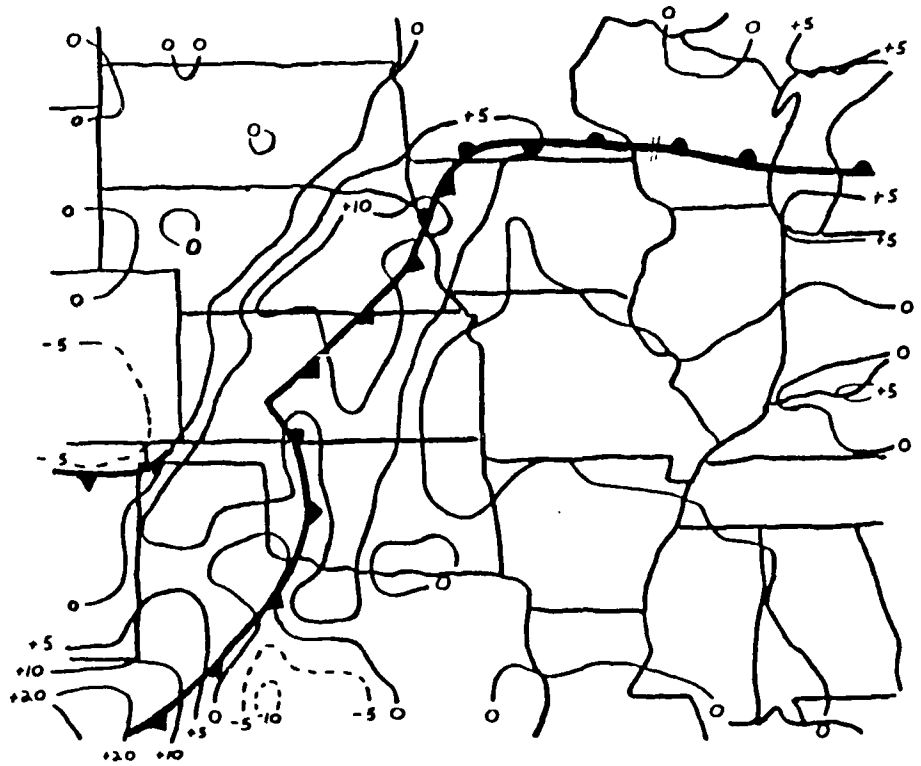

Fig. 49. Same as Fig. 48, but due to the actual wind.

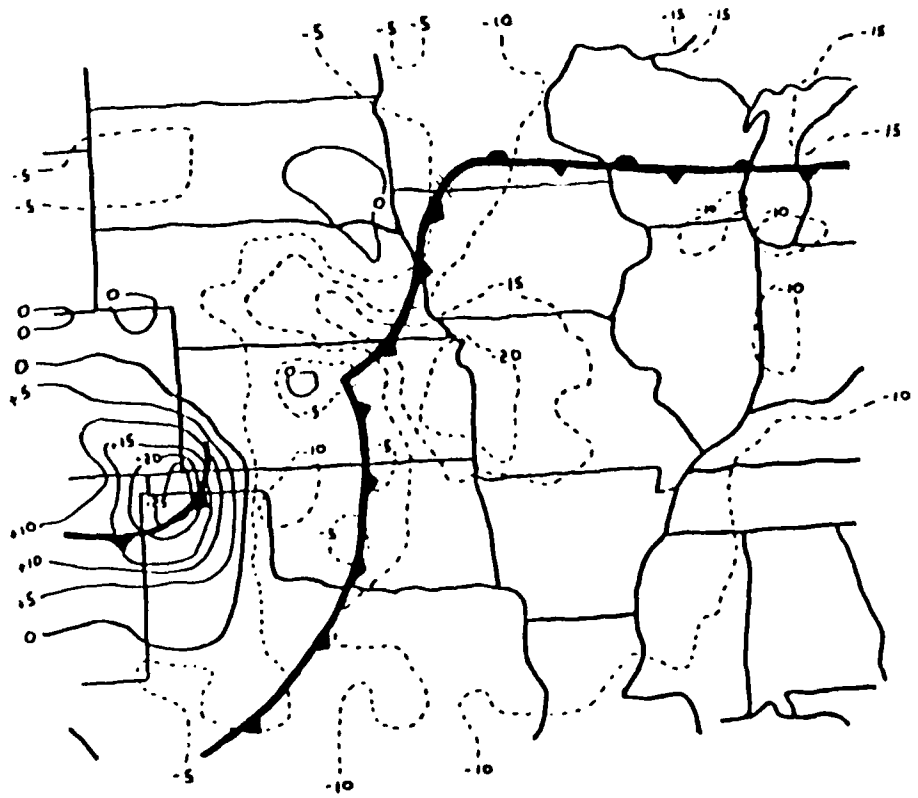

Fig. 50. Same as Fig. 45, except at 1800 G.M.T..

velocity than the geostrophic crossfrontal components over frontal section J-T were isallobaric contributions are nonexistent.

Continued development of the surface cyclone, as it moved into north-central Kansas, facilitated a different D value tendency field (Fig. 50) by 1800 G.M.T. The 1800 G.M.T. ageostrophic winds (Fig. 51) over frontal section H-L in conjunction with the magnitude of the actual, geostrophic, and isallobaric crossfrontal components (Fig. 52) initially allude to an isallobaric contribution, but a frictional contribution is suggested as well. Advocation of isallobaric influence on the actual wind crossfrontal components at frontal segments J, K, and L is supported through similar magnitudes, but in the opposite direction of actual versus geostrophic crossfrontal components. The same comparison on frontal segments H and I is ambiguous due to smaller (in opposite direction) actual versus geostrophic crossfrontal components. Similar frontogenetical forcing by the 1800 G.M.T. actual and isallobaric winds (Figs. 53 and 54, respectively) illustrated patterns favorable for "apparent" propagation over frontal section H-J. As opposed to the 31 January case study, the isallobaric contribution to "apparent" propagation included both frontogenesis ahead of the front as well as the frontolysis behind the front. Significantly, the isallobaric forcing occurred in a D tendency pattern where falls ahead and behind the front are observed. Recall that in the 31 January case study, the suggested isallobaric contribution to "apparent" propagation was limited to the frontolysis behind the front.

As observed for 1600 G.M.T., the geostrophic crossfrontal components are not supportive of the observed motion for section

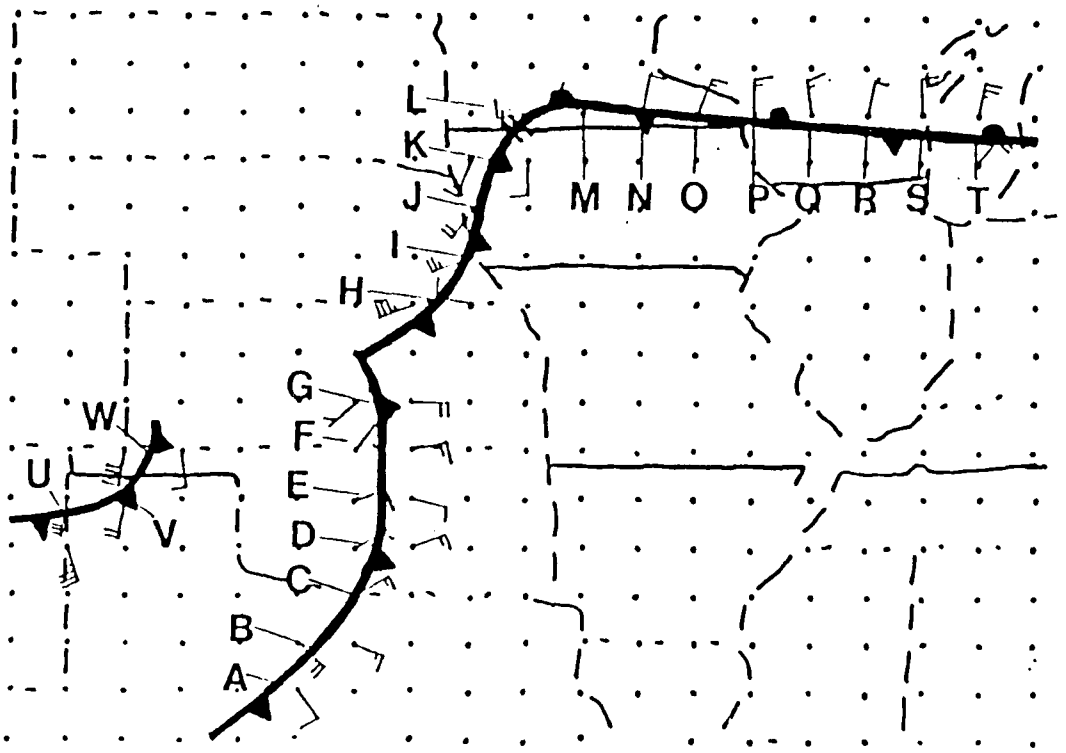

Fig. 51. Same as Fig. 46, except at 1800 G.M.T..

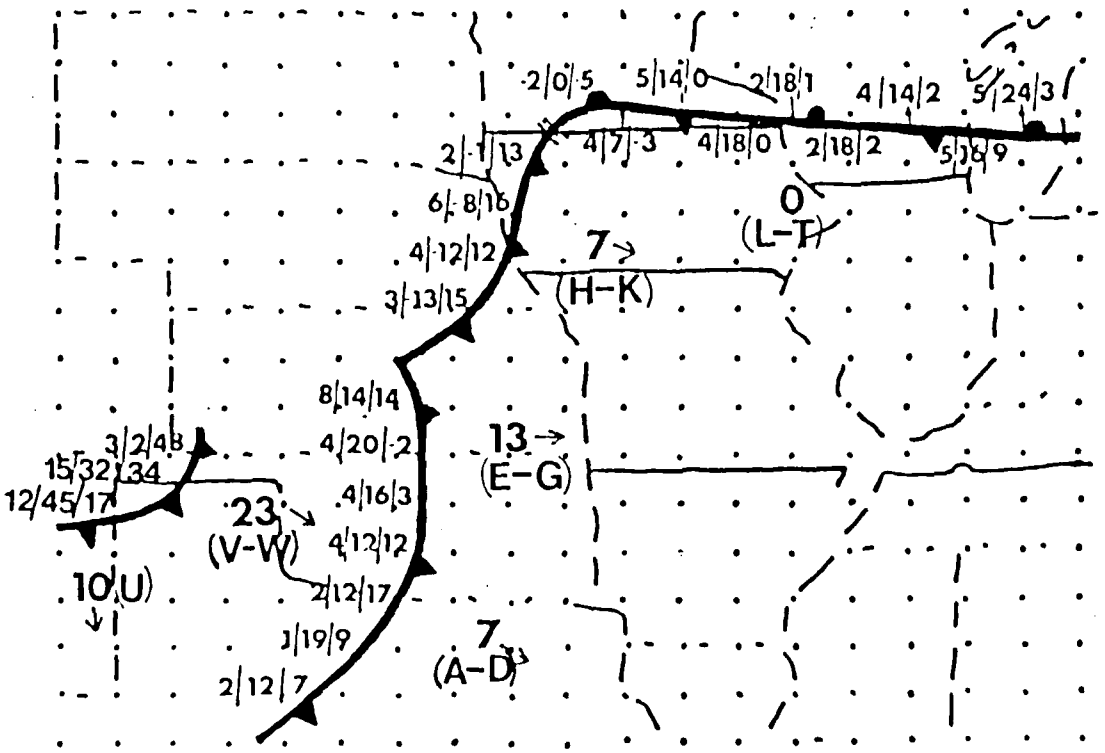

Fig. 52. Same as Fig. 47, except at 1800 G.M.T..

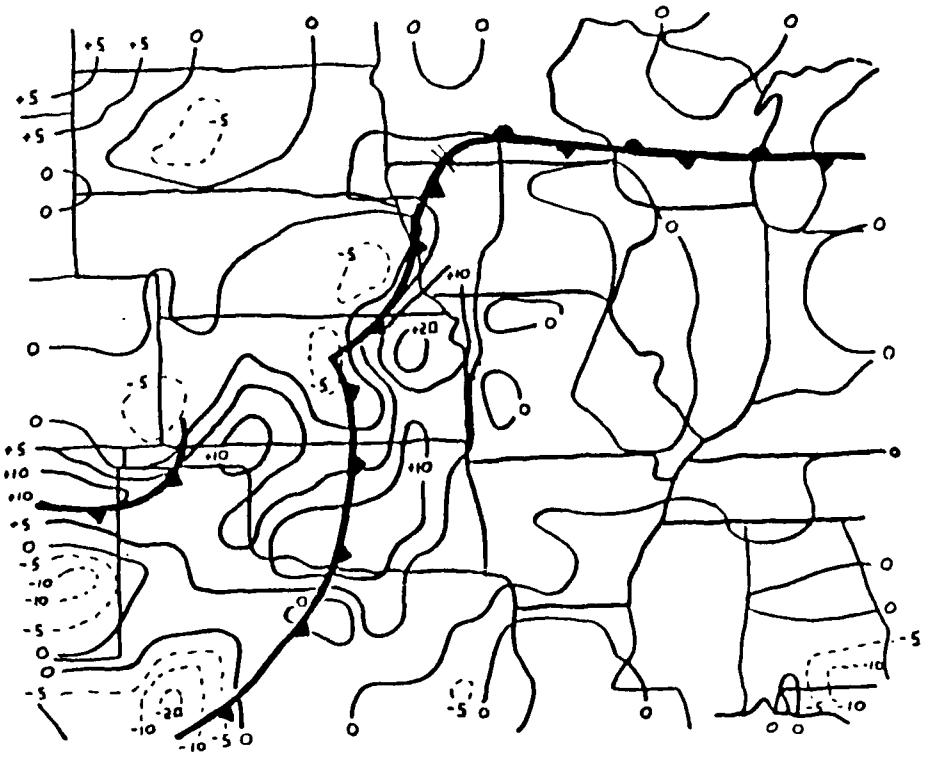

Fig. 53. Same as Fig. 49, except at 1800 G.M.T..

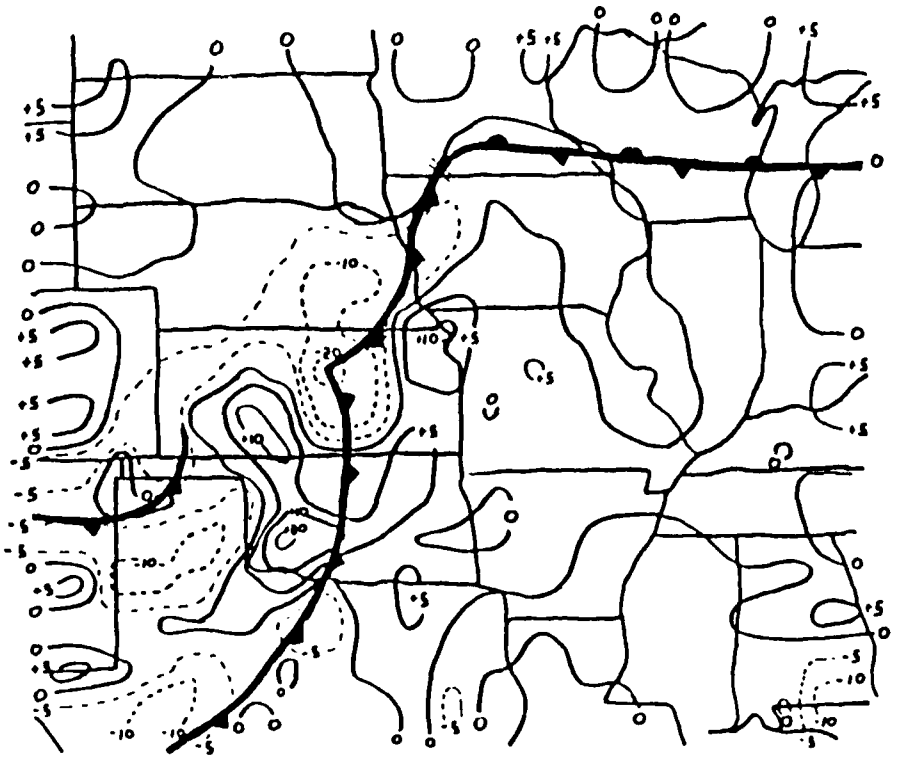

Fig. 54. Same as Fig. 48, except at 1800 G.M.T..

H-K. Unlike 1600 G.M.T. where isallobaric influence was limited to one actual wind crossfrontal component, both the 1800 G.M.T. actual crossfrontal components and frontogenetical forcing are supportive of the observed frontal motion. Actual wind crossfrontal components in better agreement with the observed frontal motion are not limited to frontal section H-K, but it is over this frontal section that an isallobaric influence is suggested.

The appearance of a D value rise rise maxima in the 2000 G.M.T. D value tendencies introduced a new isallobaric forcing field (Fig. 55) behind frontal section I-L (Fig. 56). Isallobaric contributions to actual crossfrontal components (Fig. 57) are suggested over frontal section J-L. Frontogenetical forcing due to the isallobaric wind (Fig. 58) now demonstrated frontogenesis behind and frontolysis ahead of frontal section J-K, while frontal segments L and M were still indicative of "apparent" propagation. The frontogenetical forcing due to the actual wind (Fig. 59) also demonstrated a similar pattern, but suggests that the amount of frontogenetically induced motion decreased across frontal section J-K. In summary, the appearance of D value rises behind frontal section I-K decreased the frontogenetical forcing favorable for "apparent" propagation. Where the pattern of D value falls remained across the front, "apparent" propagation was still evident. While decreased amount of frontogenetically induced motion across frontal section I-K raises doubts that the observed frontal motion is well diagnosed by the actual wind crossfrontal components and frontogenetical forcing, the combination provides a better indication of the observed frontal motion than the geostrophic crossfrontal components alone.

In this case study, the anomalous movement displayed by the front over eastern Nebraska was fairly well diagnosed by the actual wind crossfrontal components and frontogenetical forcing. The isallobaric frontogenetical forcing as a result of D value rises behind the front and D value falls ahead of the front for both 1600 and 2000 G.M.T. was not favorable for "apparent" propagation. Similarly observed patterns of frontogenetical forcing due to the actual wind allude to isallobaric contributions, but the results of the 15 November and 31 January case studies are not supportive of "apparent" propagation due solely to isallobaric forcing in the hypothesized D tendency field shown in Fig. 1. In contrast, isallobarically influenced frontogenetical forcing favorable for "apparent" propagation appeared when larger D value falls were indicated ahead of the front. Unfortunately, the isallobaric influenced frontogenetical forcing occurred during the period when thunderstorms were present in the area. The effects of the convective precipitation over the region introduce another variable to the frontogenetical forcing equation by virtue of changed temperature gradients not due to the winds alone. Due to a somewhat consistent isallobaric influence on the actual wind crossfrontal components for the front over Nebraska and Iowa, the isallobaric contribution to surface frontal motion appears more significant than in the 31 January case study. The question that immediately comes to mind is why did isallobaric influences play a more significant role for this front as opposed to the other fronts in this case study? In addition, why didn't the 31 January case study with substantially greater D value tendencies show a stronger level of influence? The answer may come from the other possible

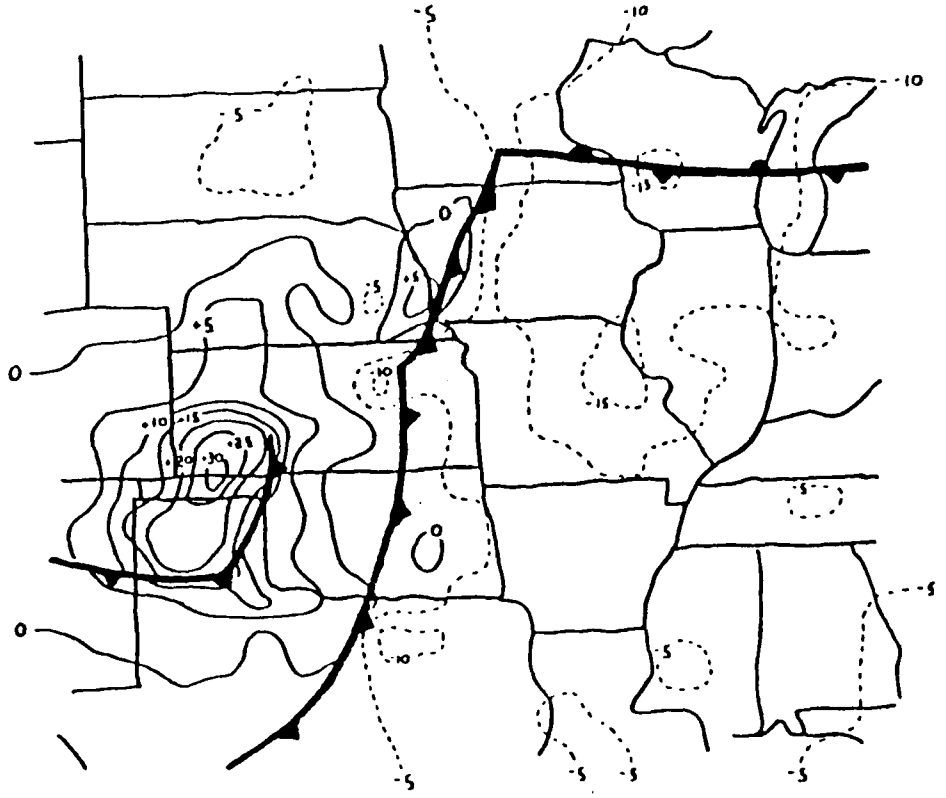

Fig. 55. Same as Fig. 50, except at 2000 G.M.T..

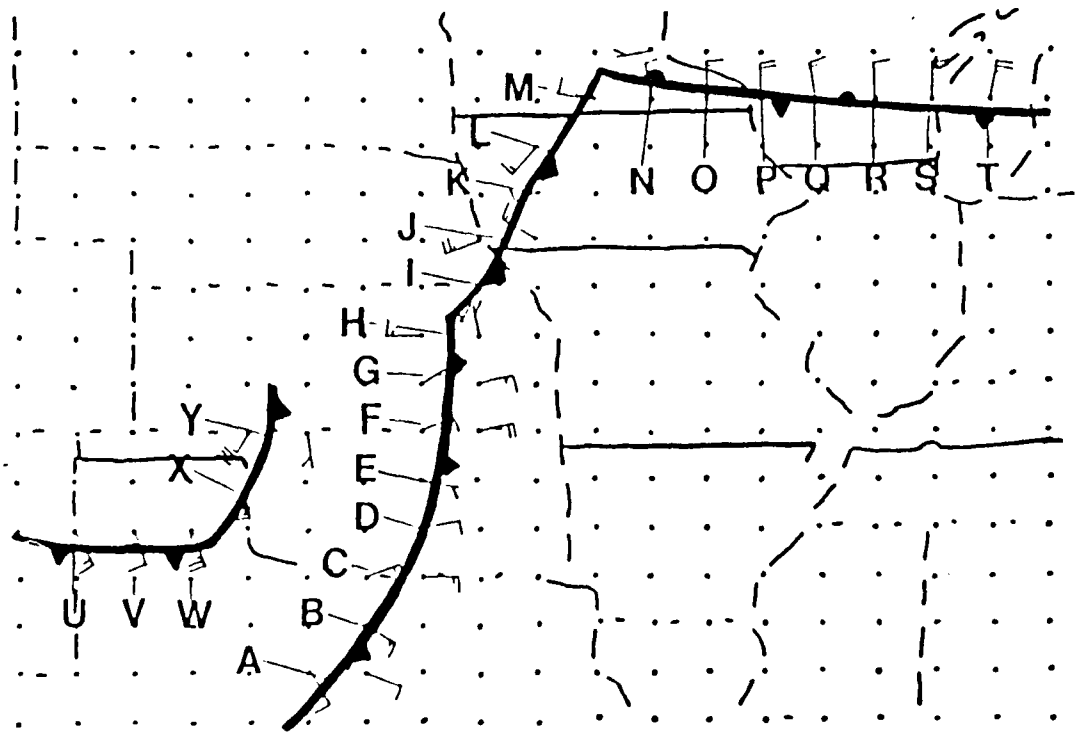

Fig. 56. Same as Fig. 51, except at 2000 G.M.T..

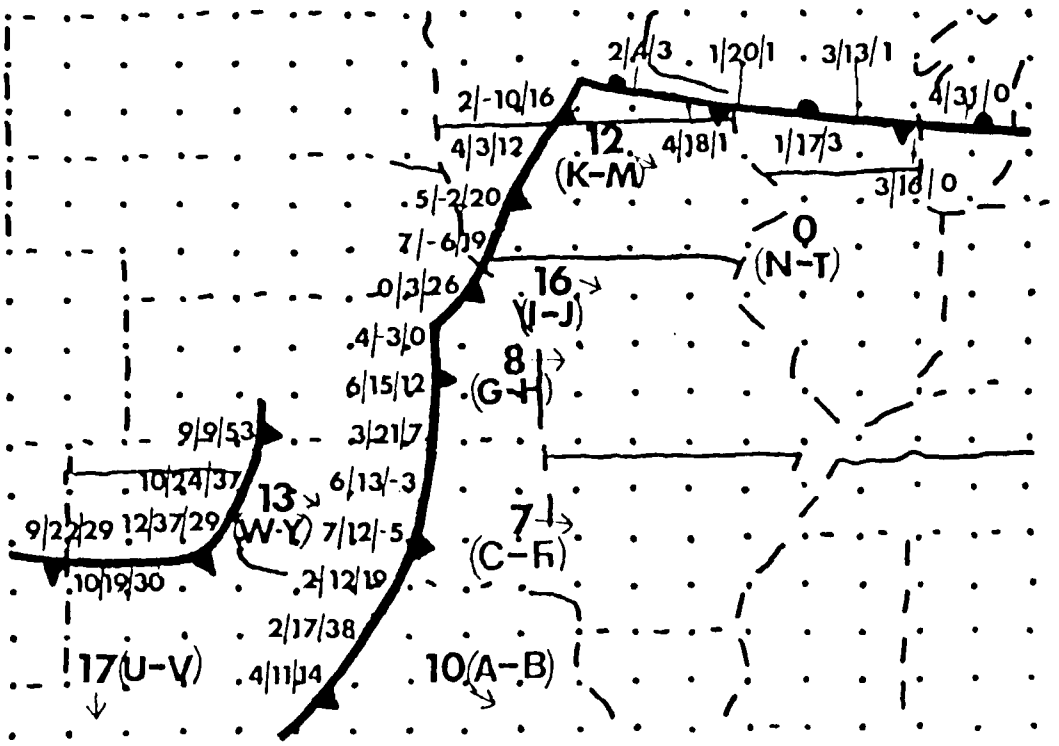

Fig. 57. Same as Fig. 52, except at 2000 G.M.T..

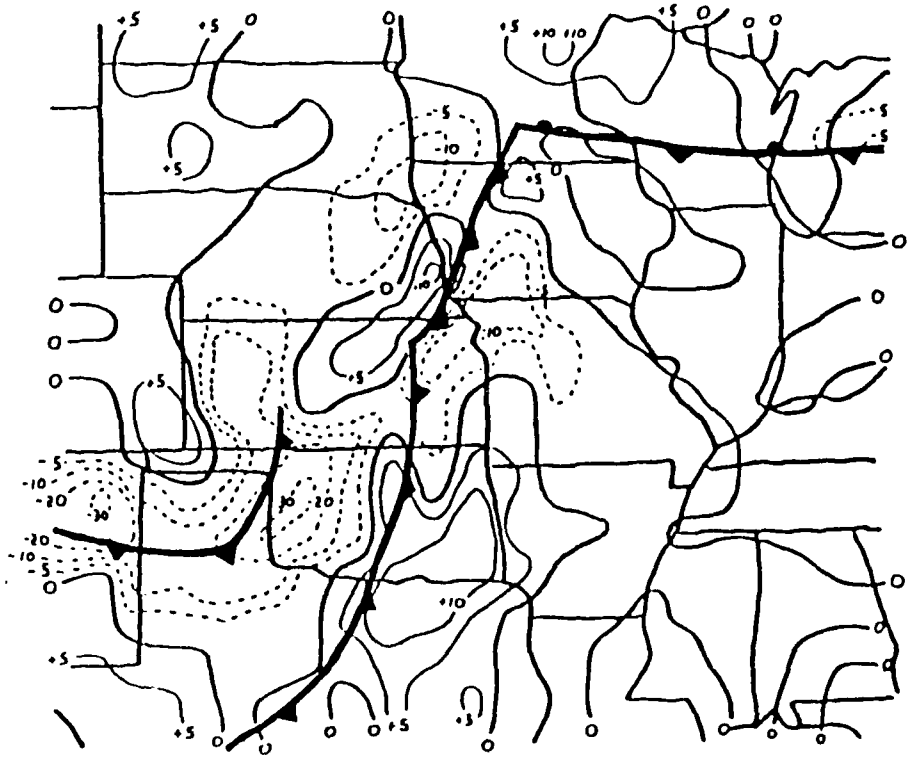

Fig. 58. Same as Fig. 54, except at 2000 G.M.T..

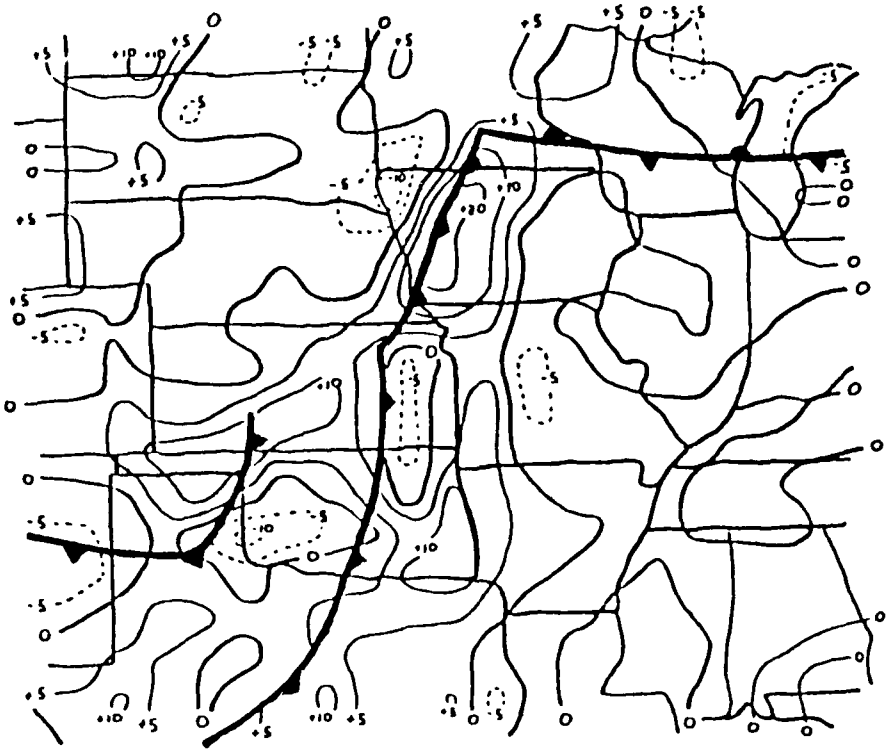

Fig. 59. Same as Fig. 53, except at 2000 G.M.T..

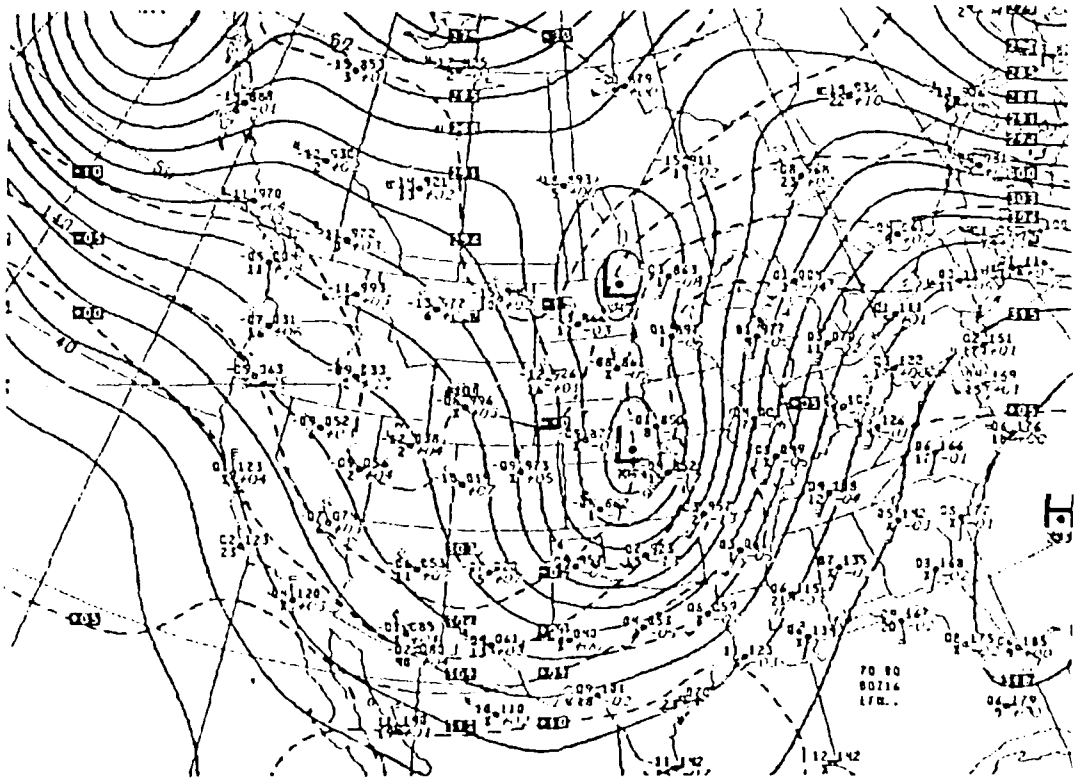

Fig. 60. National Meteorological Center 700 mb chart for 0000 G.M.T., 16 November 1988. Solid lines are height contours (decameters) and dashed lines are isotherms (°C).

contributors to surface frontal motion, such as the crossfrontal components of the upper level winds. In the 15 November case study, the upper level winds (Fig. 60) appear parallel to the frontal surface. If the upper level winds were parallel to the frontal surface, the surface frontal motion would be controlled to a larger extent by surface forces than would normally be the case. This is only a theory and without more in-depth analysis cannot be substantiated.

3.3 7 January 1989 Case Study

The 7 January case study provides another analysis of isallobaric effects on surface frontal motion associated with a developing surface cyclone. This case study exhibits two primary synoptic differences from the previous case study: First, the combination of slow movement by the developing extratropical cyclone and availability of cold air (Fig. 61). Second, a longer wavelength by the upper level shortwave (Fig. 62) conducive to benign (as compared to the 15 November case study) surface cyclone development through baroclinic instability. Subdued surface cyclogenesis concurrent with an ample supply of cold air produced generally constant isallobaric forcing (similar to the 31 January case study) on the surface fronts. D value falls and rises were observed ahead and behind of the eastern cold front, respectively extending from Minnesota to Texas at 1700 G.M.T. (Fig. 63). In contrast, both cold fronts had similar origins as the cold fronts in the 15 November case study. Initially, the eastern cold front was the result of an abrupt change

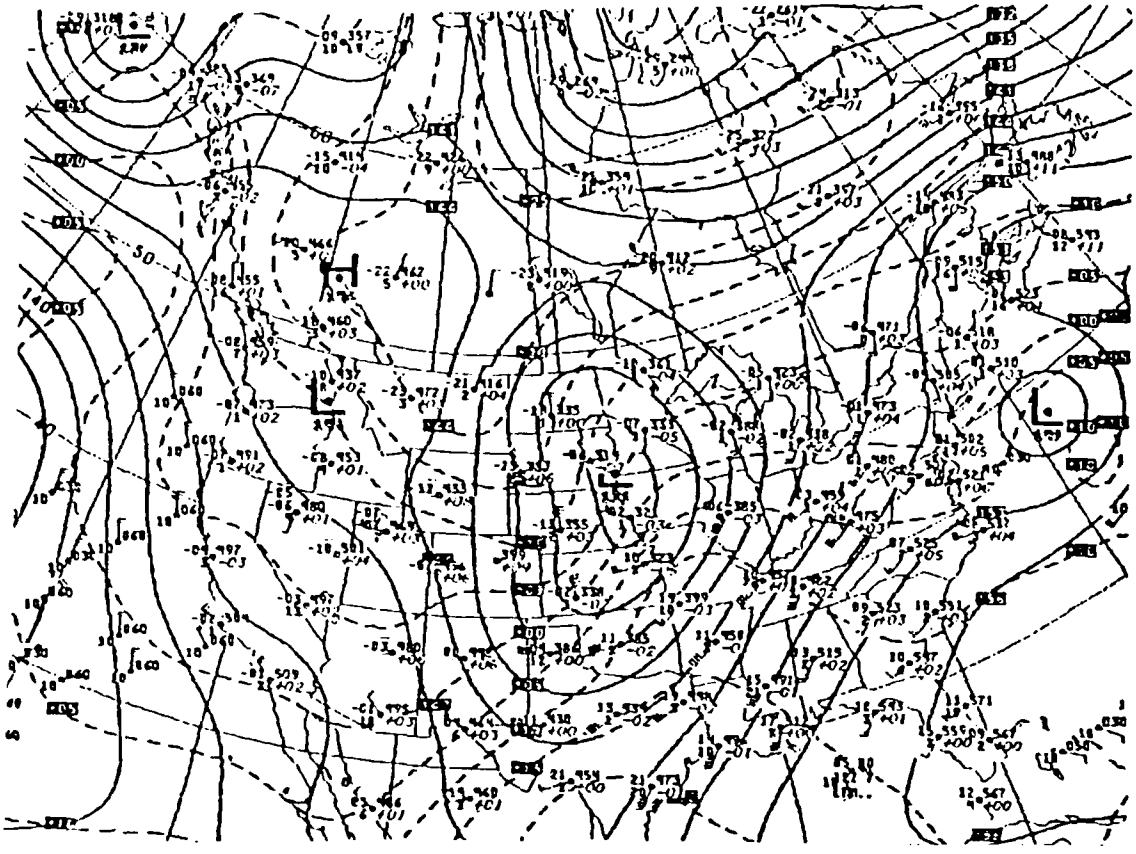

Fig. 61. National Meteorological Center 850 mb chart for 1200 G.M.T. 7 January 1989. Solid lines are height contours (decameters) and dashed lines are isotherms (°C).

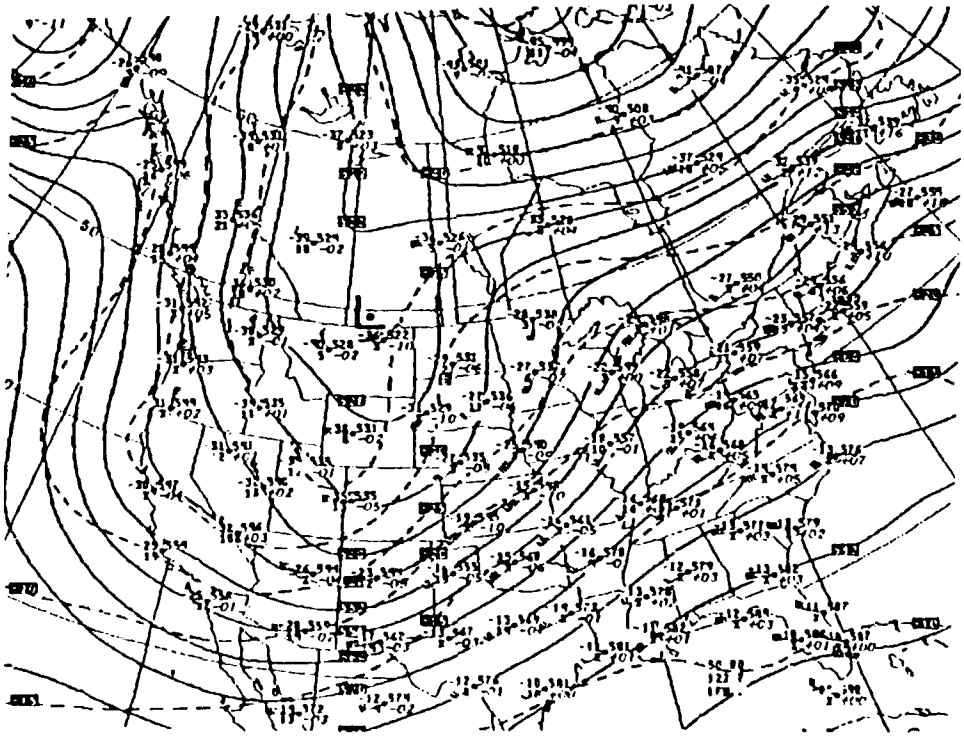

Fig. 62. Same as Fig. 61, except at 500 mb.

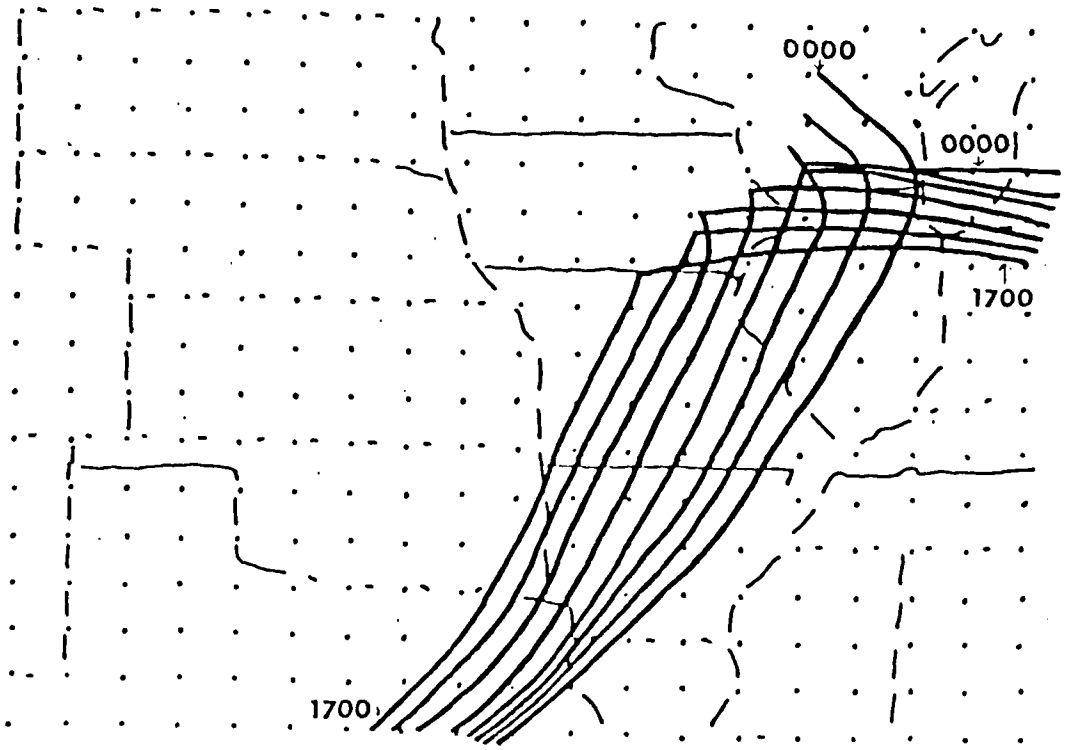

Fig. 63. Hourly frontal positions over the central United States for 1700-0000 G.M.T. 7-8 January 1989.

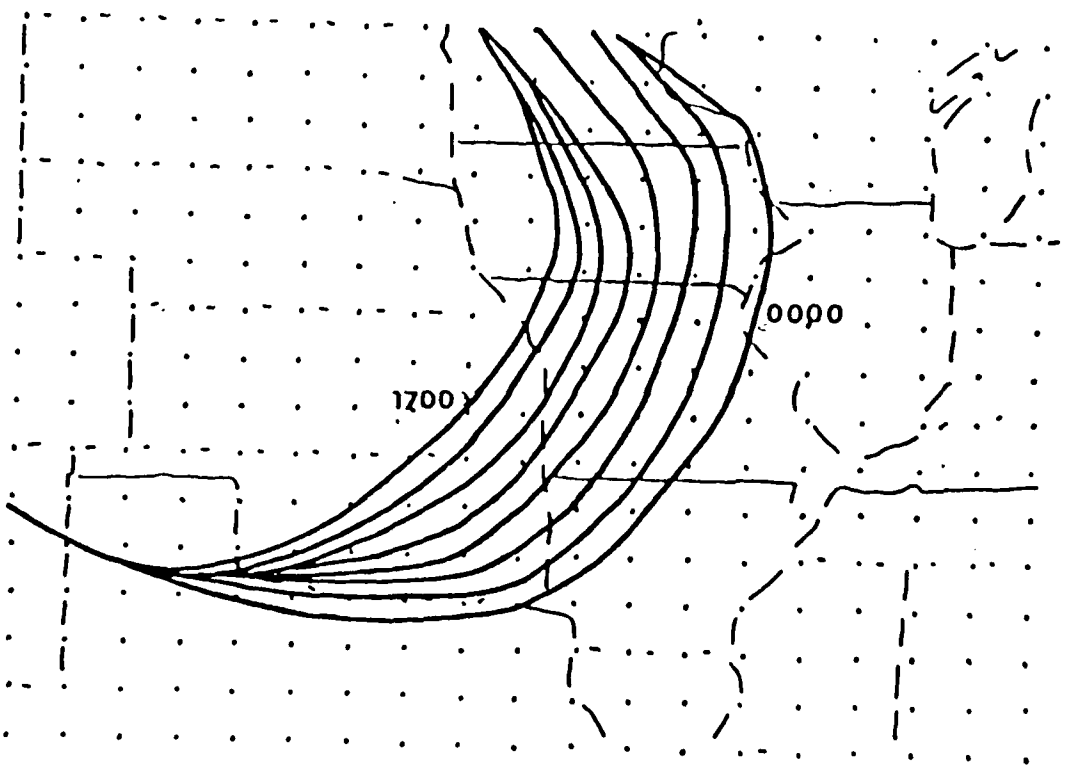

Fig. 64. Same as Fig. 63.

in moisture. The western cold front at 1700 G.M.T. (Minnesota to New Mexico, Fig. 64), originated from the cold air advection behind the surface cyclone.

Precipitation, limited at the inception of the case study (Fig. 65), rapidly developed (Figs. 66 and 67) and by 2235 G.M.T. (Fig. 68) substantial areal coverage by showers and thunderstorms was indicated. Stratiform precipitation was widespread, but small areal coverage on the NMC Radar Summaries can be attributed to the fact that it was snow. Initially therefore, it is possible to analyze the isallobaric forcing on the surface frontal motion and remove the unknown effects of convective precipitation on frontogenetical forcing.

The 1800 G.M.T. D value tendencies (Fig. 69) demonstrate the hypothesized pattern favorable for an isallobaric contribution to frontal motion over cold frontal sections A-I and a-d (Fig. 70). Even though the largest isallobaric crossfrontal components (Fig. 71) are indicated on frontal section E-J, isallobaric influence on the actual crossfrontal components is limited to frontal segments a, b, and d. Frontogenetical forcing by the 1800 G.M.T. actual and isallobaric winds (Figs. 72 and 73, respectively) suggest "apparent" propagation by isallobaric forcing over frontal sections a-c, f-h, and to a lesser extent slowed movement over frontal section E-J. Combination of the frontogenetical forcing due to the actual wind and the actual wind crossfrontal components produces a limited area where a better diagnosis of surface frontal motion than the geostrophic crossfrontal components (segments a, b, and d) is achieved. However, these are the segments where an isallobaric influence is possible.

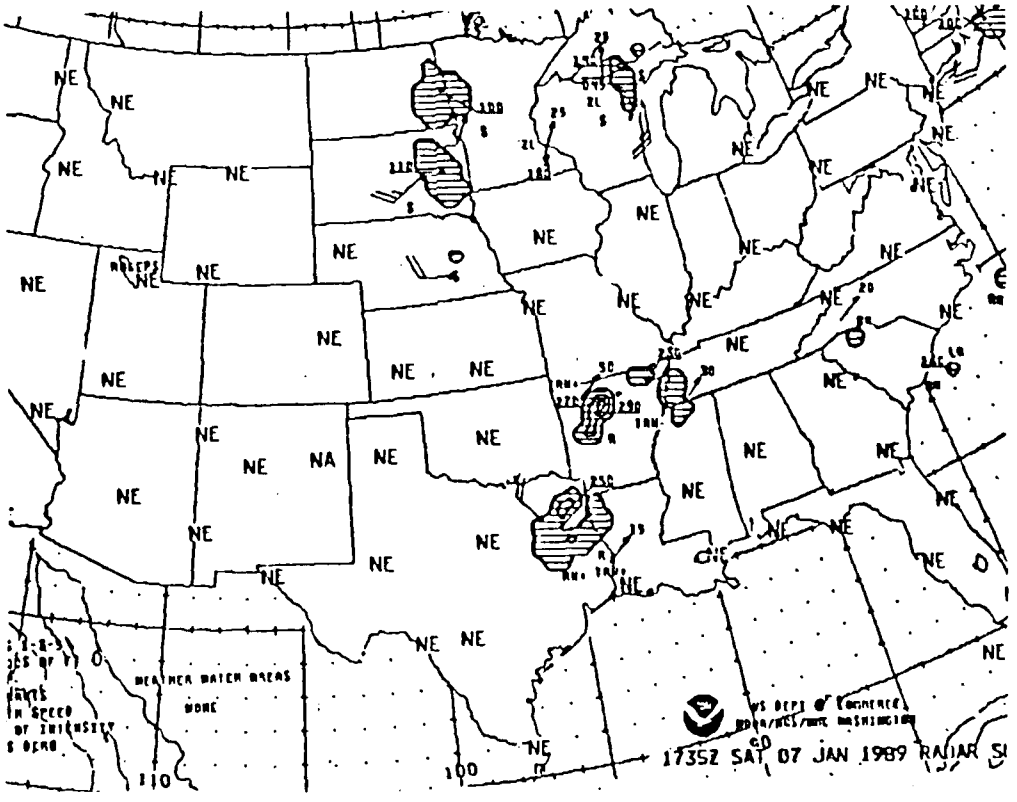

Fig. 65. National Meteorological Center Radar Summary at 1735 G.M.T. 7 January 1989. Hatched areas are precipitation. Contours are at intensity levels one, three, and five. Area movements (kts) are given by arrows with pennants. Cell movements (kts) are given by arrows with numbers. Precipitation bases and tops (X 10^2 feet) are overlined and underlined, respectively.

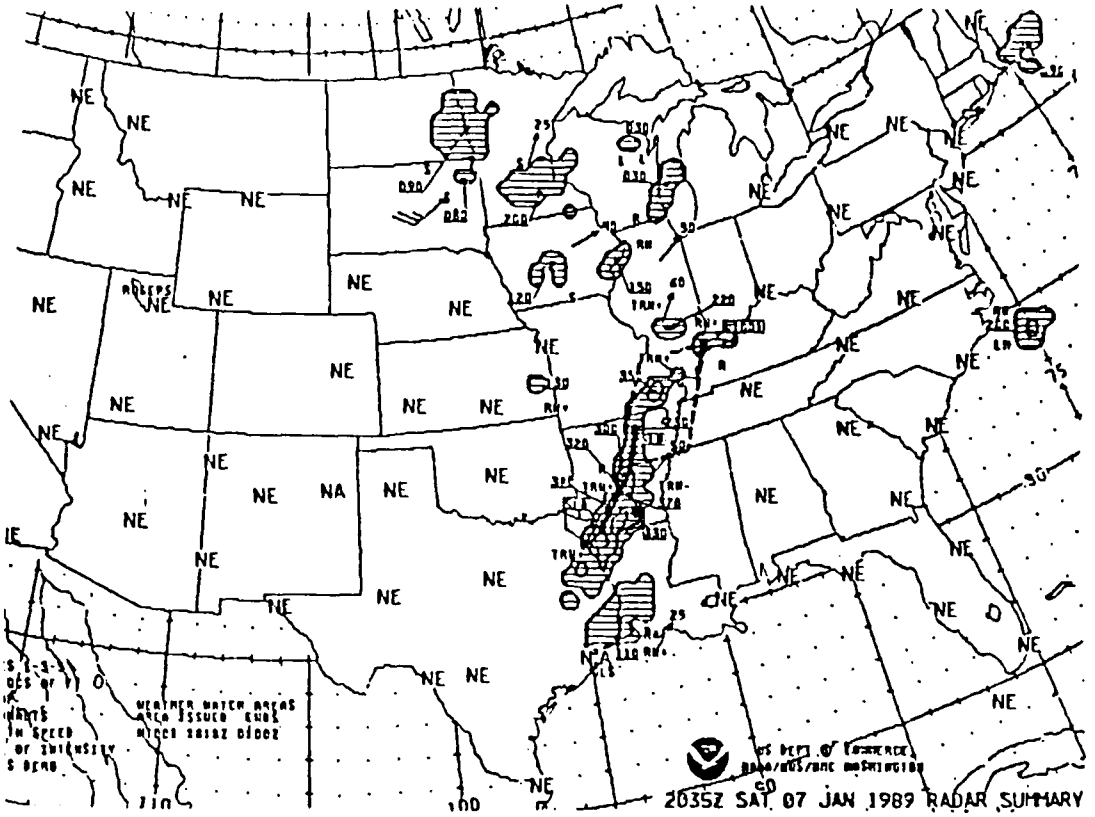

Fig. 66. Same as Fig. 65, except at 2035 G.M.T..

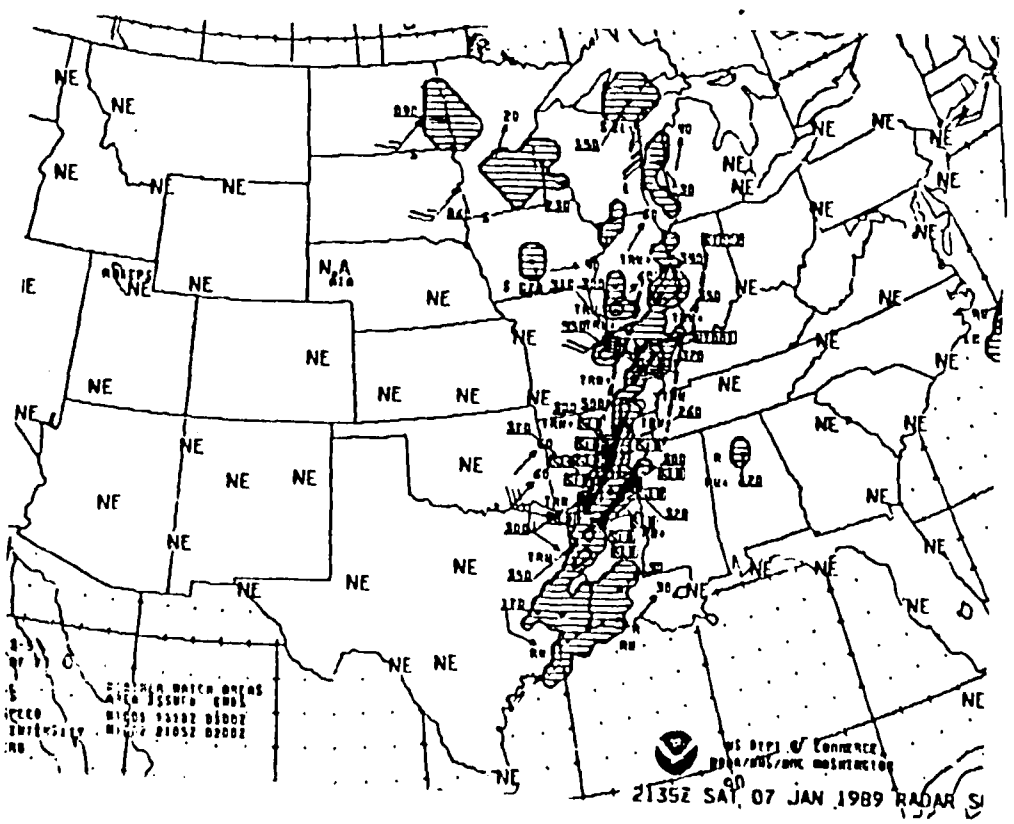

Fig. 67. Same as Fig. 65, except at 2135 G.M.T..

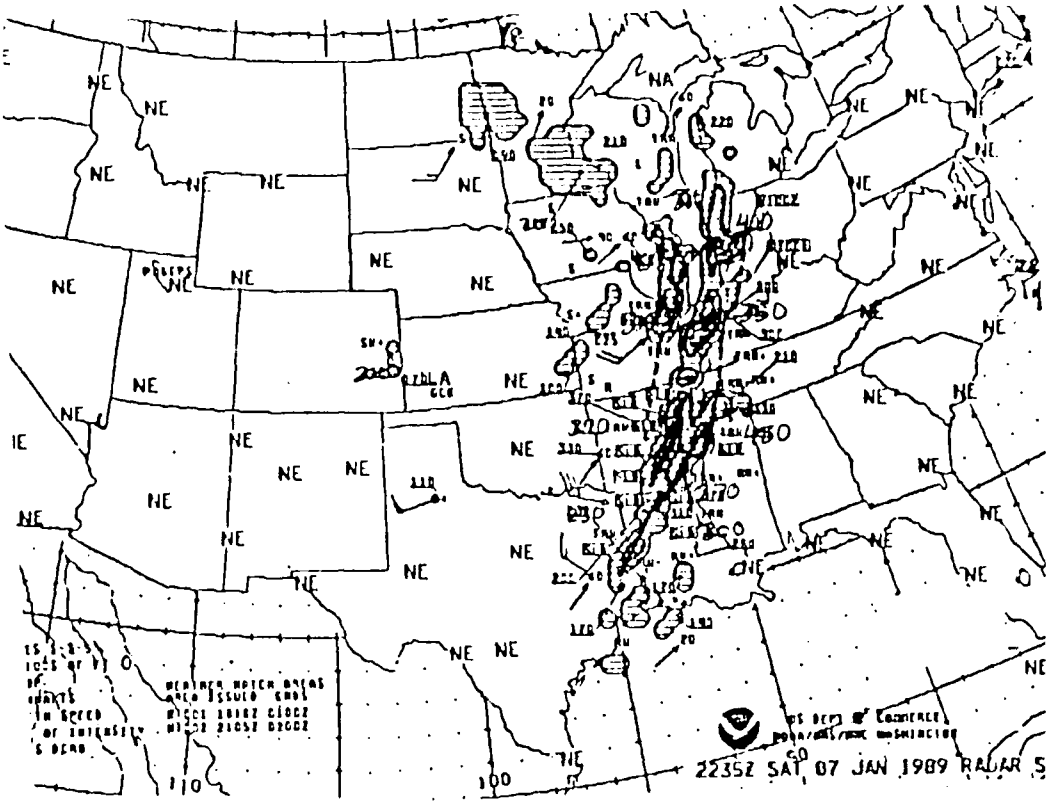

Fig. 68. Same as Fig. 65, except at 2335 G.M.T..

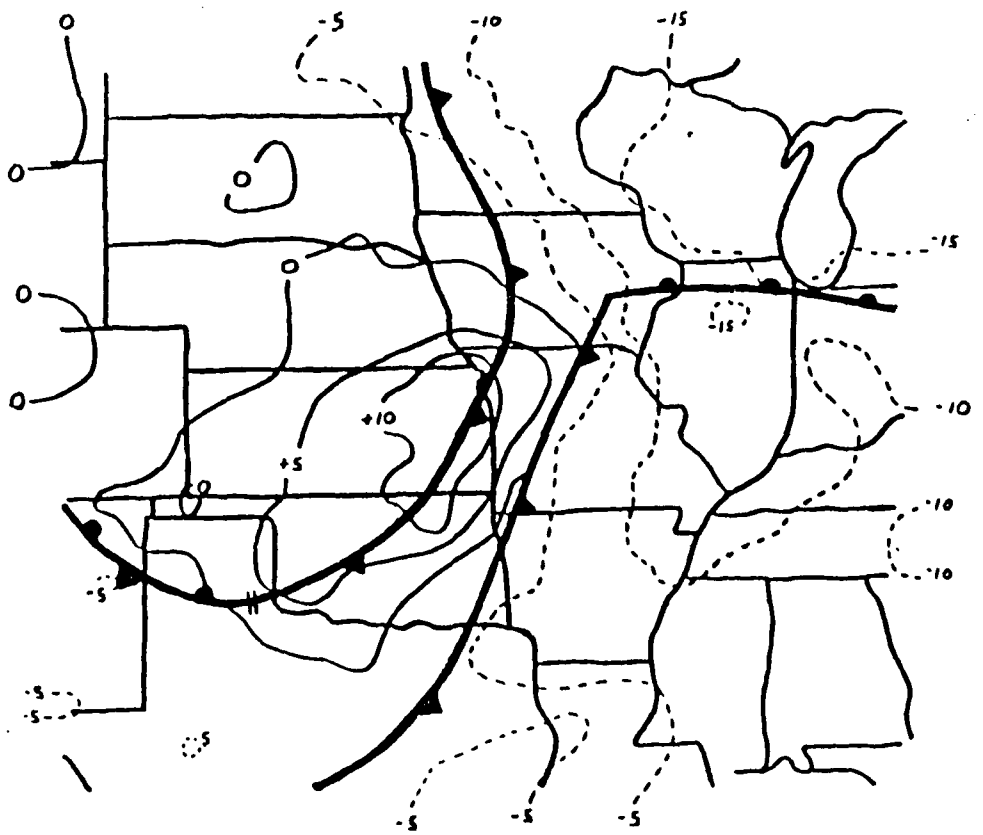

Fig. 69. Tendency of D values at 1800 G.M.T. 7 January 1989 (mhr^{-1}). Height falls are indicated by dashed lines and height rises by solid lines. Surface frontal positions are superimposed.

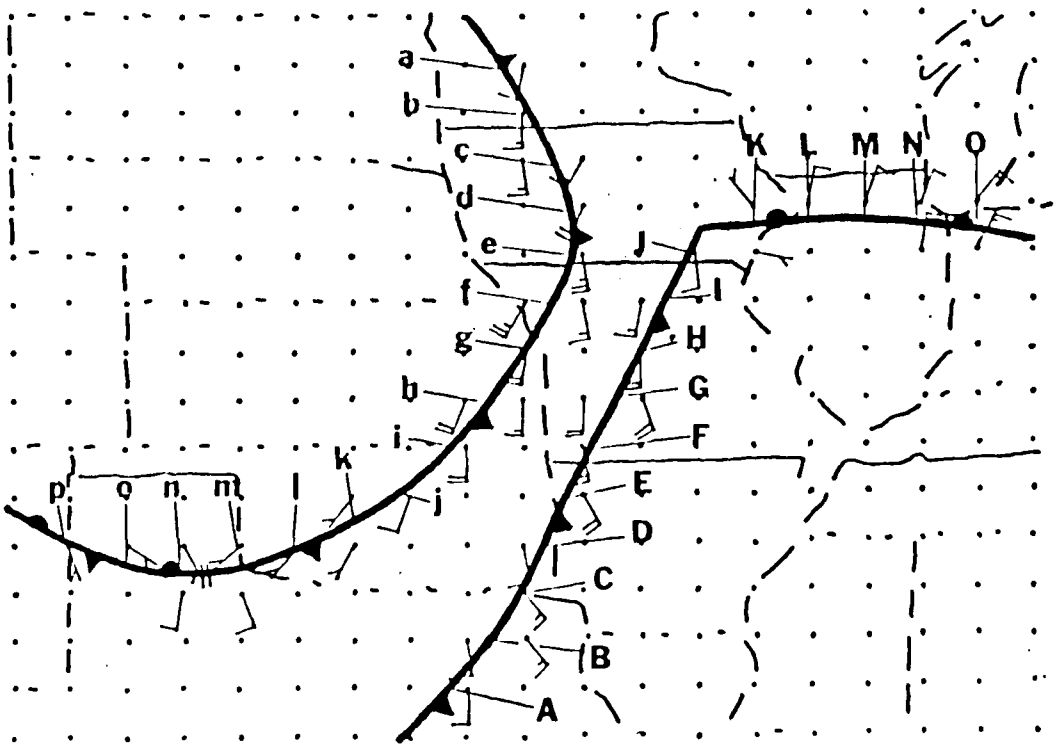

Fig. 70. 1800 G.M.T. ageostrophic winds plotted at the grid points used to determine the crossfrontal components by the actual, geostrophic, and isallobaric winds. Letters designate frontal segments on superimposed fronts.

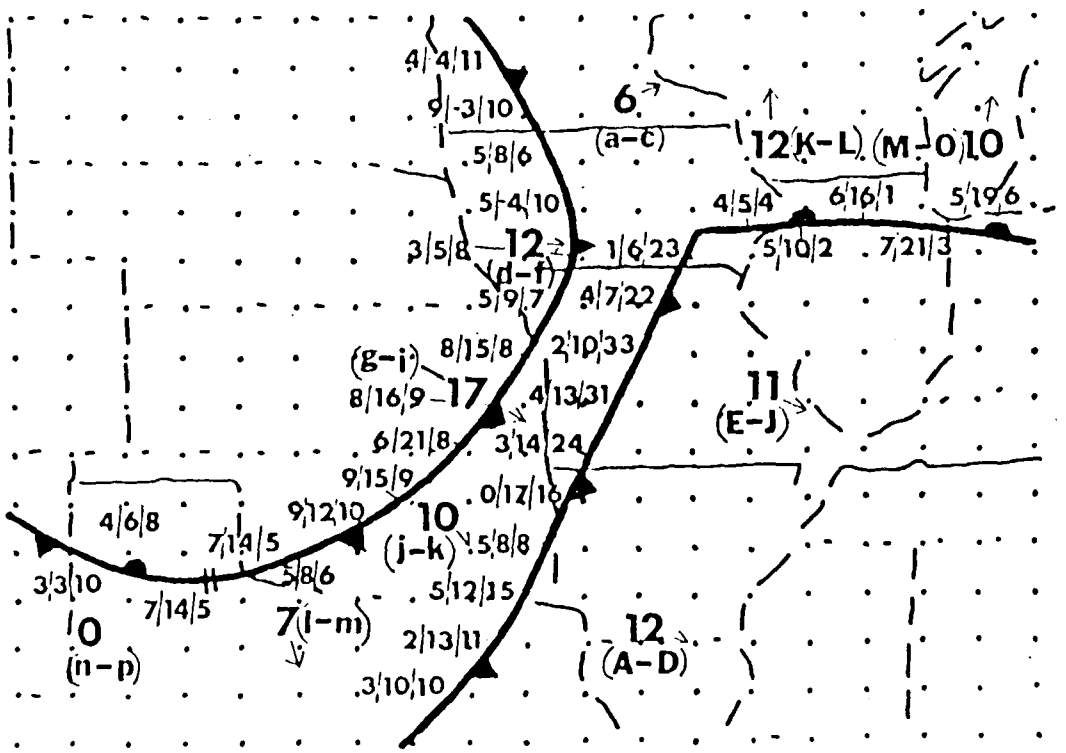

Fig. 71. Frontal velocity map for the period 1800-1900 G.M.T. 7 January 1989. Frontal velocities (m s^{-1}) are indicated by the larger numbers and correspond to the frontal segments indicated in parenthesis by the frontal velocity. Arrows indicate the approximate direction of motion. Small numbers indicate the crossfrontal component (m s^{-1}) by the actual/geostrophic/isallobaric winds. Positive (negative) cross frontal components indicate flow in the same (opposite) direction of frontal motion.

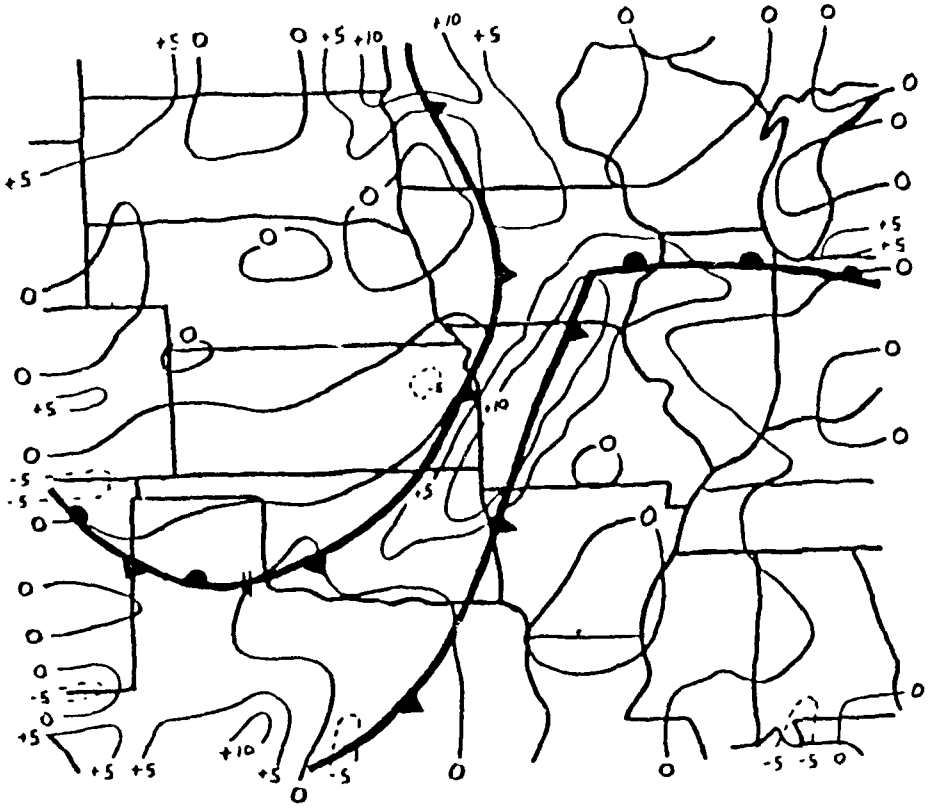

Fig. 72. Frontogenetical forcing due to the actual wind at 1800 G.M.T. 7 January 1989 ($X\ 10^{30}\ K\ km^{-1}\ hr^{-1}$). Positive (negative) values represent frontogenesis (frontolysis). Surface frontal positions are superimposed.

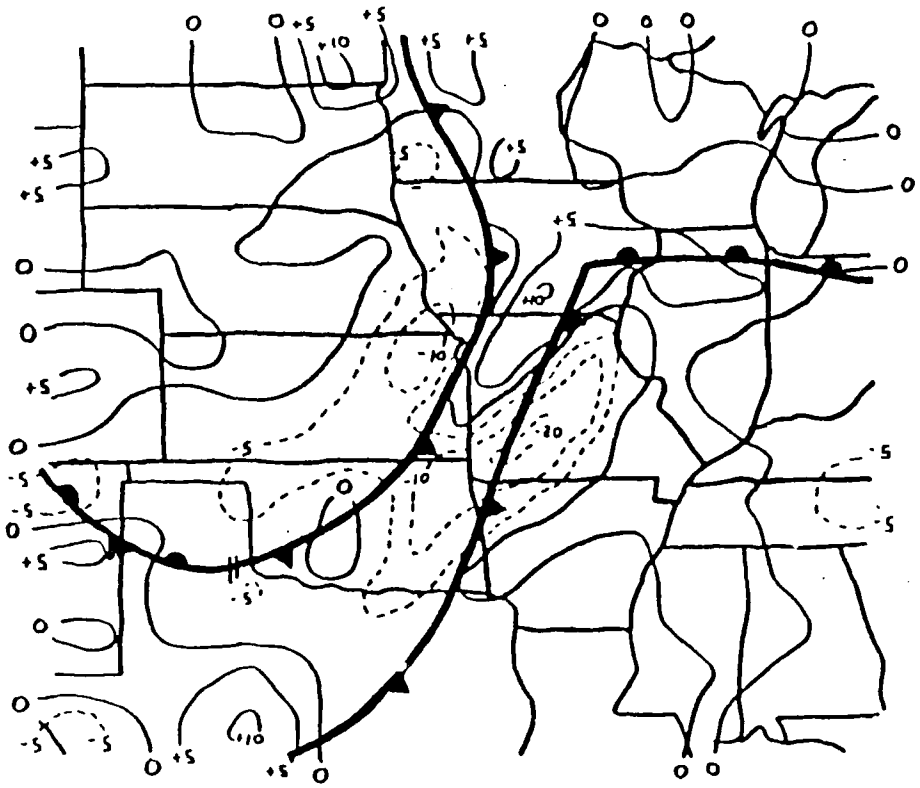

Fig. 73. Same as Fig. 72, but due to the isallobaric wind.

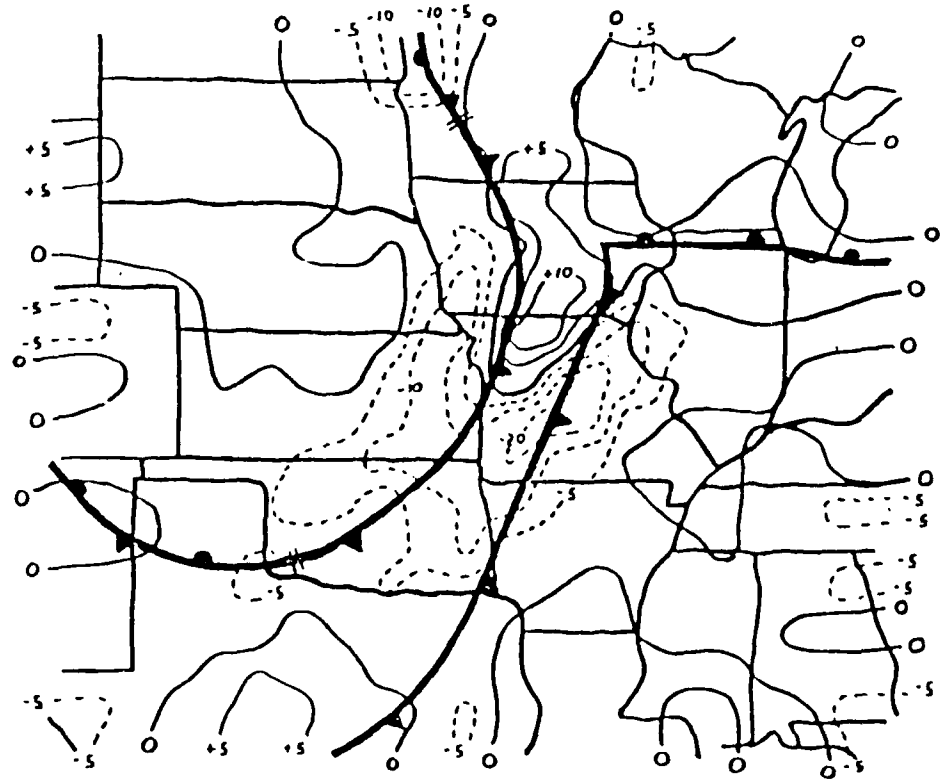

Fig. 74. Same as Fig. 73, except at 1900 G.M.T..

The actual wind frontogenetical forcing is contributing to an eastward propagation of frontal section f-h, but the suggested isallobaric influence on the actual wind frontogenetical forcing promoting the propagation occurs in a gradient of D value rises. In contrast, the "apparent" propagation potentially due to isallobaric influence on the actual wind frontogenetical forcing over frontal section a-c lies in D tendencies hypothesized as favorable for this phenomenon. Similar results are observed for the 1900 G.M.T. isallobaric (Fig. 74) and actual wind (Fig. 75) frontogenetical forcing with only minor changes observed in the D tendency field (Fig. 76). These differences in frontogenetical forcing versus the D tendencies were due to the temperature tendencies term. Notice the difference in the 1900 G.M.T. gradient of D tendencies across the frontal section over Minnesota and the frontal section extending from central Iowa to northern Missouri (Fig. 76). The 1900 G.M.T. temperatures fitted to the grid (Fig. 77), illustrate that the stronger gradient of D change values (and therefore isallobaric winds, Fig. 76) occurs in the maximum temperature gradient. As demonstrated in the 31 January case study, this combination promotes frontogenesis due to gradient of advection portion of the temperature tendencies term. In contrast, over southwestern Missouri the maximum temperature gradient (Fig. 77) is over the D rise maxima and a broad area of frontolysis occurs. The weaker temperature gradient combined with a weaker D tendency gradient associated with the front over Minnesota allowed a dominant divergence term and subsequent "apparent" propagation was indicated as in the hypothesized D tendency field (Fig. 1).

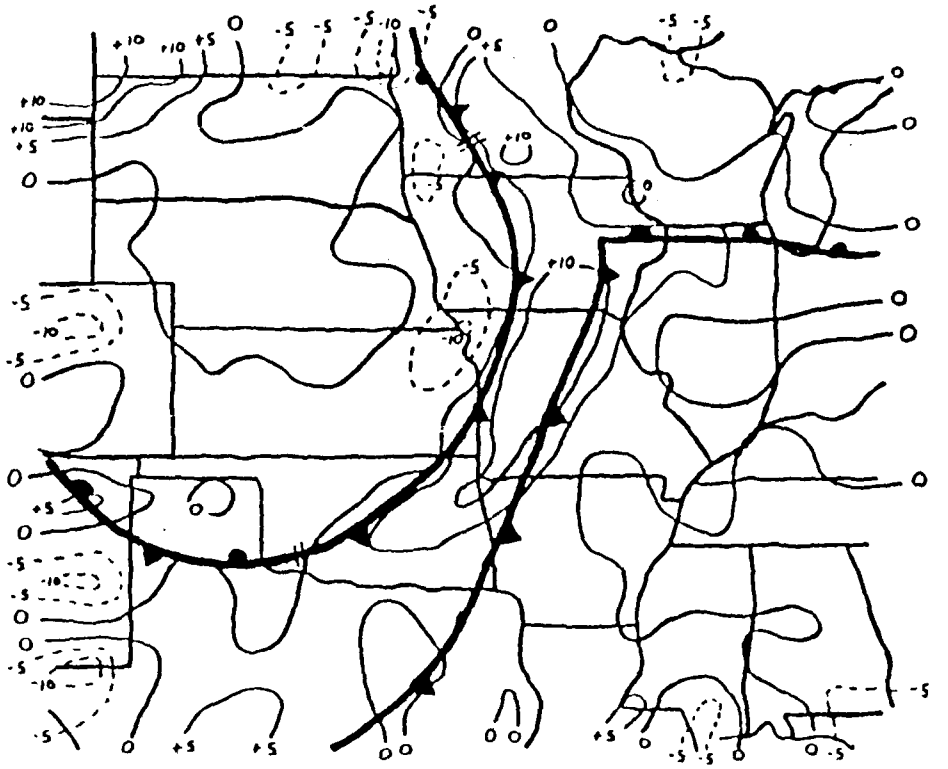

Fig. 75. Same as Fig. 72, except at 1900 G.M.T..

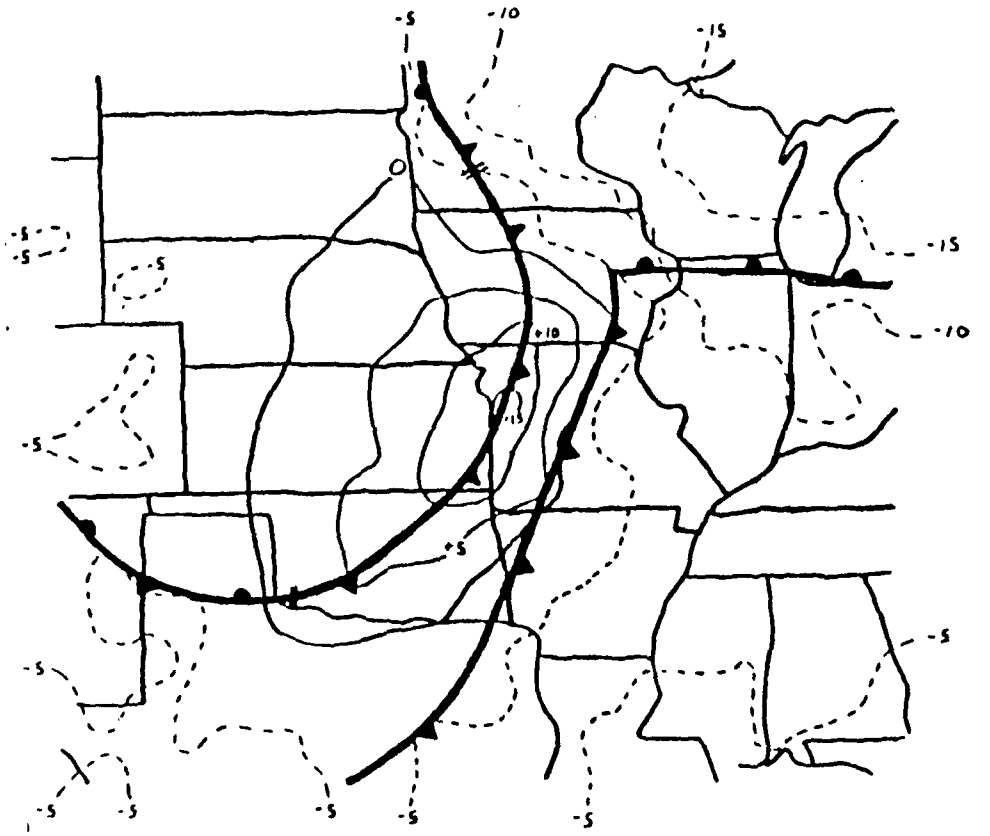

Fig. 76. Same as Fig. 69, except at 1900 G.M.T..

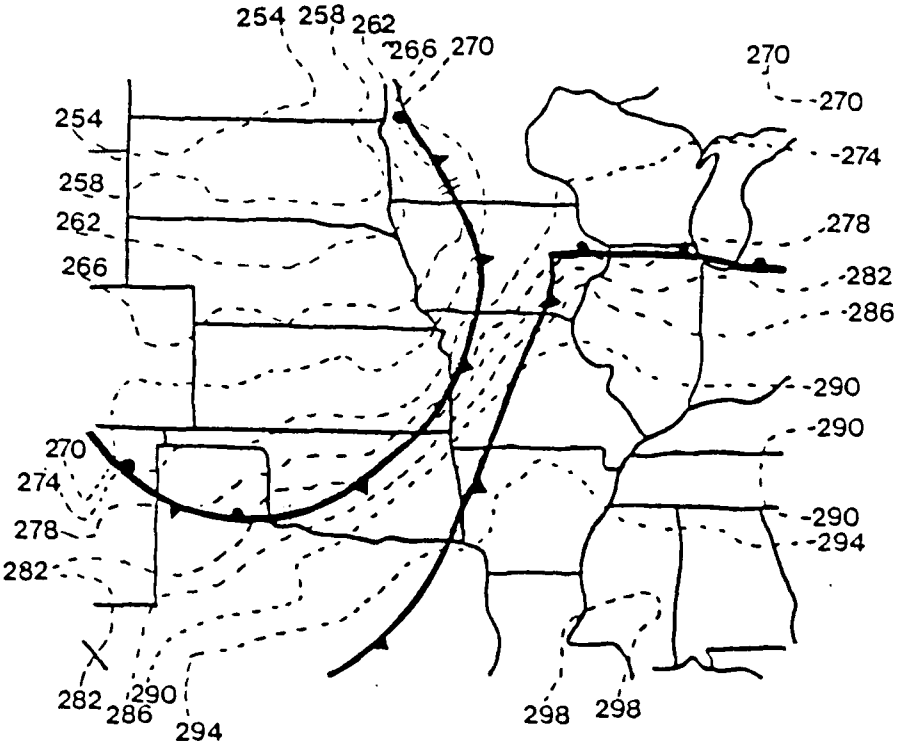

Fig. 77. Temparatures (°K) fitted to the grid points for 1900 G.M.T 7 January 1989. Dashed lines are isotherms analysed at 4°K intervals. Surface frontal postions are superimposed.

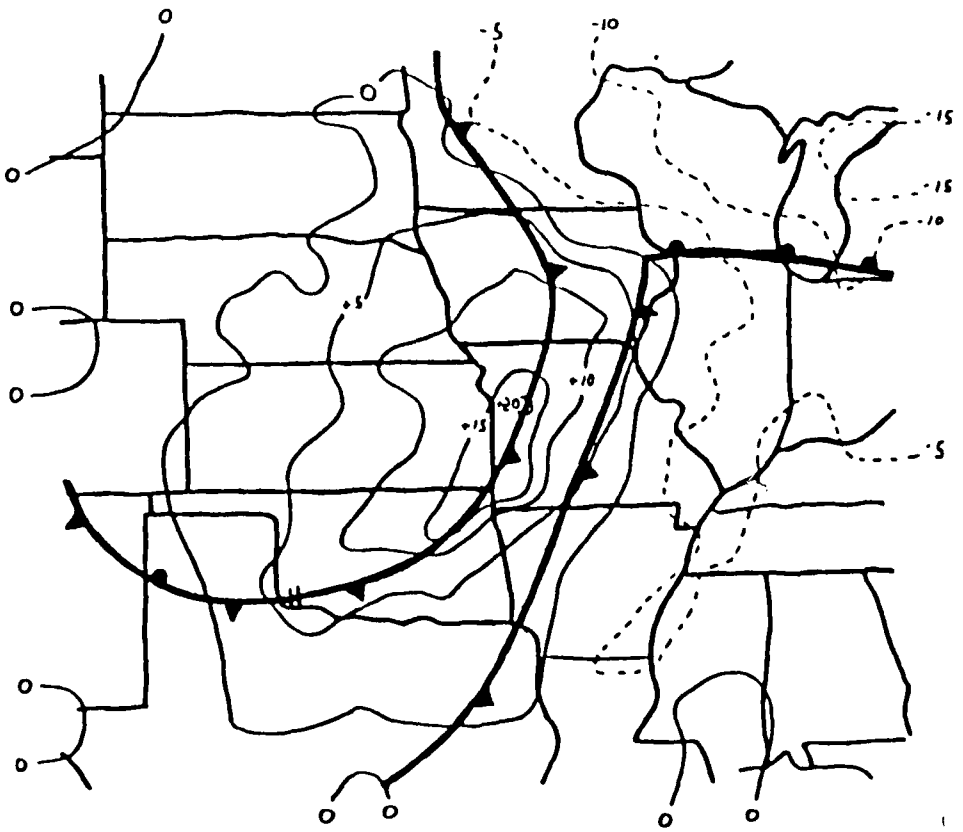

Fig. 78. Same as Fig. 76, except at 2000 G.M.T..

By 2000 G.M.T., the D value rise gradient (Fig. 78) now extended across frontal section B-K (Fig. 79). Isallobaric influence on the actual wind crossfrontal components is suggested on frontal segments a-d, l-n, and H, J, K, and L (Figs. 79 and 80). Notice that this hour had the rare occurrence of an isallobaric influence where the maximum isallobaric crossfrontal component was indicated (segment H, Fig. 79). In addition, the first occurrence of an isallobaric influence on the actual wind crossfrontal component associated with the warm front is suggested. Frontogenetical forcing due to the isallobaric wind (Fig. 81) demonstrated a change similarly observed in the 31 January case study. In particular, the sudden appearance of a large area of frontolysis. While frontolysis was occurring across both of the cold fronts in previous hours, its location was farther south and did not encompass the area indicated at 2000 G.M.T. Recall in the 31 January case study, that the frontolysis was due to a repositioned D value rise center over the maximum temperature gradient and subsequent dominance by the divergence term. In this case, the reason was due to a combination of terms. In addition, the decrease in the 2000 G.M.T. D tendency gradient (Fig. 78) over the location of the maximum temperature gradient, provides a partial explanation for the absence of frontogenesis. It is interesting to note the decreased magnitude of D value tendencies and a decreased isallobaric contribution (as compared to the 31 January case study) to the actual wind frontogenetical forcing (Fig. 82). Isallobaric contributions to frontal motion are again suggested, but the geostrophic wind crossfrontal components are more useful for diagnosing most of the observed frontal motion from 2000

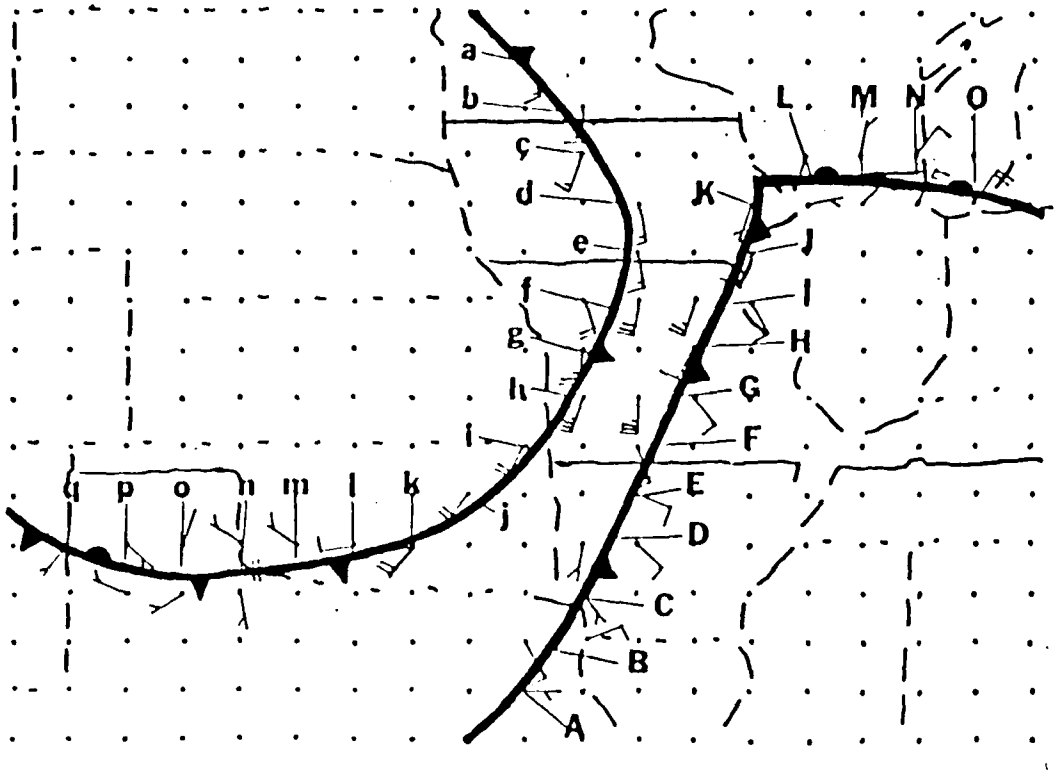

Fig. 79. Same as Fig. 70, except at 2000 G.M.T..

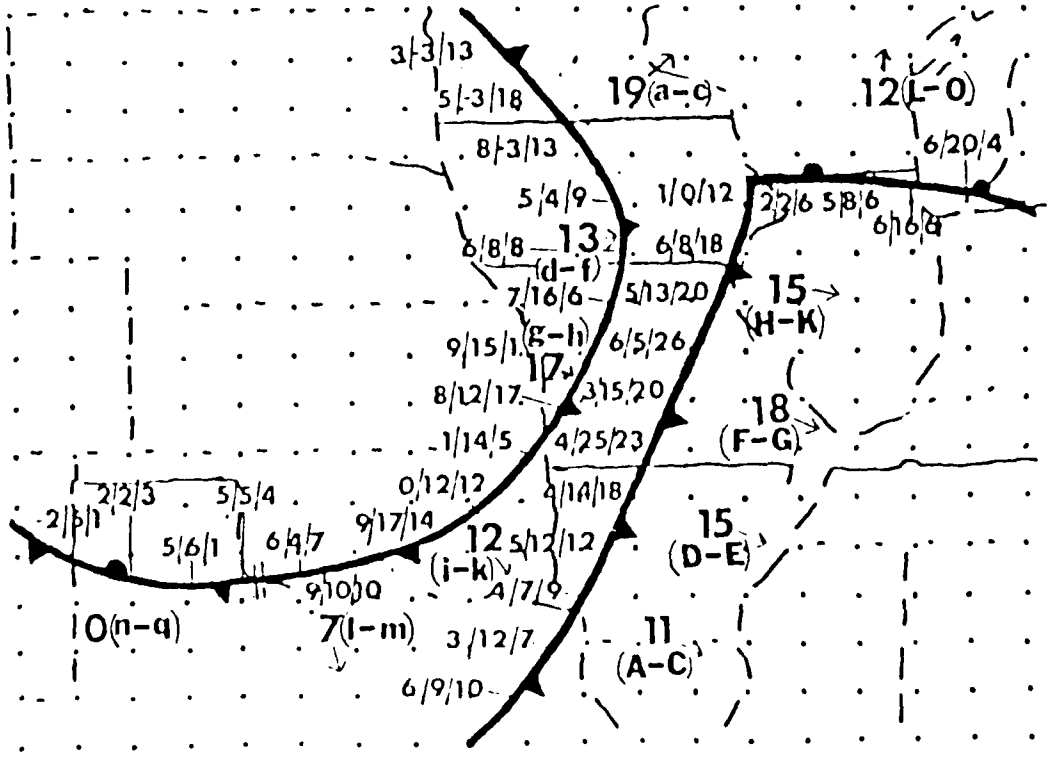

Fig. 80. Same as Fig. 71, except at 2000 G.M.T..

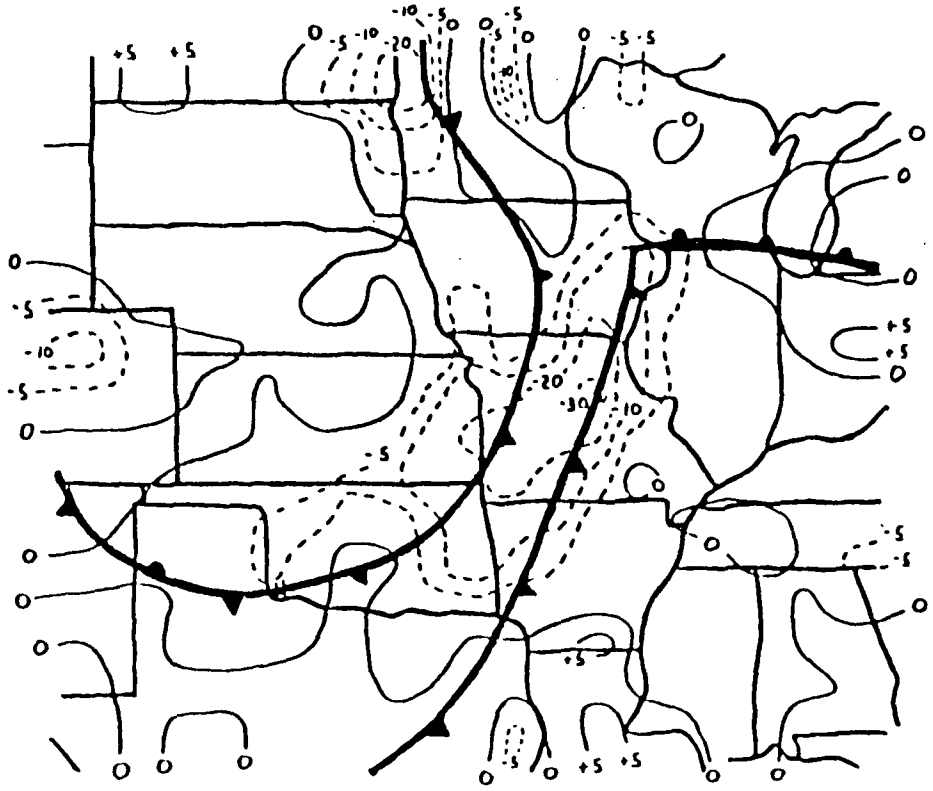

Fig. 81. Same as Fig. 74, except at 2000 G.M.T..

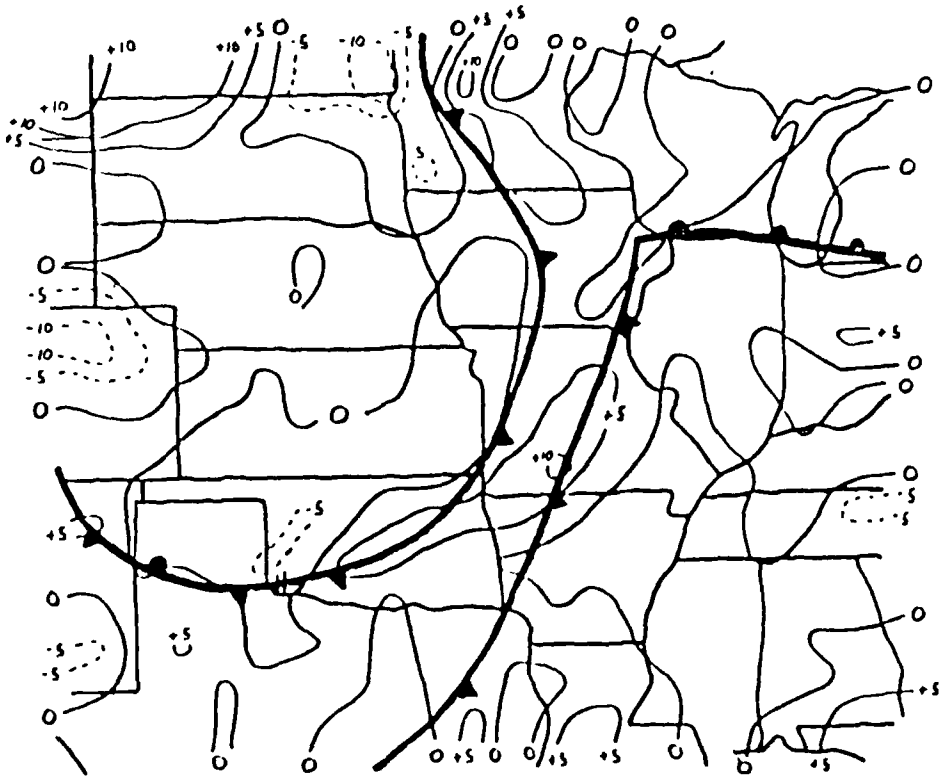

Fig. 82. Same as Fig. 75, except at 2000 G.M.T..

G.M.T. to 2100 G.M.T.

This case study was similar to the two previous case studies in that limited and somewhat random areas of isallobaric influences on the actual wind crossfrontal components were indicated. Similarities to the 15 November case study include the following: First, only one section of a cold front displayed a consistent isallobaric influence on the actual wind crossfrontal components. Furthermore, the observed movement of this frontal section was in better agreement with actual than geostrophic crossfrontal components. Second, although the D tendency field was different, the frontal section where an isallobaric influence on the actual wind crossfrontal components was suggested also indicated an isallobaric frontogenetical forcing contribution which promoted "apparent" propagation. The most significant similarity to the 31 January case study was the appearance of isallobaric induced frontolysis in the frontogenetical forcing due to the actual wind. In both case studies, this was due to the D value rise center positioned over the maximum temperature gradient. However, the decreased magnitude of isallobaric accelerations in this case study still contributed to similar patterns in the actual wind frontogenetical forcing. It is possible therefore, that the amount of isallobaric influence on the the actual wind frontogenetical forcing is directly related to the strength of the isallobaric acceleration. This hypothesis has two assumptions: Firstly, that the magnitude of the temperature gradients are similar. Secondly, other terms comprising the ageostrophic wind are similar in magnitude. While the first assumption is fulfilled in this case, the second assumption is by no

means a certainty. However, it is possible that friction at the surface is so dominant that the magnitudes of the other accelerations (besides the isallobaric acceleration) comprising the ageostrophic wind are insignificant.

4. Summary and Suggestions For Future Research

Despite the fact that the isallobaric influence of the actual wind crossfrontal components had frontogenetical forcing had to be subjectively diagnosed, this research has provided observational evidence that isallobaric forcing can be a contributor to surface frontal motion and frontogenesis. Indications of an isallobaric contribution to surface frontal motion through comparison of actual and geostrophic crossfrontal components are constrained by three assumptions:

1) The assumption of a front as a material surface.

This assumption has been debated since the inception of fronts and to date neither frontal theory nor observation has provided an answer. As noted by Reeder and Smith (1988), the assumption that a front is a material surface is useless in the case of a frontal zone which moves faster than the measured wind ahead or behind the front at any level.

2) The assumption that the winds at the grid points used to compute the crossfrontal components are representative of the force exerted by the wind on the front.

In particular, is the force imparted by the wind accurately represented on the frontal scale. Unfortunately, the answer is

is probably no. The inability to determine the significance of crossfrontal components on frontal motion opens the question of frontal location versus the location of the wind that gives a true measure of the force exerted on the front. However, Brundidge's (1965) results suggest that the most accurate measure of the force imparted on a front by the wind is close behind the frontal surface and the grid in this study does not have the resolution needed to represent the winds on the frontal scale.

3) The assumption that the frictionless isallobaric wind is representative of the isallobaric wind at the surface.

To some degree this assumption is valid; however, in theory the amount of difference between the two can be substantial (Young, 1973). The fact that stronger actual than geostrophic wind crossfrontal components were probably due to the isallobaric acceleration does suggest that there can be an isallobaric contribution to frontal motion. However, the limited areas of isallobaric influence on the actual wind crossfrontal components suggests that the isallobaric contribution to frontal motion is limited.

The actual wind frontogenetical forcing results of this study have demonstrated the occurrence of frontogenetical forcing patterns favorable for "apparent" propagation. Furthermore, this study has subjectively shown that isallobaric forcing can be a significant contributor to "apparent" propagation, but the diagnosed isallobaric influence on the actual wind frontogenetical forcing is constrained by the third assumption above as well. In the 15 November case study, convective precipitation could have contributed to the

"apparent" propagation demonstrated by the actual wind frontogenetical forcing. This study has shown that the temperature gradients associated with a front can go through a process of redevelopment. Obviously, three case studies do not give a full measure of the isallobaric influence on the actual wind frontogenetical forcing, but the results do allude to pressure tendency patterns most favorable for "apparent" propagation in the actual wind. Provided that the level of isallobaric influence is the same as observed in this study, these are as follows: First, large pressure falls ahead of the maximum temperature gradient with smaller pressure falls on or behind. Second, a weak gradient of pressure rises behind and pressure falls ahead of the maximum temperature gradient, respectively. Finally, it is possible, that when a significant pressure rise center moves over the maximum temperature gradient frontolysis will be indicated by the actual wind frontogenetical forcing. Whether or not the frontogenesis ahead of the temperature gradient will occur is uncertain.

Given the high degree of uncertainty associated with crossfrontal components, the frontogenetical forcing results provide the most promising area for future research. Recall that the frontogenetical forcing computations in this study considered only temperature. Since moisture amounts can affect the density of two different air masses, a follow-on study which includes the effects of moisture by use of the virtual temperature could easily be done. A less subjective method to define the isallobaric influence on the actual surface wind frontogenetical forcing would be to include the effects of friction on the isallobaric wind. In addition, a wider

range of pressure tendency fields should be covered to determine the limitations of the isallobaric influence on the actual wind versus the magnitude of the pressure tendency. Young (1973) has established the theoretical groundwork for inclusion of the frictional isallobaric wind. However, a study of this nature would still have uncertainty due to the other terms that comprise the ageostrophic wind. Finally, a study to determine the velocity induced on a front by the frontogenetical forcing process would be constrained by the uncertainty of temperature gradient velocity versus frontal velocity, but could establish a range of velocities versus the magnitudes of the temperature gradient.

APPENDIX A - Data Checking Methods Used

Screening for errors in the data set consisted of a three step process. First, all station data was compared to predetermined boundary values for each element. The high and low boundary values used were as follows: 75 and 0 °F for temperature, 60 and 0 °F for dewpoint, 360 and 0 degrees for wind direction, 25 and 0 kts for wind speed, and 30.50 and 29.80 inches for altimeter settings. Values outside the boundary conditions were identified and checked against the original and corrected airway reports. Second, temperatures, dewpoints, and altimeter settings at every observation location were compared to the same elements at all other reporting stations within a 130 km radius from the observation location. Values at the observation location outside the specified range for each element were identified and checked against the original teletype reports.

The ranges used were as follows: 5° F for temperature, 5 °F for dewpoint, and .05 inches for altimeter setting. Due to the high variability in wind direction and speed by local effects alone, wind direction and speed were not checked in this manner. Finally, temperature, dewpoint, wind direction, wind speed, and altimeter setting values at each observation location were identified and checked if the difference was greater than 5° F, 4° F, 35°, 5 kts, and .05 inches, respectively from the preceding hour.

A more subjective correction of improperly dissmenated elements was required in some cases. Obvious dissemination errors were easily identified and corrected. For example, the altimeter setting reported as 28.67" in a intermediate hour and reported as 29.64" in the preceding hour and 29.70" in the third hour. More difficult to identify as errors were the not impossibly large changes of a particular element. For example, large pressure changes were checked against required remarks, pressure values for the hours on either side, and against pressure changes by nearby locations. Overwhelming evidence was required to remove data that fell into this category. These data checking methods do not guarantee an error free data set as smaller errors by dissemination and data entry could pass through the error checking routines and introduce noise into the results.

In some case studies, the strengtn of the computed isallobaric wind raised doubts about the validity of the method. Confirmation of the isallobaric wind values computed was achieved by another computer program using the change of pressure formula (Eq. 17) for the isallobaric wind. Perfect agreement was found at most grid points. Small differences in the wind direction and wind speed did occur at

some grid points. These differences were most likely due to rounding by the computer as the the wind direction at each grid point was rounded to the nearest 10°. The largest differences noted were on the order of 30° and 4 kts for the wind direction and wind speed, respectively. Directional differences of this magnitude occurred where the isallobaric wind magnitudes were weak and speed differences occured where the magnitudes were exceptionally large.

APPENDIX B - Description of the Cressman (1959) Weighting Scheme

Since an objective analysis produces an approximation of the value of an observed or computed parameter at grid points, consideration of the error produced by the objective analysis scheme is necessary. The computer code used for the Cressman (1959) weighting scheme is a modified form of the code presented by Inman (1970). A general discussion will be used to qualitatively asses the error introduced by the objective analysis method. Let T^s represent the temperature of a given observation location where s is the scan number. The correction $C^s_{i,j}$ applied to the grid point i,j under consideration by the temperature of the observation location is calculated by

$$C^s_{i,j} = W\, T^s / W. \qquad \text{(B1)}$$

W in Eq. (B1) is a distance dependent weight factor that is determined by the distance of the observation location from the grid point using the equation below.

$$W = ((R^2 - d^2)(R^2 + d^2)^{-1}), \tag{B2}$$

where d is the distance between the grid point and the observation location and R is the radius of influence specified. The magnitude of the weighting factor W from Eq. (B2) based on the distance between the grid point and the observation location is depicted in Fig. B1. The total correction applied to the grid point is a weighted average of all the observation locations within the radius of influence. When the distance (d) between the grid point and the observation location is larger than R, the station element will not influence the correction applied to the grid point (W = 0). When the correction due to all stations within the radius of influence has been computed, the estimate of temperature at the grid point is calculated by

$$T^s_{i,j} = T^{s-1}_{i,j} + c^s_{i,j}. \tag{B3}$$

For the first scan, $T^{s}_{i,j}$ represents the first guess field. As McDonnell (1967) noted, first guess fields are not absolutely necessary for a successful application of the technique where sufficient data are available. Therefore, a zero first guess field was used. Before the next scan is executed, the current estimate of T^s is made at the observation location. The estimate is made from values at the four surrounding gridpoints using the bilinear interpolation formula as given by Inman (1970),

$$T^s_p = T^s_1 + (T^s_4 - T^s_1)\Delta y/b + (T^s_2 - T^s_1)\Delta x/a - (T^s_2 - T^s_3 + T^s_4 - T^s_1)\Delta x\Delta y/ab, \tag{B4}$$

where T_p^s is the estimate of temperature at the observation location, T^s with a numbered subscript is the temperature at one of the four surrounding grid points, Δx is the distance in the x-direction from the y-coordinate of grid points one and four, Δy is the distance in the y-direction from the x-coordinate of the grid points, a is the distance between grid points along the x-axis, and b is the distance between grid points along the y-axis. Illustration of the terms in Eq. (B4), presented in Fig. B2, will help clarify the subsequent discussion. The formula assumes a square grid is used. For the latitude/longitude grid used, the y-direction grid spacing remains constant however, the x-direction spacing between points varies with latitude. The x-direction grid spacing in Fig. B2 was computed by taking the cosine of the station (p) latitude times the distance in the y-direction. In the worse case scenario, where the station latitude is the same as the latitude of grid points three and four or grid points two and one, the distance a would be approximately 1.4 km too long or short. Therefore, the approximation of a square grid in the bilinear interpolation formula does not introduce serious error. The computer code also allows use of observation locations outside the grid which permits the use of exterior grid points in the calculations discussed earlier.

Each field fitted to the grid was done using two scans, the first scan used a radius of influence of 160 km and the second scan had a radius of influence of 60 km. The requirement of a least two stations to be part of the correction was imposed on the first scan only. If two stations were not within the radius of influence during the first scan, the radius of influence was increased by the distance

between grid points in the y-direction (111.19 km) until the requirement was fulfilled. The two scan approach had a smoothing effect on the field fitted to the grid point on the first pass and smaller scale variations within the field were introduced in the second pass by the use of a much smaller radius of influence. However, a distance weighting scheme is not the best objective analysis procedure according to Thiebaux and Pedder (1987). They noted that the use of a distance weighting scheme can lead to large biases in the grid point data, due to no consideration being given to the observation locations relative to one another. For example, if two stations are within the radius of influence for a particular grid point and they are both located in approximately the same direction and distance from the grid point, the correction by each observation location is given the same weight which may produce a somewhat erroneous value for the grid point.

APPENDIX C - Computation of Station Pressures, Virtual Temperatures, Gravity Variations, and Data Smoothing

In order to increase the number of observations available for each hour, missing temperatures, dewpoints, and altimeter settings were replaced by taking the average value of the hour before and after the hour under consideration. If the respective element was missing either the hour before or after, no value for the missing element was calculated. Altimeter settings were converted to station pressures (P_{sr}) using

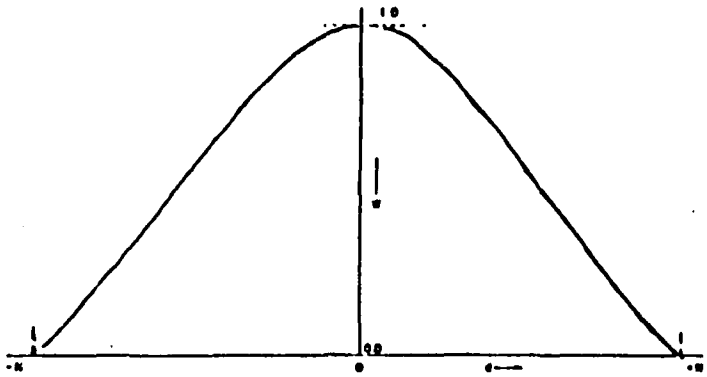

Fig. B1. Curve of the weighting function W vs. distance d. (After Cressman, 1959).

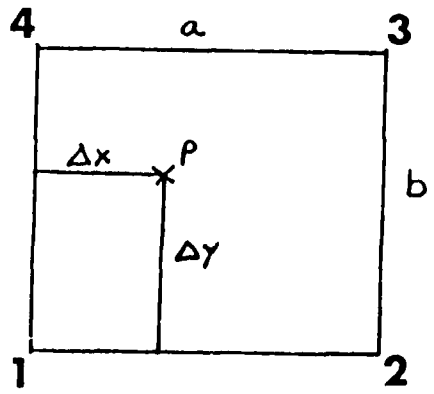

Fig. B2. Illustration of the values used in the bilinear interpolation formula. (After Inman, 1970).

$$P_{ST} = [A^n - (P_o^n L/T_o)Z_{ele}]^{1/n}, \quad (C1)$$

where P_o is the standard atmospheric sea level pressure (1013.25 mb), A is the altimeter setting (mb), L_o is the standard atmospheric lapse rate (6.5^o Kkm^{-1}), T_o is the standard atmospheric sea level temperature (288^oK), Z_{ele} is the elevation of the station above sea level (m), and $n = L_o R_d g^{-1} = .19$. Virtual temperature (Tv) was computed from the approximation

$$T_v = T(1 + 0.61w), \quad (C2)$$

where w is the actual mixing ratio (Kg Kg^{-1}). The actual mixing ratio may be determined by

$$w = 0.622e(P_{ST} - e)^{-1}, \quad (C3)$$

where e is the actual vapor pressure (mb). The actual vapor pressure was determined from the method used by Koehler (1979).

$$e = e_s \exp[-(L/R_v)(1/T_d - 1/T)], \quad (C4)$$

where e_s is the saturation vapor pressure (mb), L is the latent heat of evaporation ($m^2 s^{-2}$), Rv is the water vapor gas constant ($m^2 s^{-2} {}^oK^{-1}$), Td is the dewpoint temperature (^oK), T is the temperature, and a value of 5430^oK was used for the ratio $L R_v^{-1}$. The saturated vapor pressure was calculated from the approximation given by Tetens (1930).

$$e_s = 6.11 \times 10^{(aT/b+T)}, \quad \text{(C5)}$$

where the values used for the constants (a = 7.5, b = 237.5) are for over a water surface and T is the temperature (°C). Variations in gravity (g) due to elevation and latitude of the observation location was computed from the following (Haltiner and Martin, 1957):

$$g = 980.62(1-0.00259\cos 2\phi)(1-3.14 \times 10^{-7}z), \quad \text{(C6)}$$

where ϕ is the latitude and z is the elevation (m). The five-point formula from Cressman (1959) used to smooth station elevations and the total frontogenetical forcing by the actual, ageostrophic, and isallobaric winds was

$$A = 0.5A + 1/8\Sigma A, \quad \text{(C7)}$$

where ΣA is the sum of the values of A at the four nearest grid points.

APPENDIX D - Sensistivity Study on Frontogenetical Forcing

Winds in the area of interest were measured at the standard height of 3.0 m (10 feet) above the surface. Reported wind directions and speeds represent a two minute average for all nonmilitary locations (one-minute for Air Force observations). The use of measurements taken as much apart as 20 minutes before or after as being representative of the actual surface wind over the region

opens questions to the validity of the resultant frontogentical forcing for the actual wind. To obtain a qualitative measure of possible error, (wind direction and wind speed) 50 randomly selected stations from 1900 G M.T. on the 31 Jan 89 case study were changed by either subtraction or addition of 10^{o} and 2 kts, respectively. After the results were obtained for the altered conditions given above, the same 50 observation locations wind direction and wind speed were altered by random subtraction or addition of 20^{o} and 4 kts, respectively. Observation locations and the changed wind velocities are listed in table D1. A count of the missing and altered stations in table D1 yields only 47 stations; this is due to three numbers being repeated by the random number generator used. Subtraction of the missing stations leaves a total of 40 changed wind velocities. During this hour 293 stations reported wind velocities, hence the 40 changed stations represents almost 14% of the total reporting stations. Locations of the 40 stations are depicted in Fig. D1.

Frontogentical forcing by the actual wind, actual wind with 40 stations altered by 10^{o} and 2 kts, actual wind with 40 stations altered by 20^{o} and 4 kts are displayed in Figs. D2-D4. Perusal of these figures reveals little change in the frontogenetical forcing pattern observed for the actual wind. Some magnitude changes are noted, but given the nonlinear terms in Eq. (24) the results were better than anticipated. The smoothing effect of the Cressman (1959) objective analysis scheme undoubtedly was the major reason why more dramatic changes were not noted. These results imply some error due to different measurement times and short measurement times for the actual wind. However, the error would appear to be manifested in the

magnitude and not in the horizontal pattern of the frontogenetical forcing.

NO.	ID	WIND	10 DEG 2 KT	20 DEG 4 KT
	BJI	M	M	M
1	MKG	2217	2115	2013
2	SBN	2217	2319	2421
3	OLU	2614	2512	2410
4	PIR	3516	3618	0120
5	AQQ	1307	1205	1103
6	IMT	2103	2201	0000
7	HRO	2211	2109	2007
8	BFF	2917	3015	3113
	TPL	M	M	M
9	MWA	1710	1612	1514
10	JXN	2310	2408	2206
11	TYS	2117	2019	1921
12	ESF	2420	2518	2616
13	TUP	2216	2118	2020
14	TCL	2012	2110	2208
15	LAF	2120	2222	2324
16	LFT	2010	1908	1806
17	MMO	2215	2317	2419
	ONM	M	M	M
18	MLU	2210	2312	2414
	FDY	M	M	M
19	BYH	2020	1918	1816
20	OWL	3315	3417	2519
21	LAR	2630	2528	2426
	HBR	M	M	M
22	ALS	1705	1807	1909
23	P35	2222	2120	2018
24	JBR	2216	2318	2420
25	MLI	2419	2517	2615
26	CVO	2219	2121	2023
27	HSV	2117	2219	2321
28	BNI	2225	2123	2021
29	ICT	2413	2515	2617
30	PTK	2316	2214	2112
31	LIC	2617	2719	2821
	VDO	M	M	M
	DYR	M	M	M
32	MLC	2015	1913	1812
33	TIK	2222	2324	2426
34	GCK	2614	2514	2412
35	SNY	2725	2827	2929
36	TOP	2313	2415	2517
37	BVV	2412	2310	2208
38	CEW	2006	2108	2210
39	P07	3411	3309	3207
40	BAU	2707	2809	2911

Table D1. Summary of the stations where the wind velocities were altered. the direction and magnitude of the changes are indicated in the last two columns.

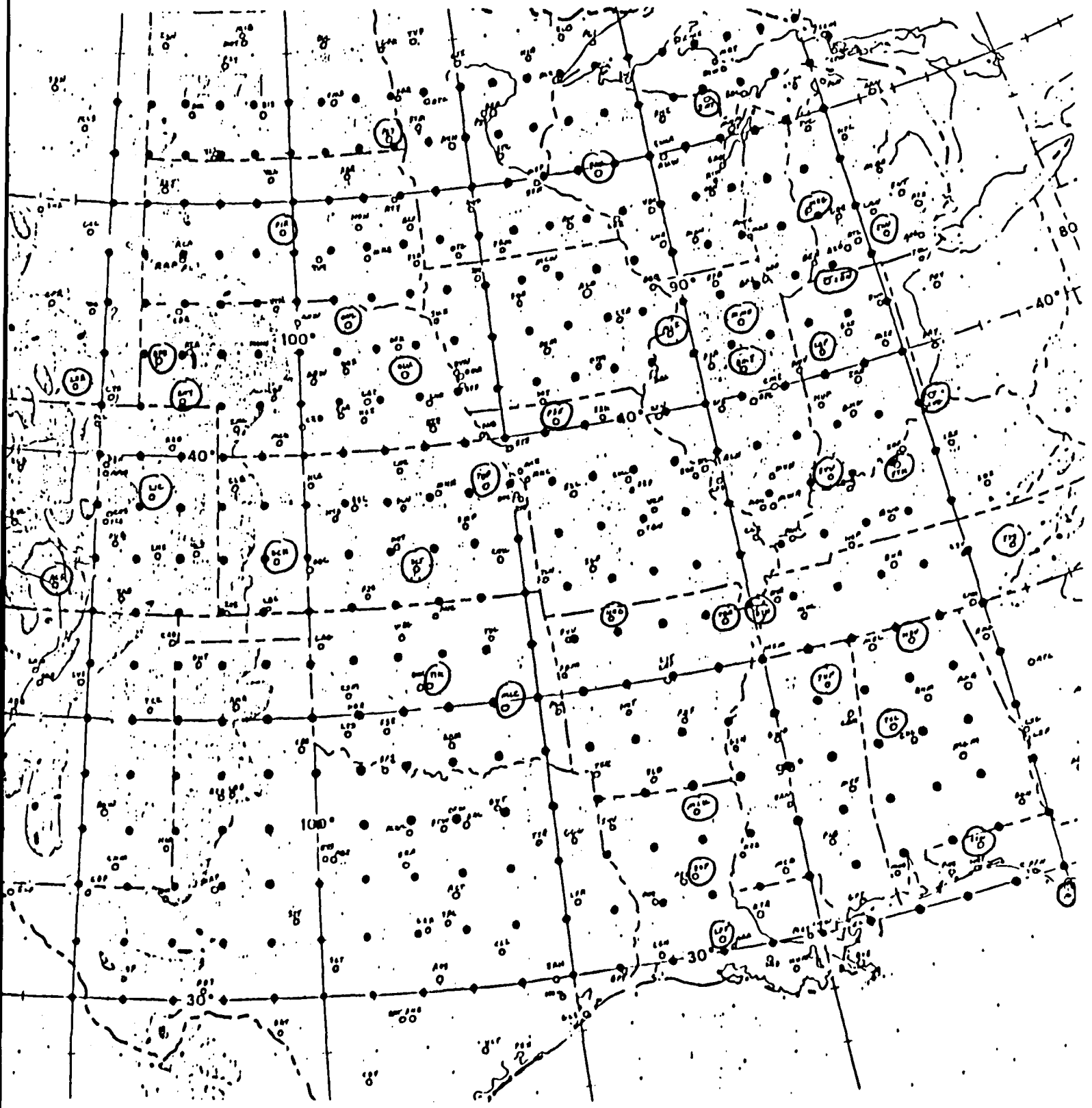

Fig. D1. Location of the 40 stations where the actual winds were altered. Stations listed in Table D1. are circled.

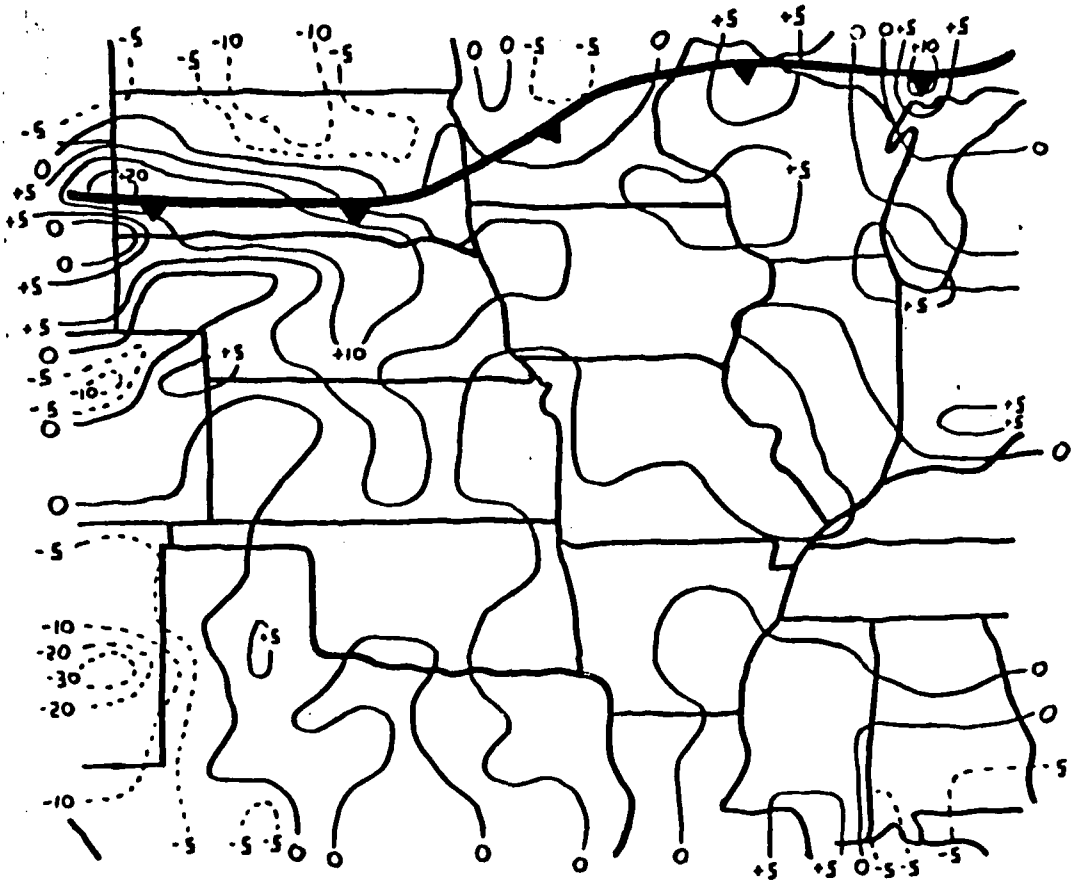

Fig. D2. Frontogenetical forcing due to the actual surface winds at 1900 G.M.T. 31 January 1989 (X 10^{3} °K $km^{-1}hr^{-1}$). Positive (negative) values represent frontogenesis (frontolysis). Surface frontal position is superimposed.

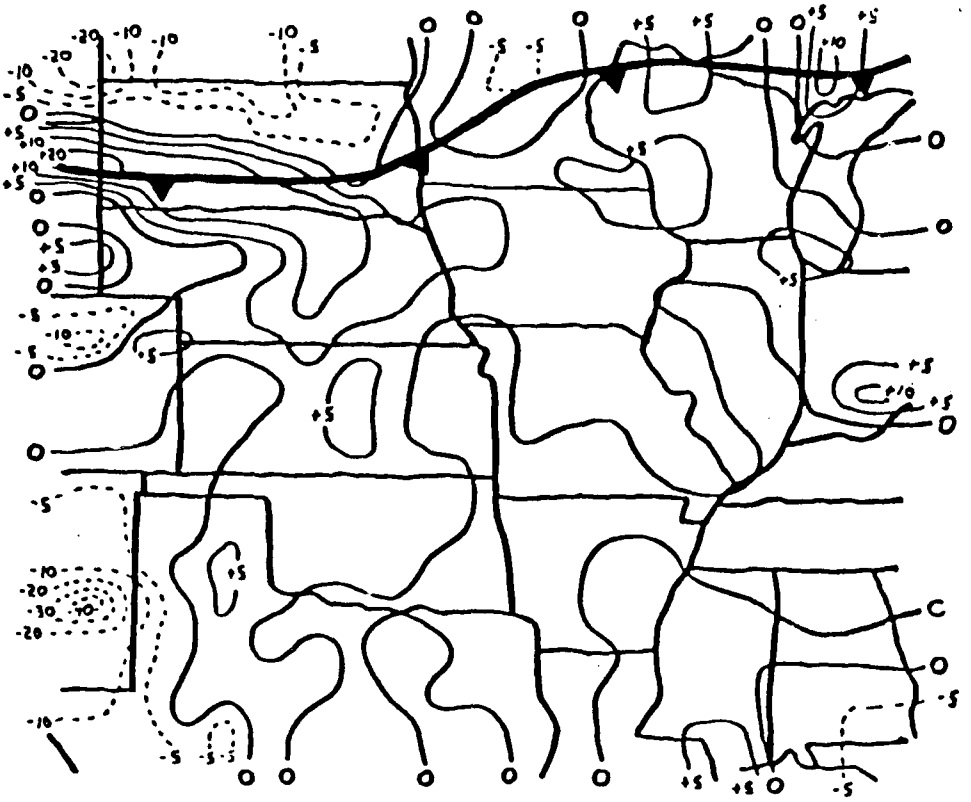

Fig. D3. Same as Fig. D2, but with changed wind velocities (10°, 2 kts).

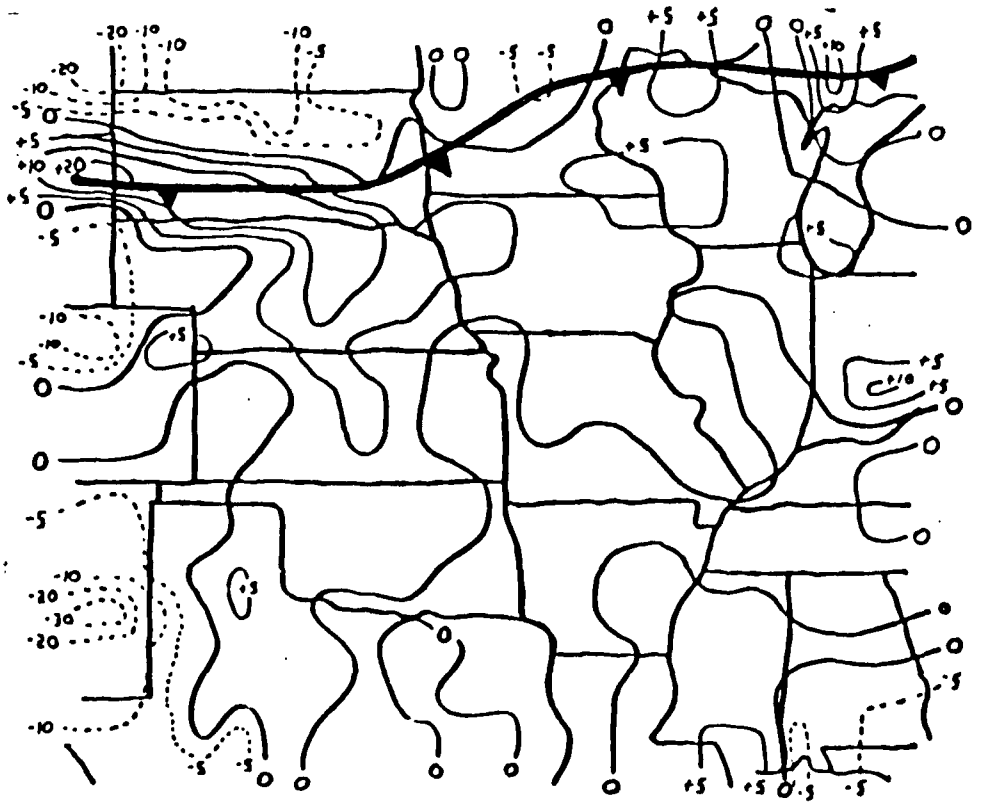

Fig. D4. Same as Fig. D2, but with changed wind velocities (20°, 4 kts).

REFERENCES

Bellamy, J. C., 1945: The use of pressure altitude and altimeter corrections in meteorology. J. Meteor., 2, 1-79.

Bergeron, T. 1937: On the physics of fronts. Bull. Amer. Meteor. Soc., 18, 265-275.

Bond, N A., and R. G. Fleagle, 1985: Structure of a cold front over the ocean. Quart. J. R. Meteor. Soc., 111, 739-759.

Bonner, W. D., and J. Paegle, 1970: Diurnal variations in boundary layer winds over the south-central United States in summer. Mon. Wea. Rev., 98, 735-744.

Browning, K. A., and G. A. Monk, 1982: A simple model for the synoptic analysis of cold fronts. Quart. J. R. Meteor. Soc., 108, 435-452.

Brundidge, K. C., 1965: The wind and temperature structure of nocturnal cold fronts in the first 1420 feet. Mon. Wea. Rev., 93, 587-603.

Brunt, D., and C. K. M. Douglas, 1928: The modification of the strophic balance for changing pressure distribution, and its effect on rainfall. Mem. Roy. Meteor. Soc., 3, 29-51.

Cressman, G. P., 1959: An operational objective analysis system. Mon. Wea. Rev., 87, 367-374.

Haltiner, G. J., and F. L. Martin, 1957: Dynamical and Physical Meteorology. New York, McGraw-Hill, 470pp.

Hobbs, P. V., and P. O. V. Pearson, 1982: The mesoscale and microscale structure and organization of clouds and precipitation in midlatitude cyclones. Part V: The struture of narrow cold-frontal rainbands. J. Atmos. Sci., 39, 280-295.

Hoskins, B. J., and F. P. Bretherton, 1972: Atmospheric frontogenesis models: Mathematical formulation and solution. J. Atmos. Sci., 29, 11-37.

Inman, R. L., 1970: Papers on operational objective analysis schemes at the National Severe Storms Forecast Center. Tech. Memo ERTLM-NSSL 51., 91 pp.

Jascourt, S. D., S. S. Lindstrom, C. J. Seman, and D. D. Houghton, 1988: An observation of banded convective development in the presence of weak symmetric stability. Mon. Wea. Rev., 116, 175-191.

Koehler, T. L., 1979: A case study of height and temperature analysis derived from Nimbus-6 satellite soundings on a fine mesh model grid. Ph.D. Dissertation, Department of Meteorology, University of Wisconsin-Madison, 185 pp.

McDonell, J. E., 1967: A summary of the first-guess fields used at the National Meteorological Center. Tech. Memo WBTMNM3-38., U. S. Weather Bureau, 17 pp.

Moore, J. T., and P. D. Blakley, 1988: The role of frontogenetical forcing and conditional symmetric instability in the midwest snowstorm of 30-31 January 1982. Mon. Wea. Rev., 116, 2155-2171.

Petterson, S., 1956: Weather Analysis and Forecasting, Vol 1. McGraw-Hill, 428 pp.

Reeder, M. J., 1986: The interaction of a cold front with a prefrontal thermodynamically well-mixed boundary layer. Aust. Meteor. Mag., 34, 137-148.

-----, and R. K. Smith, 1986: A comparison between frontogenesis in the two-dimensional Eady model of baroclonic instability and summertime cold fronts in the Australian region. Quart. J. Roy. Meteor. Soc., 112, 293-313.

-----, and -----, 1987: A study of frontal dynamics with application to the Australian summertime "cool change." J. Atmos. Sci., 44, 687-705.

Sangster, W.E., 1960: A method of representing the horizontal pressure gradient force without reduction of station pressures to sea level. J. Meteor., 17, 166-176.

-----, 1967: Diurnal surface geostrophic wind variations over the Great Plains. Preprints, Fifth Conf. on Severe Local Storms, St. Louis , MO, 146-153. Amer. Meteor. Soc.

-----, 1987: An improved technique for computing the horizontal pressure-gradient force at the Earth's surface. Mon. Wea. Rev., 115, 1358-1369.

Saucier, W. J., 1955: Principles of Meteorological Analysis. Chicago Press, 438 pp.

Smith, R. K., and M. J. Reeder, 1988: On the movement and low level structure of cold fronts. Mon. Wea. Rev., 116, 1927-1944.

Tetans, O. 1930: Z. Geophysics., 6.

Thiebaux, H. J., and M. A. Pedder, 1987: Spatial Objective Analysis: with applications in atmospheric science. Academic Press, 299 pp.

Young, J. A., 1973: A theory for isallobaric air flow in the planetary boundary layer. J. Atmos. Sci., 30, 1584-1592.